CHAPTER II

Synthesis, Characterization, Chiroptical and Cyclic Voltammetric Studies on Dioxouranium (VI) Complexes of Aldimine Derivatives of L-/D-Histidine and X-ray Crystal Structure of (N-Orthovanillidene-L-histidinato) (2,2'-bipyridyl) Dioxouranium (VI) Monohydrate Monomethanolate.

Abstract

Several new dioxouranium(VI) complexes, mostly mixed mononuclear ones, have been synthesized using N-(salicylidene)-L-histidine (S-L-$HisH_2$), N-(orthovanillidene)-L-histidine (OV-L-$HisH_2$) and the corresponding D-histidine derived ligands (S-D-$HisH_2$; OV-D-$HisH_2$). They have been characterized by elemental analysis and different physico-chemical studies including IR, UV-visible, 2D NMR (H-H COSY), CD spectroscopy and cyclic voltammetry. The crystal and molecular structures of $[UO_2(OV\text{-}L\text{-}His)(bipy)].CH_3OH.H_2O$, have been determined by X-ray crystallography. Crystal data are :

M_r = 763.54, triclinic, P1,

a = 7.817(4), b = 9.181(6), c = 10.801(12) Å,

α = 92.01(7), β = 103.51(7), γ = 114.18(5)°,

V = 680.1(5) Å^3, Z = 1, D_m = 1.85 (flotation),

D_x = 1.864(4) M gm^{-3}, λ(MoK$_\alpha$) = 0.71069 Å,

μ = (MoK$_\alpha$) = 5.74 mm^{-1}, F(000) = 368, T = 295 K,

R = 0.041 for 2818 reflections. The tridentate aldimine

ligand forms, together with bipyridine, the coordination sphere around the UO_2^{2+} entity. Methanol and water molecules are hydrogen bonded to each other [2.932(26)Å] and the water molecule is also bonded to the carboxylate O atom [2.956(15)Å]. The complexes of L-histidine derived ligands possess CD curves which are quasi-enantiomeric to those containing D-histidine residues. Chiroptical studies supported by NMR data, help to ascertain the relative contributions of configurational, conformational and vicinal factors to the observed CD curves. In the potential window -0.80 to -1.20V, most of these complexes exhibit one quasi-reversible reduction wave, corresponding to forming the analogous dioxouranium(V) species on the cyclic voltammetric time scale. The i_{pc}/i_{pa} values throw light on the factors like compactness of the aldimine chelate rings and extent of M→L π bonding, influencing the electrochemical behaviour of these complexes.

Introduction

The different facets of the coordination chemistry of aldimine derivatives of amino acids of the first transition metals as well as the ligands themselves, have received considerable attention, because of their relevance to various enzymic (vitamin B_6 catalysed) and nonenzymic reactions of α-amino acids[1,2,4-8,32,80]. Such reactions involving a number of electron and hydrogen shifts, are controlled mainly by subtle conformational effects around the N-Cα bond.

Molecular structures of a large number of metal-imine acid complexes including those of copper, have been determined through X-ray analyses[6,31,32,80]; the 1:1 complexes in such cases are mostly bridged through carboxylate oxygen atoms. Besides this, precise 2D NMR studies are difficult in such paramagnetic systems; although 1D NMR data of some of the free ligands and the corresponding diamagnetic Al(III),

Zn(II) complexes have been published, the major difficulty associated with such octahedral complexes, is the formation of several diastereoisomers with small energy barrier, thereby complicating the ^1H NMR spectra[2,6,9]. The diamagnetic UO_2^{2+} entity serves here as a good probe for elucidating the ^1H NMR spectra of such ligand systems.

Although the salicylidenamine chirality (SA) rule has been used extensively for explaining the CD spectra of the free ligands, only limited application of this rule has so far been made, for the interpretation of the chiroptical data (e.g., the statement regarding absolute configuration/ conformation in terms of a coupled oscillator model) of the corresponding metal complexes[1,6,80]. In recent years the subject of determination of absolute configuration of in situ transition metal complexes of ligating natural products from circular dichroism within the d-d bands, has received considerable attention; but such studies usually need complex formation of the organic molecules with a metal cluster, in order to restrict the conformational freedom[26].

In this study the pentagonal/hexagonal planar coordination geometry of the UO_2^{2+} entity has been used as a matrix for complexing two sets of chiral ligands derived from L-/D-histidine and ascertain their absolute configuration/ conformation with the help of the SA chirality rule and NMR

data; the coordination mode of the ligand and overall coordination geometry around the UO_2^{2+} entity, have been ascertained in one case through X-ray crystal structure determination. The choice of histidine for this work has obvious reasons, e.g., the histidyl residue is perhaps the most important metal-binding site in biological systems and histidine is present in a large number of enzyme active centres[6,80,142-144]. The rich coordination chemistry of the dioxouranium(VI) species and that several physico -chemical aspects of dioxouranium(VI) compounds, e.g., photochemistry, circularly polarized luminescence spectroscopy, etc., have been the subject of recent publications, makes this study an interesting one[16,17,44-48,71,145,147-150].

In view of the recent developments on the subject of conformational control of electrochemical behaviour and vice versa[75-77], as well as the cyclic voltammetric studies on dioxouranium(VI) complexes[46,48], electrochemical studies on the pertinent complexes especially the quasi-enantiomeric ones, are undertaken using cyclic voltammetry; it is a temporal method in which the duration of the potential scan occurs within the time domain of the mean life times associated with the conformational changes. In this chapter we try to correlate the conformational aspects of the chelate rings (compactness/sterically demanding nature), as revealed by the electrochemical parameters of the cyclic

voltammetric waves, with the chiroptical inferences drawn from CD spectra and the extent of M→L π bonding (indicated from ^{1}H NMR study).

Experimental Section

Materials. Orthovanillin (Fluka), salicylaldehyde (Kemphasol), L-histidine monohydrochloride monohydrate (E.Merck, Germany), D-histidine monohydrochloride monohydrate (Sigma, U.S.A.), 2,2'-bipyridyl (B.D.H), 1,10-phenanthroline monohydrate (B.D.H) and uranyl nitrate hexahydrate G.R. (LOBA, Bombay) were used as such. The solvents were purified by the usual laboratory procedures[10].

(a) Preparation of ligands

OV-L-HisHK.2H$_2$O, S-L-HisHK : L-histidine monohydrochloride monohydrate (0.21g, 1 mmol) was dissolved by warming with KOH (0.12g, 2 mmol) in 25 ml methanol-water (5:1 v/v) mixture. To this warm solution orthovanillin (0.19g, 1.25 mmol) or salicylaldehyde (0.155g, 1.25 mmol) in 10 mL methanol was added, the resulting mixture was stirred for 1h and then evaporated to dryness on a steam bath. The dryness was treated with diethyl ether to remove the excess orthovanillin or salicylaldehyde and then with dry methanol to dissolve the ligand, leaving behind KCl. The filtered

methanolic solution was reduced to dryness in vacuo and the resulting product was finally dried over $CaCl_2$ in a vacuum desiccator.

Yields of these hygroscopic, orange-yellow to yellow colored ligands were around 50-60%. Purity was checked through elemental analyses.

(b) Preparation of complexes

$K_2[UO_2(OV\text{-}L\text{-}His)_2].4H_2O$: To a warm solution of OV-L-HisHK $.2H_2O$ (0.36g, 1 mmol) in 15 ml methanol, $UO_2(NO_3)_2.6H_2O$ (0.25g, 0.5 mmol) in 8 ml water was added, the mixture was stirred for 0.5 h, followed by concentration to about 10 mL on a steam bath and then left undisturbed for 3h. The precipitated compound was filtered, washed with methanol-water (4:1 v/v), methanol, diethyl ether and dried over $CaCl_2$ in vacuo.

Alternatively, the ligand may be obtained in situ by reacting orthovanillin (0.15g, 1 mmol) in 5 mL methanol with a 15 mL methanol-water (1:1 v/v) solution of L-histidine monohydrochloride monohydrate (0.21g, 1 mmol) in KOH (0.112g, 2 mmols), followed by reaction with $UO_2(NO_3)_2.6H_2O$ (0.25g, 0.5 mmol) in 5 mL methanol.

$[(UO_2)_2(S\text{-}L\text{-}His)(S\text{-}L\text{-}HisH)_2(H_2O)_2].4H_2O$

This compound may be prepared either by using a solution of S-L-HisHK (0.3g, 1 mmol) in 15 mL methanol or the ligand obtained in situ from salicylaldehyde (0.125g, 1 mmol), L-histidine monohydrochloride monohydrate (0.21g, 1 mmol), KOH (0.14g, 2.5 mmol) and following the above-mentioned procedure.

$[UO_2(OV\text{-}L\text{-}His)(bipy)].3H_2O$, $[UO_2(OV\text{-}L\text{-}His)(phen)].H_2O$, $[UO_2(S\text{-}L\text{-}His)(bipy)].2H_2O$, $[UO_2(S\text{-}L\text{-}His)(phen)].4H_2O$

A warm solution of $OV\text{-}L\text{-}HisHK.2H_2O$ (0.36g, 1 mmol) or S-L-HisHK (0.3g, 1 mmol) in 15 mL methanol, was mixed with 2,2'-bipyridyl (0.15g, 1 mmol) or 1,10-phenanthroline monohydrate (0.2g, 1 mmol) in 5 mL methanol, followed by the addition of a solution of $UO_2(NO_3)_2.6H_2O$ (0.5g, 1 mmol) in 5 mL water, the resulting mixture was worked up through the aforesaid sequence of manipulations.

All these complexes may also be prepared by an alternative procedure, involving formation of the ligands in situ, followed by reaction with 2,2'-bipyridyl or 1,10-phenanthroline and $UO_2(NO_3)_2.6H_2O$ in 1:1:1 molar proportion in methanol-water (4:1 V/V) medium. For the N-(orthovanillidene) complexes the amount of KOH was restricted to 0.056g (1 mmol), whereas for the other system a slight excess of KOH (0.084g, 1.5 mmols) had to be used.

$[UO_2(OV\text{-}L\text{-}His)(bipy)]\cdot CH_3CH\cdot H_2O$

This complex was obtained by recrystallization of $[UO_2(OV\text{-}L\text{-}His)(bipy)]\cdot 3H_2O$ from methanol-water (4:1 V/V) mixture. The third recrystallization product was used for x-ray diffraction measurement.

Yields of these complexes were ca. 45-55%. They are insoluble in diethyl ether, slightly soluble in methanol, ethanol and moderately soluble in dimethyl formamide, dimethyl sulfoxide.

Physical measurements

IR spectra (4000-200 cm^{-1}) were recorded in nujol mull using CsI optics and in CsI phase on a Pye Unicam SP3-300 IR spectrophotometer and on a Perkin Elmer 983 IR spectrophotometer respectively. Electronic spectra in methanol were recorded on a Shimadzu (UV-240) spectrophotometer. CD spectra were recorded on a Jobin Yvon dichrograph RJ Mark III. 300 MHZ ^1H NMR spectra (1D & 2D) were recorded on a Varian VXR 300 S NMR spectrometer at 25°C, some of the ^1H NMR spectra were also recorded on a Varian XL-100 spectrometer. The acid dissociation constants of the partly deprotonated ligands in $[(UO_2)_2(S\text{-}L\text{-}His)(S\text{-}L\text{-}HisH)_2(H_2O)_2]\cdot 4H_2O$, were measured (Systronics digital pH meter, model 335) in methanol-water (3:2 V/V) at constant ionic strength (0.1M $NaClO_4$) at 30°C by

Bjerrum's method (using the equation $\bar{n}_H = nA - P - [H^+] + [OH^-] / A$) applying the Kelvin-Wilson titration technique; pK_a values were obtained by the least-square method from the $\bar{n}_H$-B values[12,139-141]. Although there is possibility of calculating the pK_a values upto the third stage of dissociation (the aquo groups), this could not be done here due to the formation of $Na_2U_2O_7$ after a certain stage of titration. Electrochemical studies were performed with a Bioanalytical systems (BAS) model CV-27 electroanalytical apparatus. The solvent (DMSO) used in the electrochemical measurements was purified by distillation from phosphorus pentoxide under a dry nitrogen atmosphere and stored over molecular sieves (3Å). The supporting electrolyte, tetrabutylammonium perchlorate, $[NBu_4]ClO_4$, was prepared from tetrabutylammonium hydroxide by literature procedure and dried overnight at 100°C under vacuum[57]. The three-electrode (CV) measurements were carried out under a purified dinitrogen atmosphere in a gas-tight cell by using a BAS planar platinum-inlay working electrode, a platinum wire auxiliary electrode and a saturated calomel electrode (SCE); the SCE was connected to the test-solution through a vycor tip. The reported potentials are uncorrected for junction contribution. The solvent-supporting electrolyte (DMSO-0.1M $[NBu_4]ClO_4$) base line was checked, prior to electrochemical measurements of the relevant complexes.

Controlled-potential coulometric experiments were conducted by use of either the BAS CV-27 instrument or a BAS PWR-3

potentiostat functioning in conjunction with the CV-27 unit. The latter configuration afforded a faster rate of electrolysis. The working electrode for coulometry was a piece of platinum foil (4.2 cm x 2.2 cm). The reference electrode was as described above. The wide glass tube containing the platinum coil auxiliary electrode was filled-up with an appropriate mixture of solvent-supporting electrolyte and kept isolated from the sample solution by a vycor glass disk. A steady stream of dinitrogen gas was maintained through the vigorously stirred solution during electrolysis. The potentials for exhaustive electrolysis were 0.1 to 0.2 V past the cathodic-peak potential of the appropriate cyclic voltammogram of each complex. An identical experiment performed on supporting electrolyte alone, enabled a correction for background charge to be made.

Potential measurements have a precision of $\pm$ 0.005 V and coulometric measurements (n) of $\pm$ 10%.

X-ray crystallography

Crystal and diffraction data are summarized in Table II-1. The intensities were corrected for Lorentz and polarisation effects. The absorption correction was included by emperical ϕ-scan method. The structure was solved by direct and Fourier methods using SHELX 76 (Sheldrick, 1976) and SHELXS 86

(Sheldrick, 1990) programs. Least-squares refinement with nonhydrogen atoms anisotropically converged to R = 0.041 and R_w = 0.037. Scattering factors for neutral atoms and anomalous dispersion corrections were taken from the literature[151-155]. All calculations were performed on the VAX 8650 computer system. Atomic coordinates are listed in Table II-2, bonding distances and angles in Table II-3 and anisotropic temperature factors in Table II-4.

Results and Discussions

The analytical data of these complexes are listed in Table II-5. Molar conductances measured in dilute methanolic solutions (ca.10^{-4}M, because of solubility problem), are usually lower then literature data, e.g., 40 and 70-75 $\Omega^{-1}cm^2mol^{-1}$ are typical values for nonelectrolytes and 1:1 electrolytes respectively[11]. For complex 5 (Table II-5) experimental pK_a values of 6.82 and 7.87 refer to unneutralised/coordinated phenolic -OH groups[12].

The TGA curve (ca.7°C/min, air) (Figure II-4) of $[UO_2(OV\text{-}L\text{-}His)(bipy)].CH_3OH.H_2O$ indicates that the extraspheric hydrogen bonded H_2O/CH_3OH molecules are not completely eliminated until a temperature of 175° is attained[25], which is also revealed by X-ray data (Figure-1).

Structure : $[UO_2(OV\text{-}L\text{-}His)(bipy)].CH_3OH.H_2O$ crystallizes in the triclinic space group P1. The atom-numbering scheme, the unit cell and ORTEP diagrams are shown in Figures II-1 to II-3 respectively. The molecule is centred on seven coordinate uranium in pentagonal bipyramidal stereochemistry. The phenoxide oxygen, imine nitrogen and one of the carboxyl oxygen atoms of the tridentate imine acid together with the two nitrogen atoms of 2,2'-bipyridyl, occupy the five corners of the equatorial coordination pentagon. Binding by the uranyl oxygen atoms in the two apical sites completes the pentagonal bipyramid. The two nitrogen atoms of 2,2'-bipyridyl have slightly different U-N bond lengths[156]. The axis of the C(3)-C(4) bond linking the imidazole ring, is orientated in a similar fashion as in other β-aryl amine acid derived systems[32,80].

The O-U-O axis shows a 3.6° deviation from linearity and the equatorial plane is puckered[157,158]. With respect to the O(1)-U axis the carboxyl oxygen and azomethine nitrogen atoms are 4.2°-4.3° below the equatorial plane and the phenoxide oxygen atom is 0.9° above it; one [N(4)] of the two nitrogen atoms of 2,2'-bipyridyl is on the equatorial plane, while the other one [N(5)] is 2.2° above it. In terms of the O(2)-U axis the three donor atoms of the imine acid residue are 0.2-1.4° above the equatorial plane; [N(4)] is 3.5° above the equatorial plane and [N(5)] is

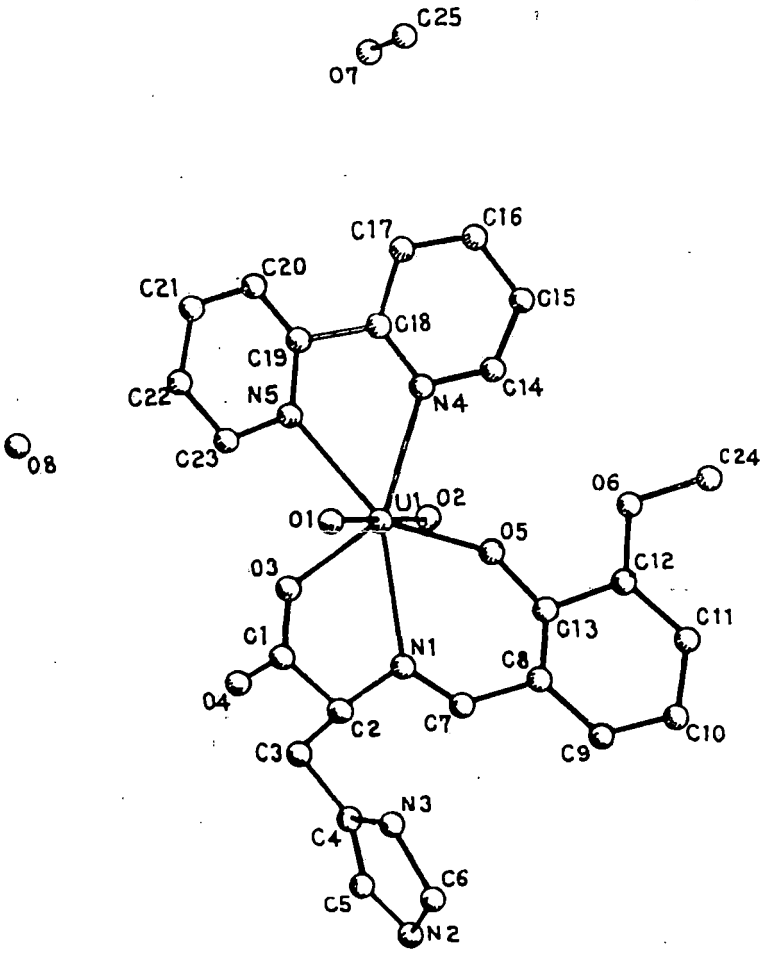

Figure II-1: Atom numbering scheme of $[UO_2(OV\text{-}L\text{-}His)(bipy)]\cdot CH_3OH\cdot H_2O$.

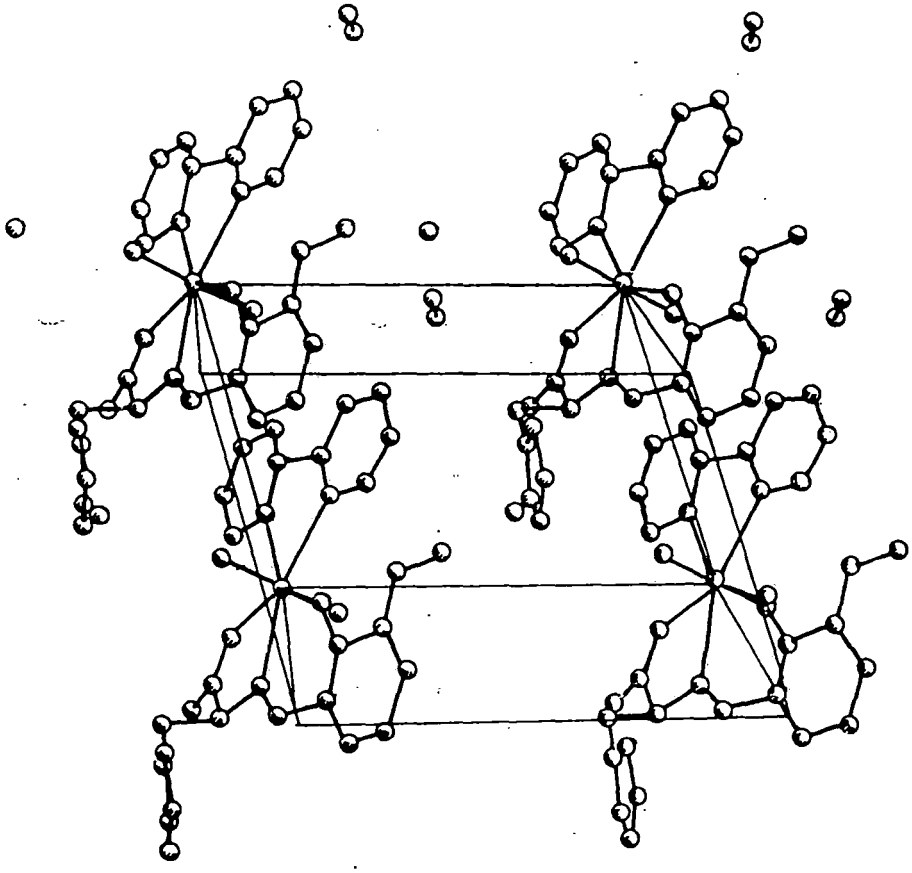

Figure II-2: Molecular packing in crystals of

$[UO_2(OV\text{-}L\text{-}His)(bipy)]\cdot CH_3OH\cdot H_2O$.

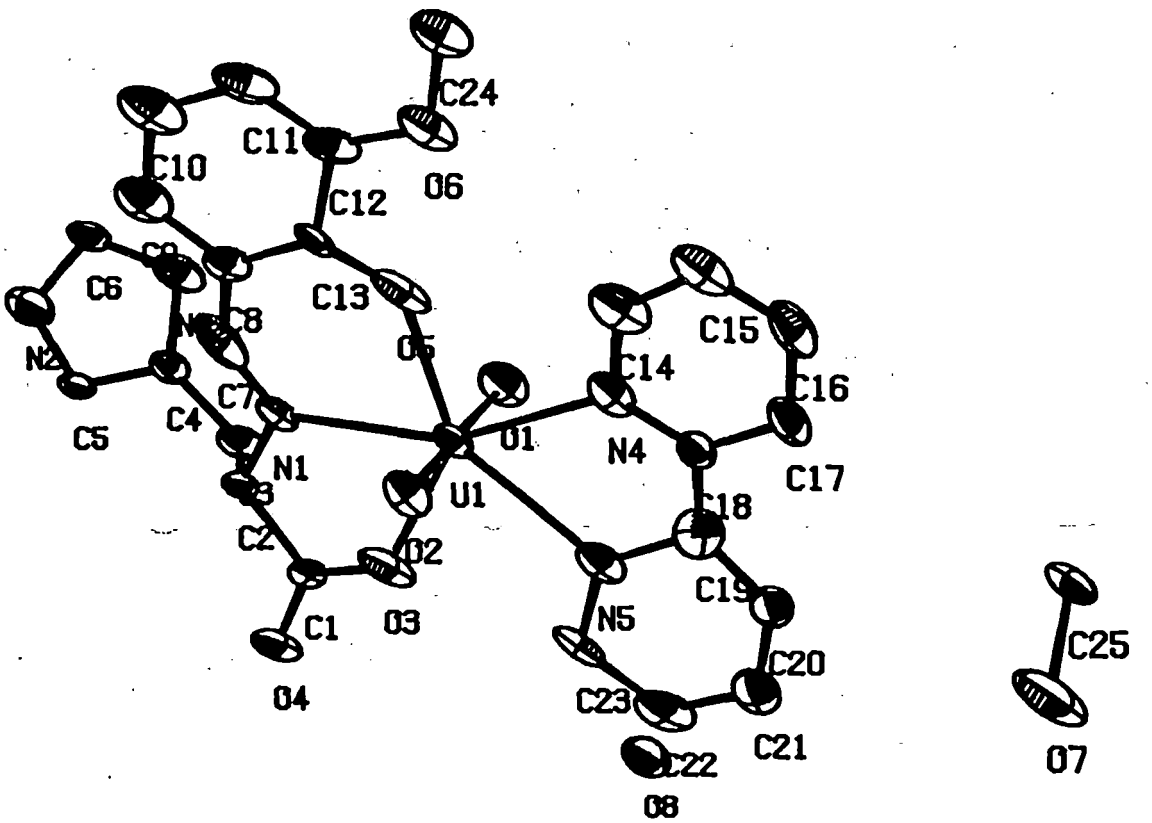

ORTEP

Figure II-3: ORTEP diagram of $[UO_2(OV\text{-}L\text{-}His)(bipy)].CH_3OH.H_2O$. Thermal ellipsoids represent 40% probability.

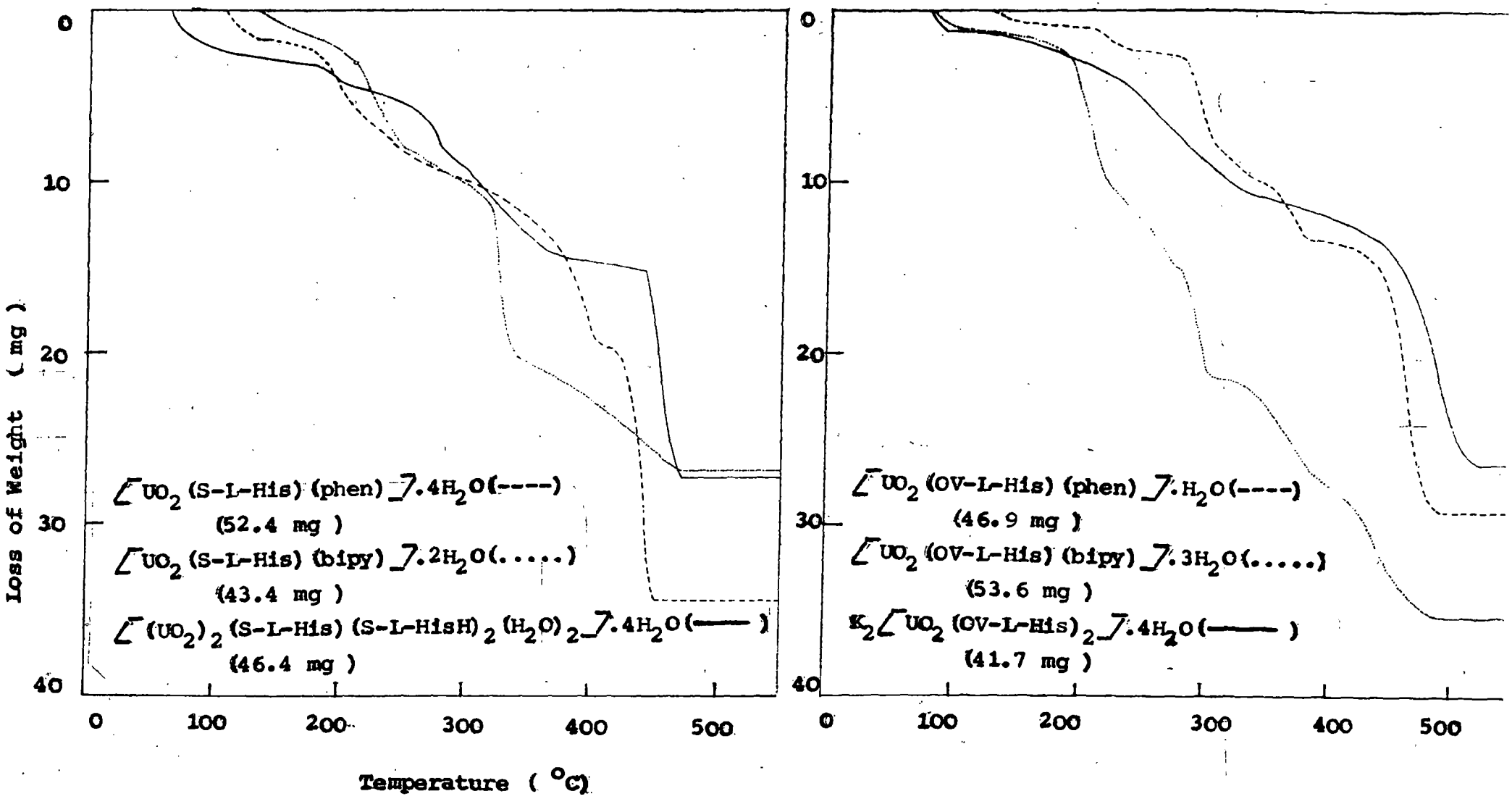

FigureII-4: TGA curves .

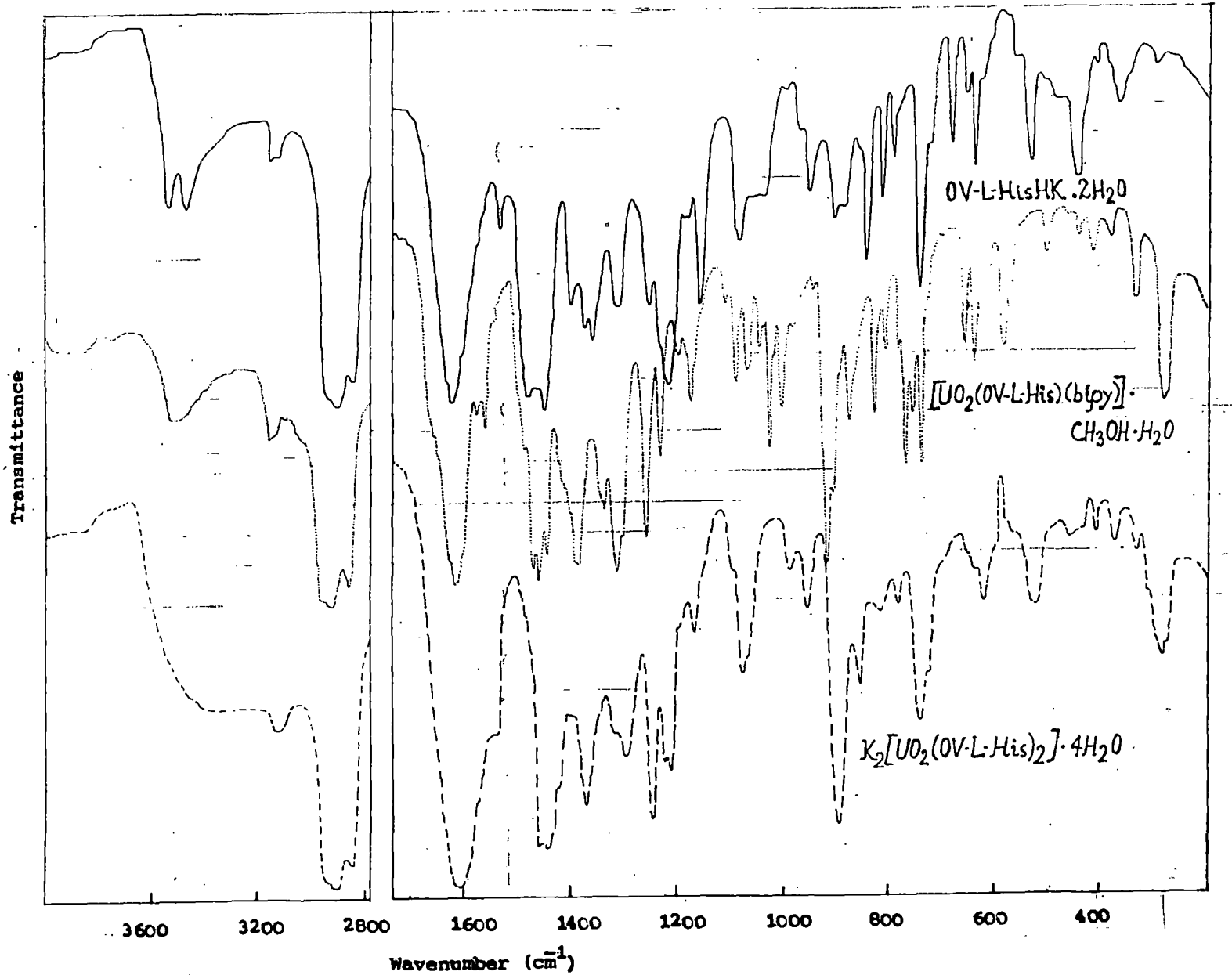

Figure II-5. I.R. spectra of OV-L-HisHK.$2H_2O$, $[UO_2(OV\text{-}L\text{-}His)(bipy)].CH_3OH.H_2O$ and $K_2[UO_2(OV\text{-}L\text{-}His)_2].4H_2O$ in nujol using CsI optics.

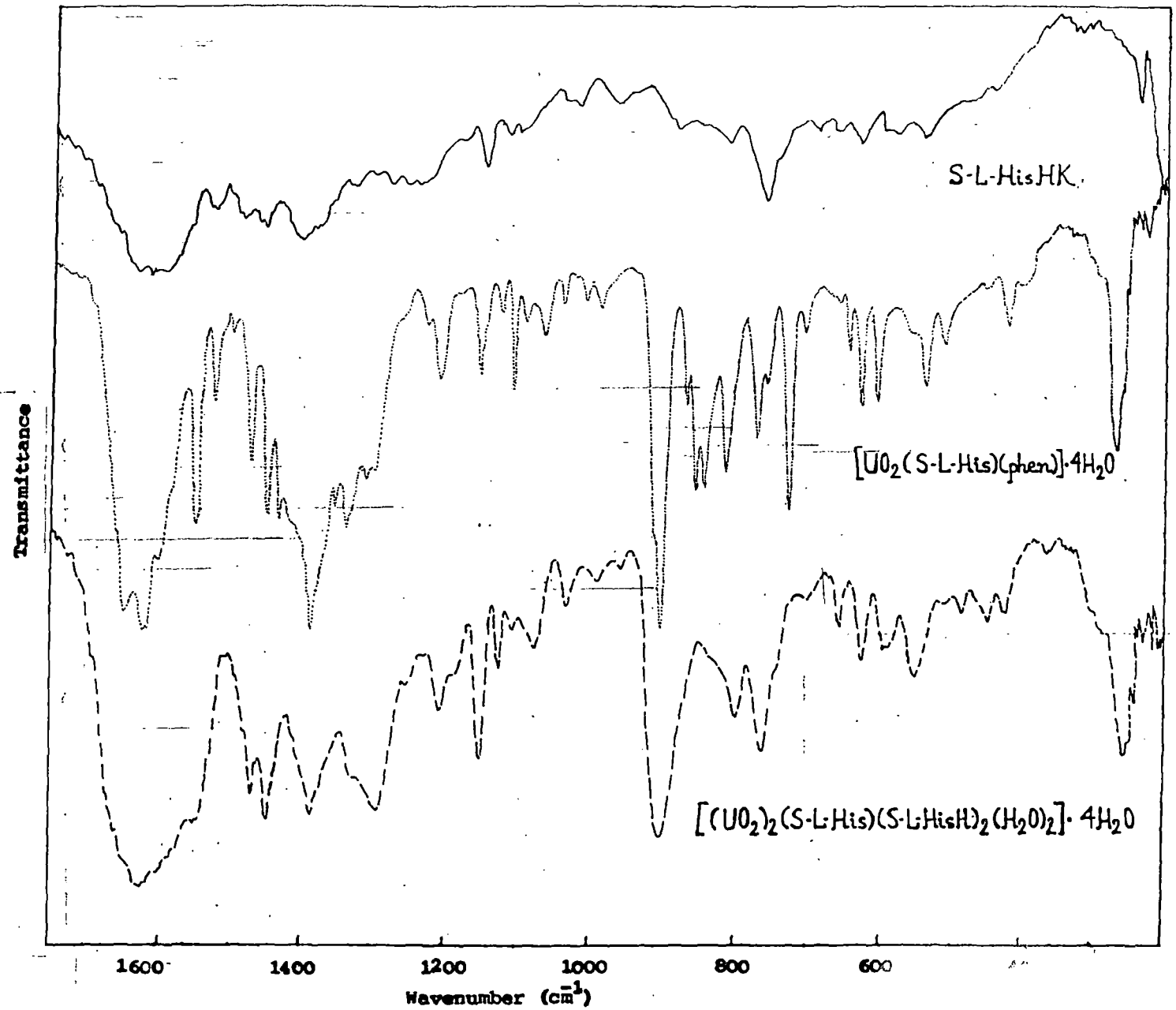

Figure II-6: I.R. spectra of S-L-HisHK, in KBr , $[UO_2(S\text{-}L\text{-}His)(ph$ and $[(UO_2)_2(S\text{-}L\text{-}His)(S\text{-}L\text{-}HisH)_2].4H_2O$ in CsI medium.

1.2° below it, i.e., the two aromatic rings of the neutral donor molecule are slightly bent with respect to its X-axis[63]. The chelate ring puckerings can be easily visualised using a Darling model[159,160]. This diamagnetic mononuclear complex with L-amino acid residue, has been used here as a model for understanding its ^{1}H NMR and CD spectra and also those of other related species.

IR spectra. A comparative study (Table II-6; Figures II-5 and II-6) of the IR spectra of OV-L-HisHK.$2H_2O$ and $[UO_2(OV\text{-}L\text{-}His)(bipy)].CH_3OH.H_2O$, reveals the following features : the ν (CH=N) mode is lowered on coordination and in some of these complexes this IR band is split[16,18,161]; the broad free ligand band due to the ν (C-O) mode coupled with the δ(OH) vibration of the phenolic -OH group, changes to a sharp band of the ν (C-O) mode (phenoxide group)[13]; the $\Delta(\nu_{as} - \nu_s)$ value of the $-CO_2^-$ group is 190 cm^{-1} and it is consistent with unidentate carboxylate coordination[21,22]. Comparable IR data are observed for the other pertinent complexes except for $[(UO_2)_2(S\text{-}L\text{-}His)(S\text{-}L\text{-}HisH)_2(H_2O)_2].4H_2O$, where a broad band is observed at 1619 cm^{-1} due to the presence of two types of azomethine groups (vide ^{1}H NMR data) as well as coordinated aquo groups; the nature of the IR bands around 1210-1190 cm^{-1} is also different, due to the presence of unneutralised ligand protons[13].

Tridentate imine acid coordination is inferred in all these cases except for $[(UO_2)_2^{\oplus}(S\text{-}L\text{-}His)(S\text{-}L\text{-}HisH)_2(H_2O)_2]\cdot 4H_2O$ where one of the azomethine groups remains free (vide NMR data); all the 1:1 (M:L) complexes (serial numbers 2-4, 6 & 7, Table II-5) attains an equatorial coordination number of five; for the 1:2 (M:L) complex (Serial No.1, Table II-5) an equatorial coordination number of six is possibly achieved.

In most cases the asymmetric stretching frequency (ν_3) of the UO_2^{2+} entity is a sharp peak accompanied by a shoulder[23]; its doubly degenerate bending frequency (ν_2), which is usually split, appears in the region 268-256 cm^{-1} as a prominent peak, accompanied by shoulders[24].

NMR spectra : Several relevant ^1H NMR spectra are shown in Figures II-7 to II-15; they include H-H COSY (2D NMR spectra) data on most of them. These figures indicate the assignments of different proton signals as well as dominant conformers to which they correspond, as inferred from CD spectra (vide later)[1]. Table II-7 lists the chemical shift values of protons of major conformers of the ligands and those of the corresponding complexes along with the Δ ($= \delta_{complex} - \delta_{ligand}$) ppm values for the latter. Some of the important coupling constants from first-order analysis of expanded 1D spectra and related data together with the population (estimated from the time averaged ^1H NMR spectra) of conformers, have also been

tabulated (Table II-8)[2].

A perusal of the ^1H NMR spectrum (Figure II-7) of OV-L-HisHK $.2H_2O$ along with its expanded runs over relevant regions, reveals the following important aspects :- the ligand consists of two conformers (89% and 11% respectively), the dominant one being I and a smaller contribution from the other one arising from anticlockwise rotation about the $C_\alpha - C_\beta$ bond (Scheme I); the additional

Scheme I

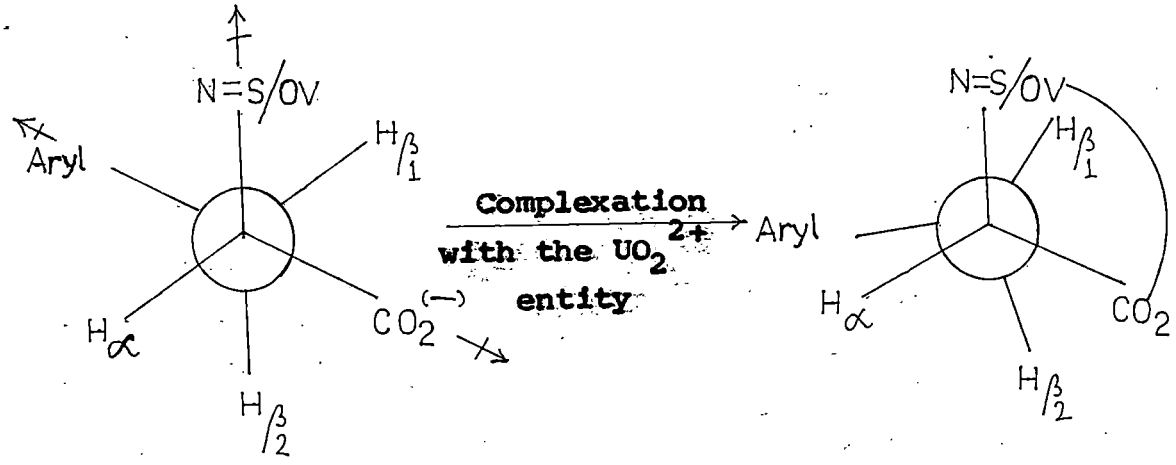

S-L-HisH$^-$ / OV-L-HisH$^-$;

Aryl = imidazole group;

Arrows indicate electric vectors.

$170^\circ < H_\alpha CCH_{\beta_1} < 180^\circ$

$60^\circ < H_\alpha CCH_{\beta_2} < 70^\circ$

The curved line indicating the chelate ring with UO_2^{2+} entity.

signals for the later conformer appear at δ 7.48 ($CH=N$), 5.23 (H_α) and 3.71 ($C_5.OCH_3$) ppm. The relative conformational population around the $C_\alpha - C_\beta$ bond could also be calculated (89% and 11% respectively) from the coupling constant values ($^3J_{\alpha\beta_1}$ and

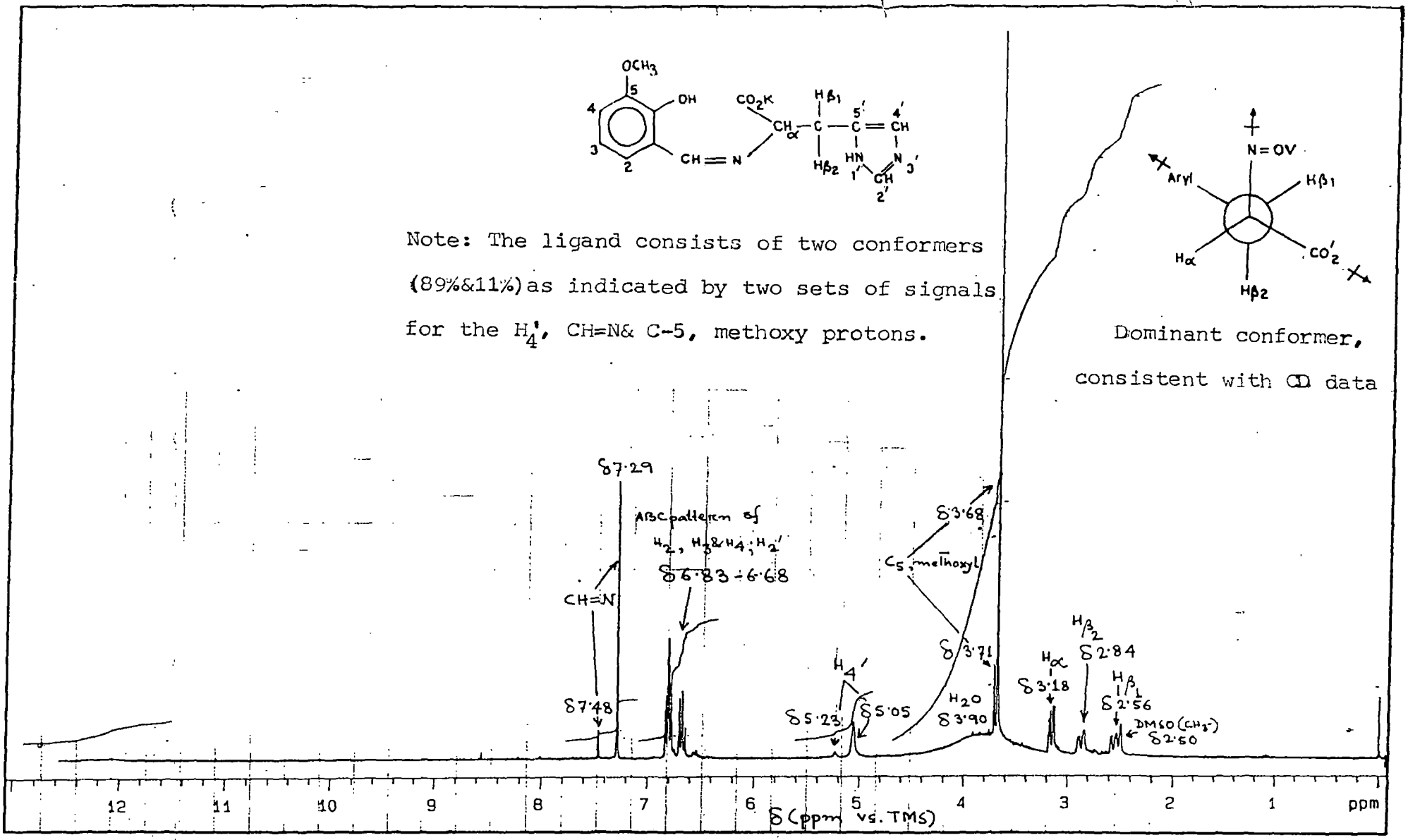

Figure II-7(a): 300 MHz ^{1}H NMR spectrum of OV-L-HisHK .2H$_2$O in DMSO.

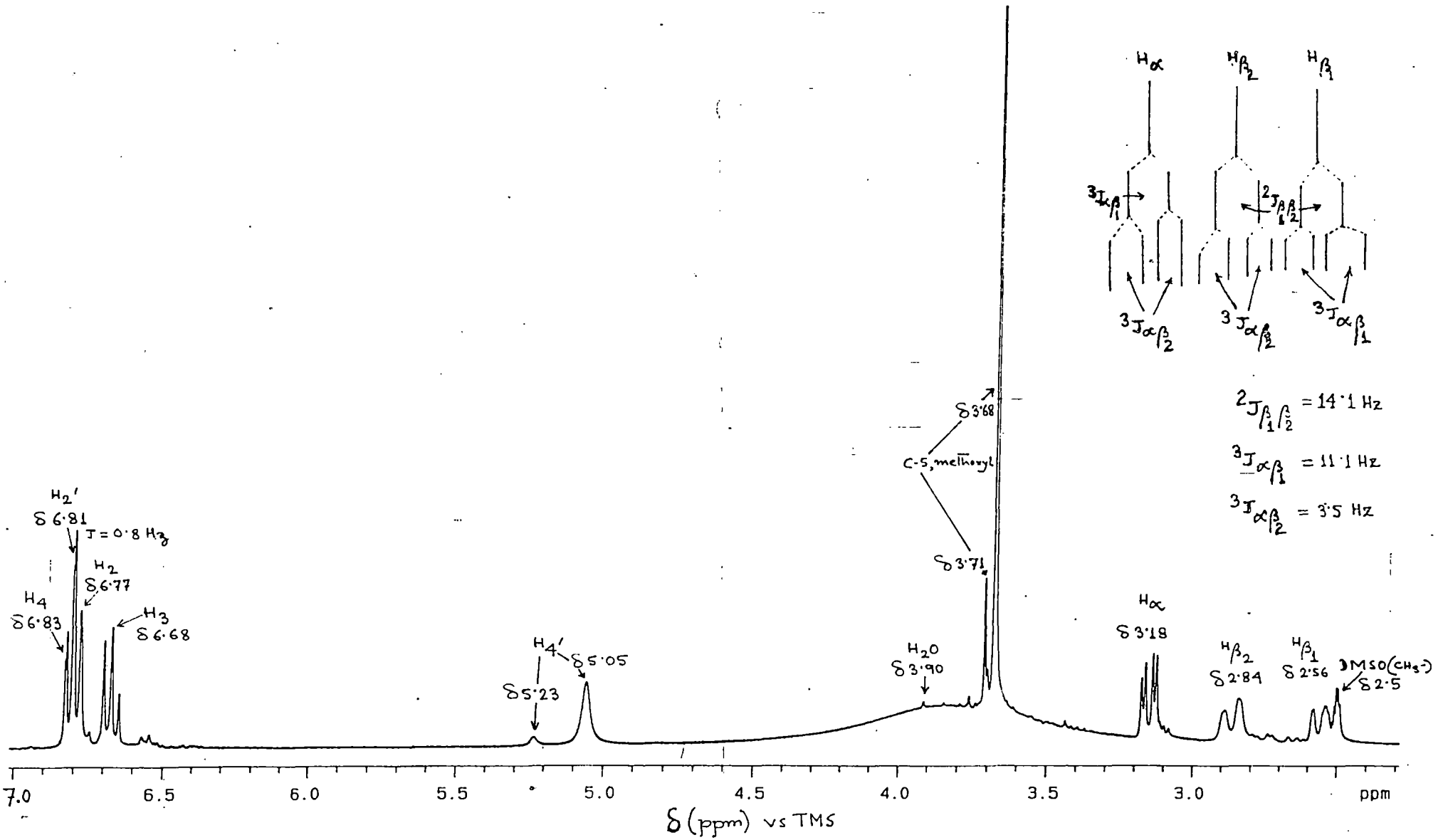

Figure II-7(b): 300 MHz ^{1}H NMR spectrum of OV-L-HisHK.2H$_2$O in DMSO showing the expansion of the region δ 7.0-2.3 ppm .

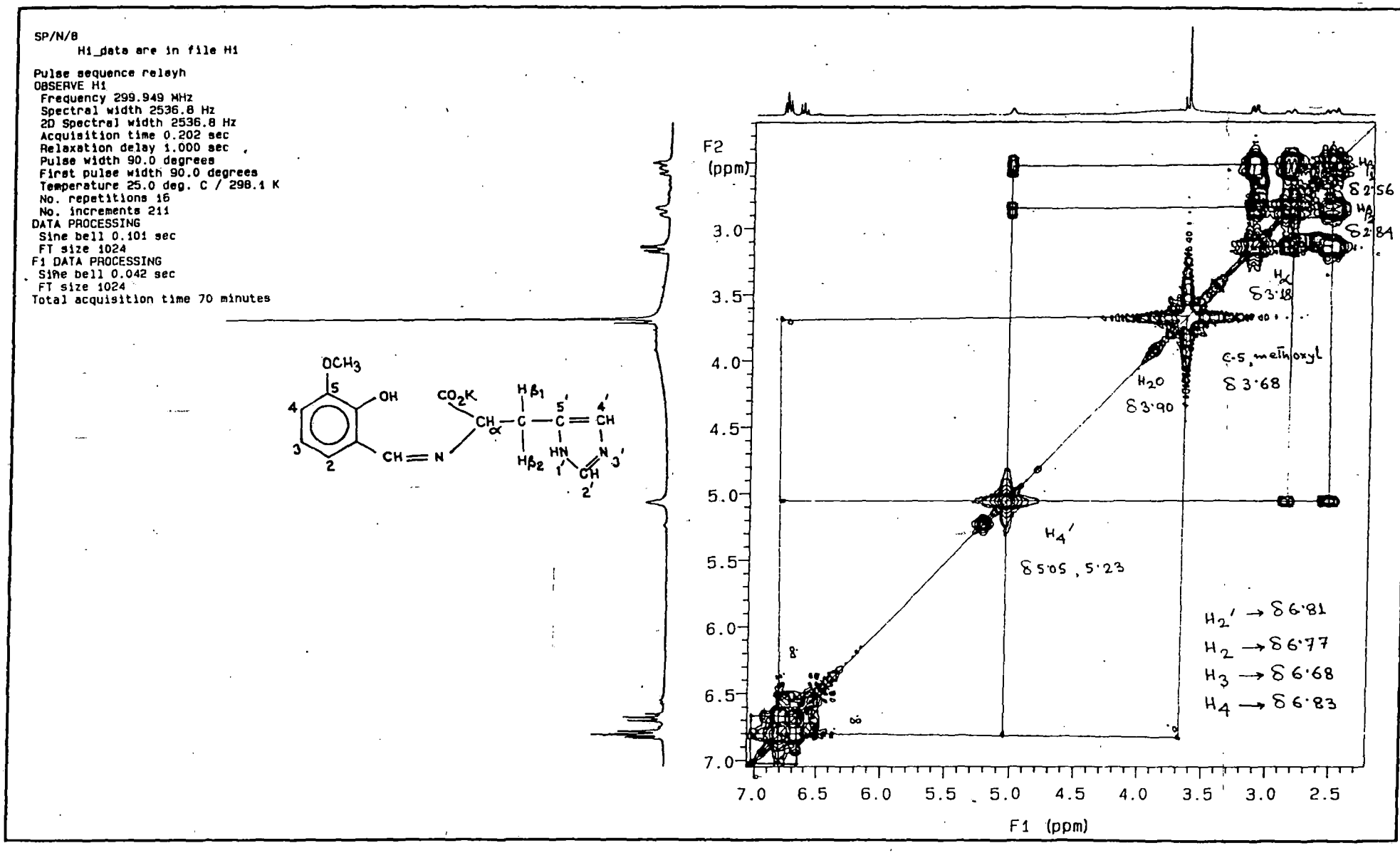

Figure II-7(c): 300 MHz 2D H-H COSY spectrum (symmetrized) of OV-L-HisHK.2H_2O.

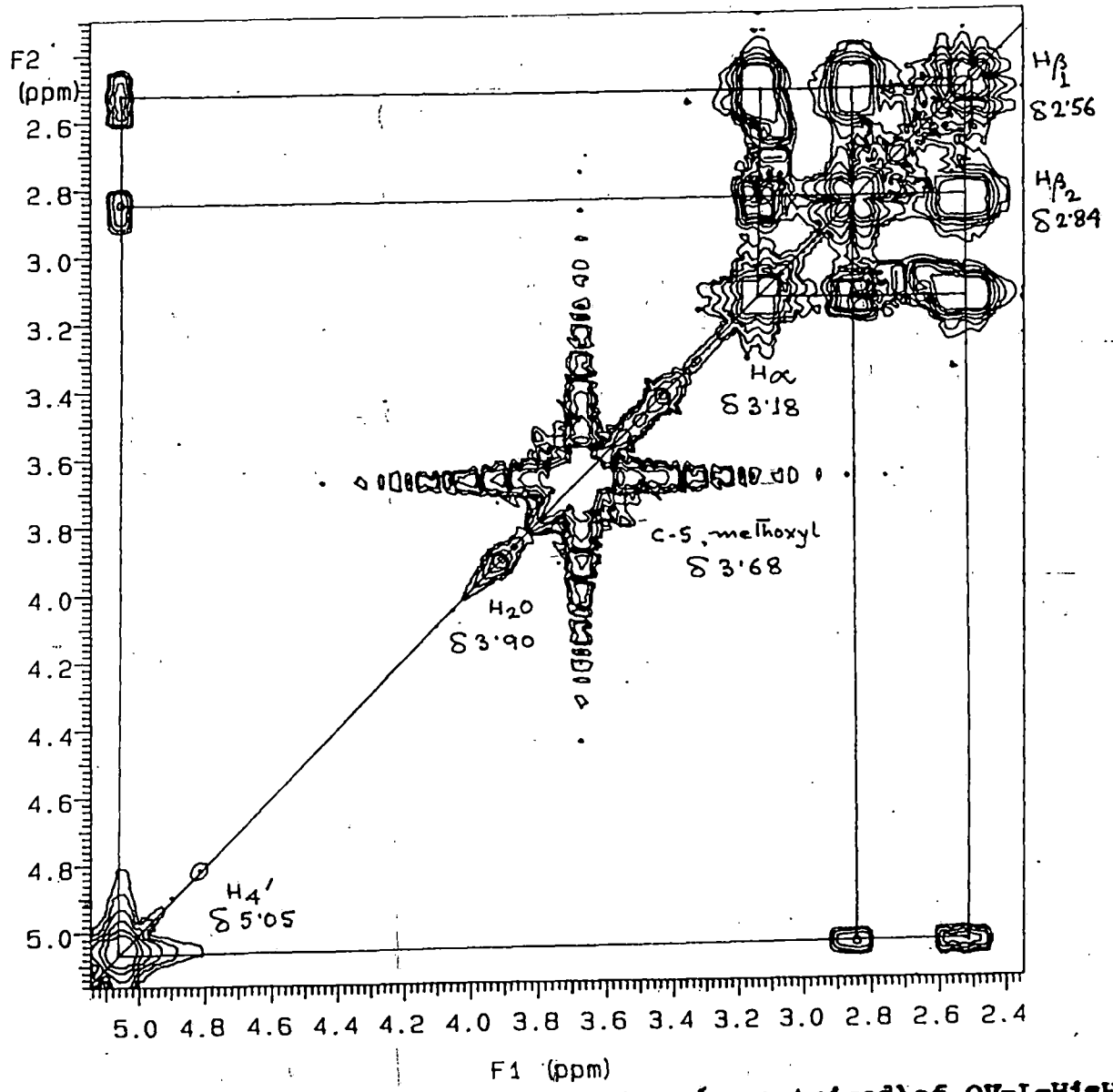

Figure II-7(d): 300 MHz H-H COSY spectrum (symmetrized) of OV-L-HisHK.2H_2O showing the expansion of the region δ 5.0-2.4 ppm .

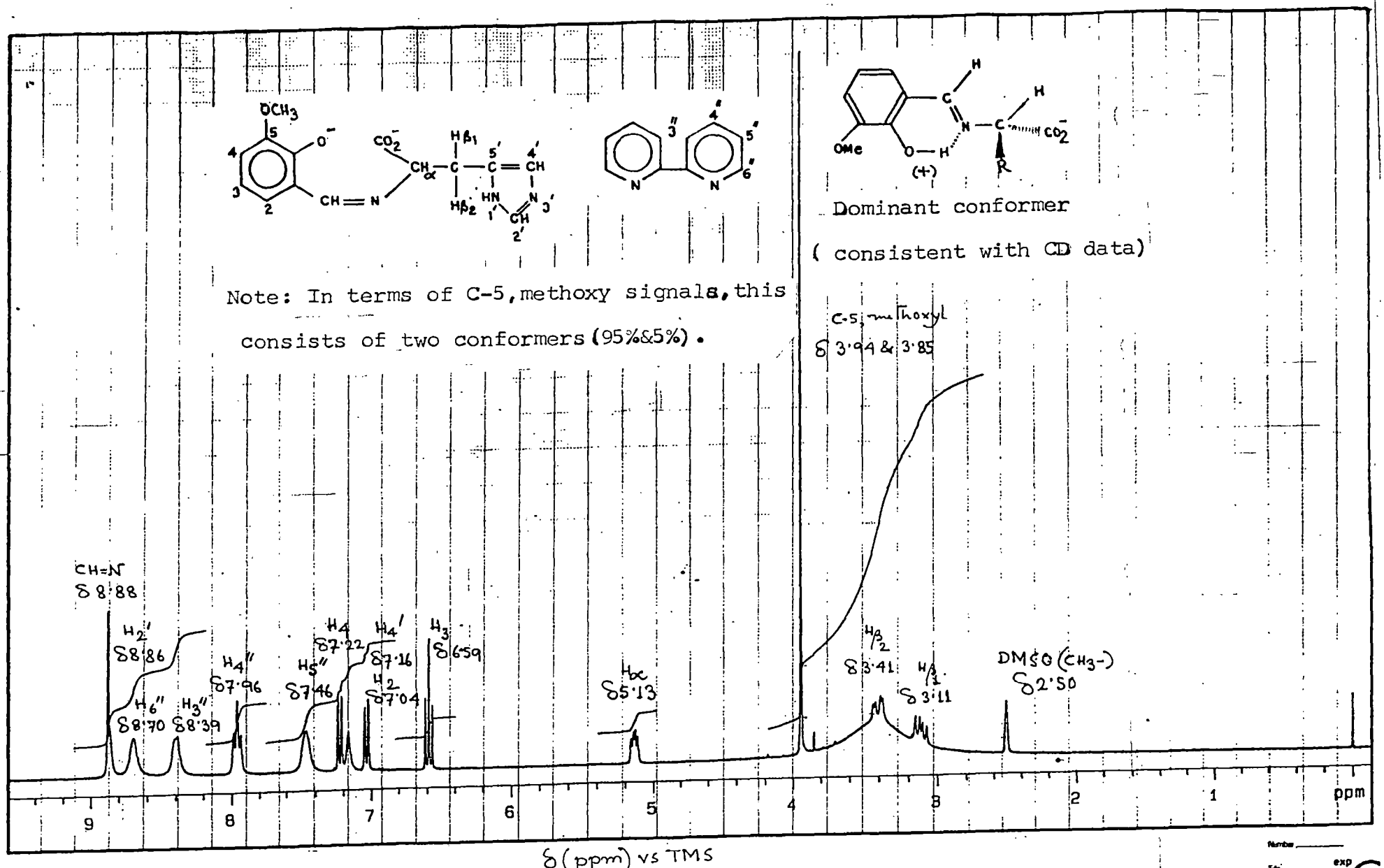

Figure II-8(a): 300 MHz ^1H NMR spectrum of $[UO_2(OV\text{-}L\text{-}His)(bipy)].3H_2O$ in DMSO.

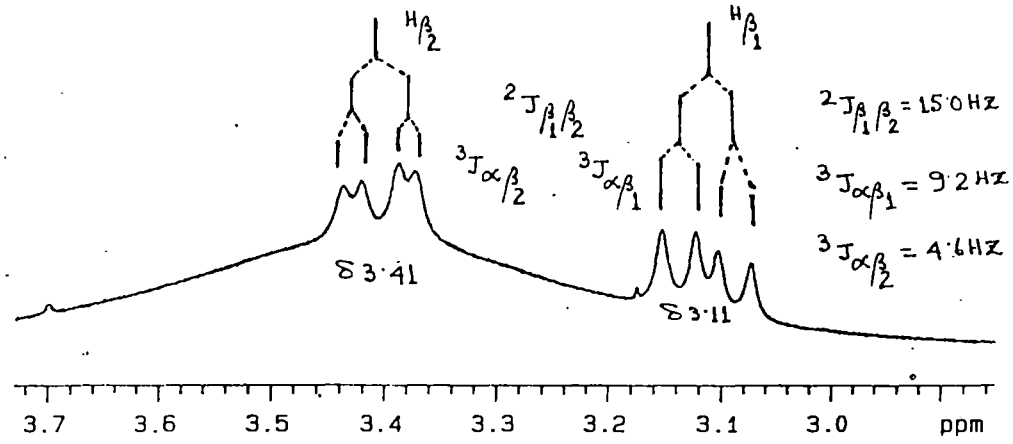

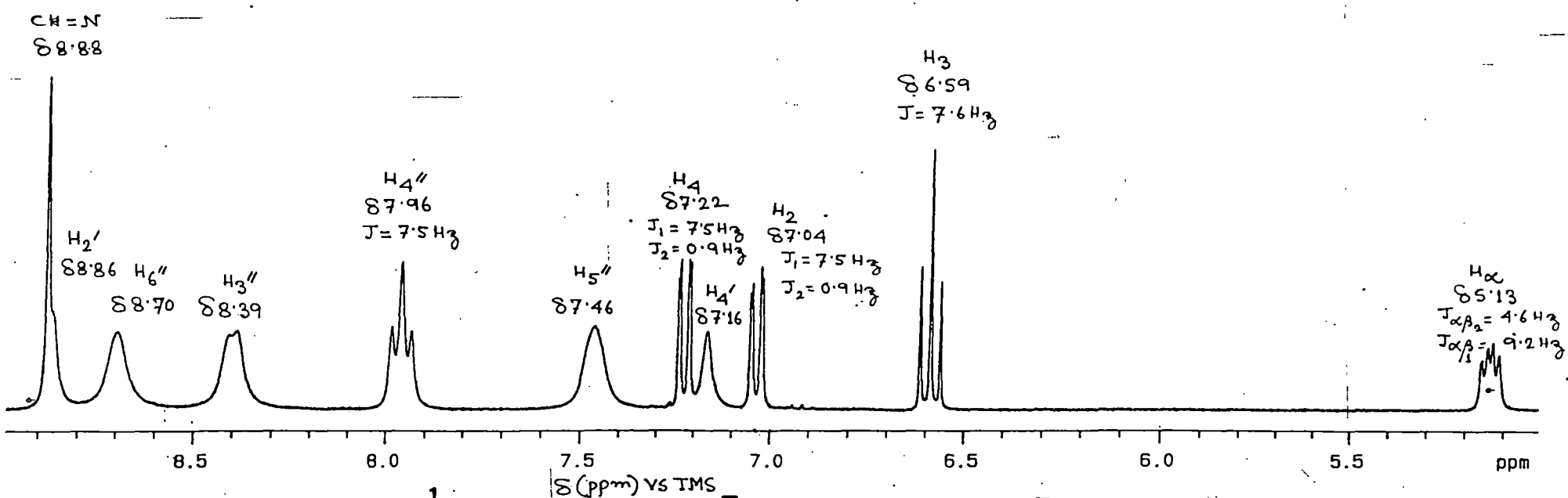

FigureII-8(b): 300 MHz ^1H NMR spectrum of $[UO_2(OV\text{-}L\text{-}His)(bipy)].3H_2O$ in DMSO showing the expansion of δ 8.9-5.1 ppm and δ 3.7-2.5 ppm region .

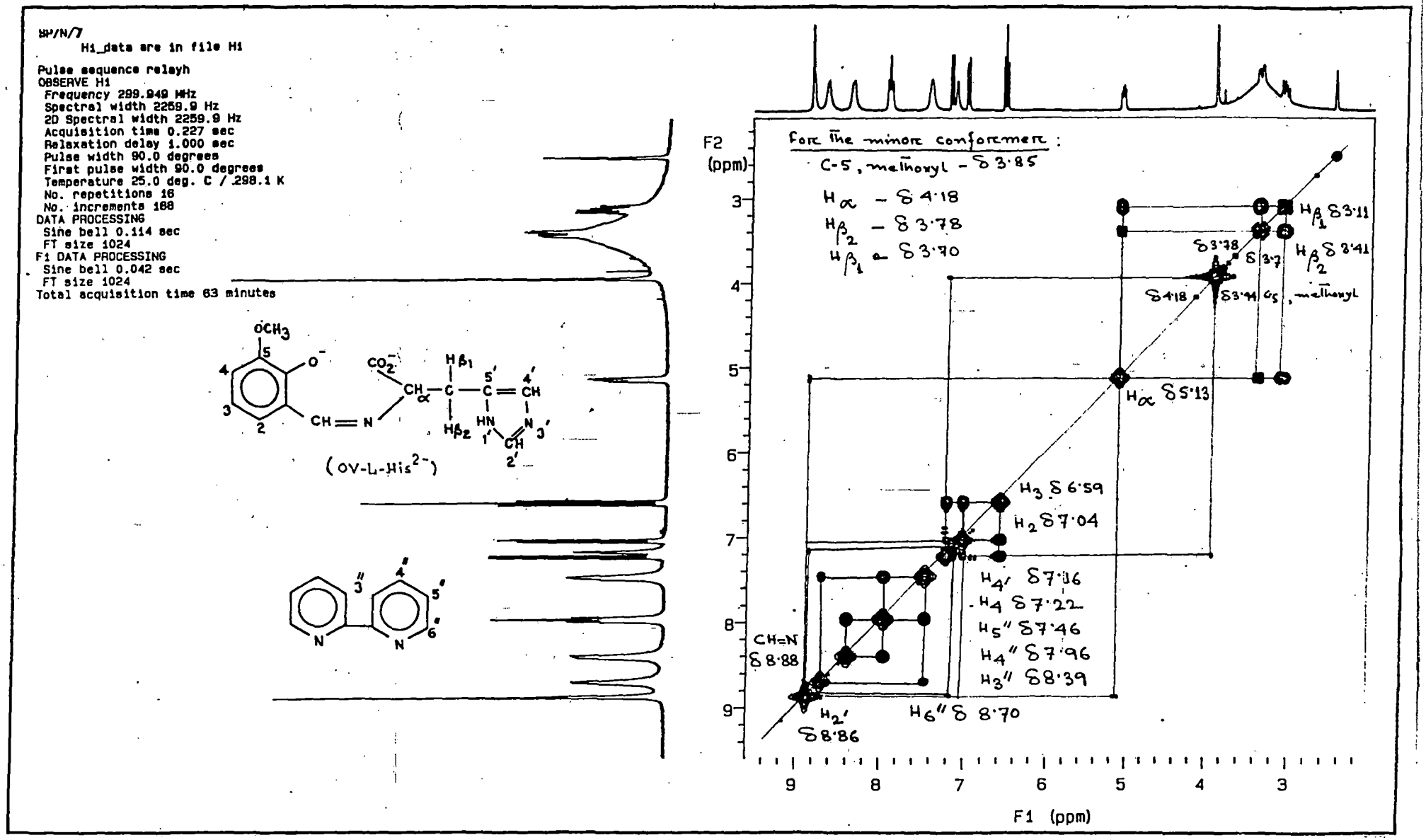

Figure II-8(c): 300MHz H-H COSY spectrum (symmtrized) of $[UO_2(OV\text{-}L\text{-}His)(bipy)].3H_2O$.

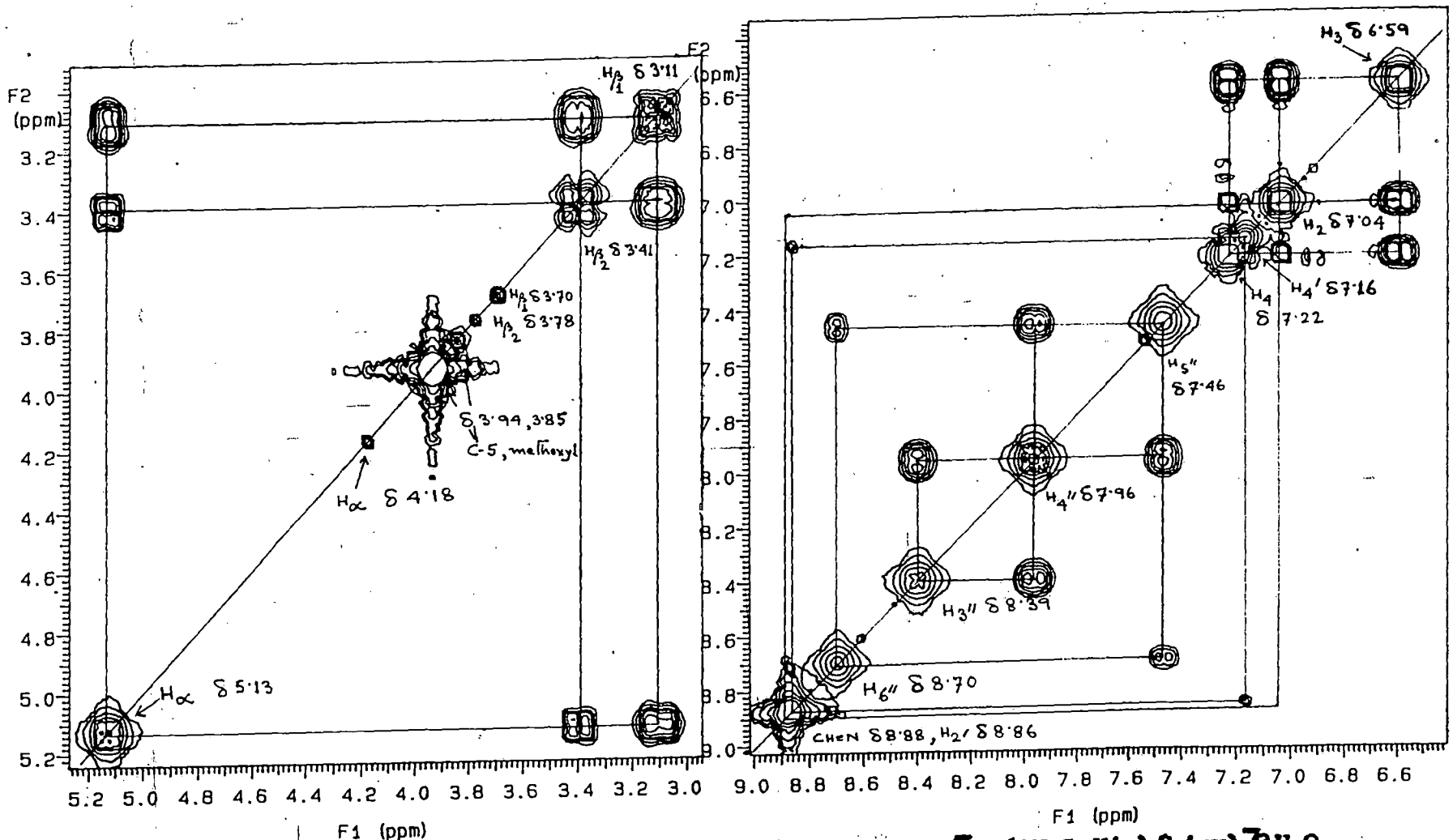

FigureII-8(d): 300 MHz H-H COSY spectrum (symmetrized) of $[VO_2(OV\text{-}L\text{-}His)(bipy)]\cdot 3H_2O$ showing the expansion of δ 9.0-6.5 ppm and δ5.2-3.0 ppm region .

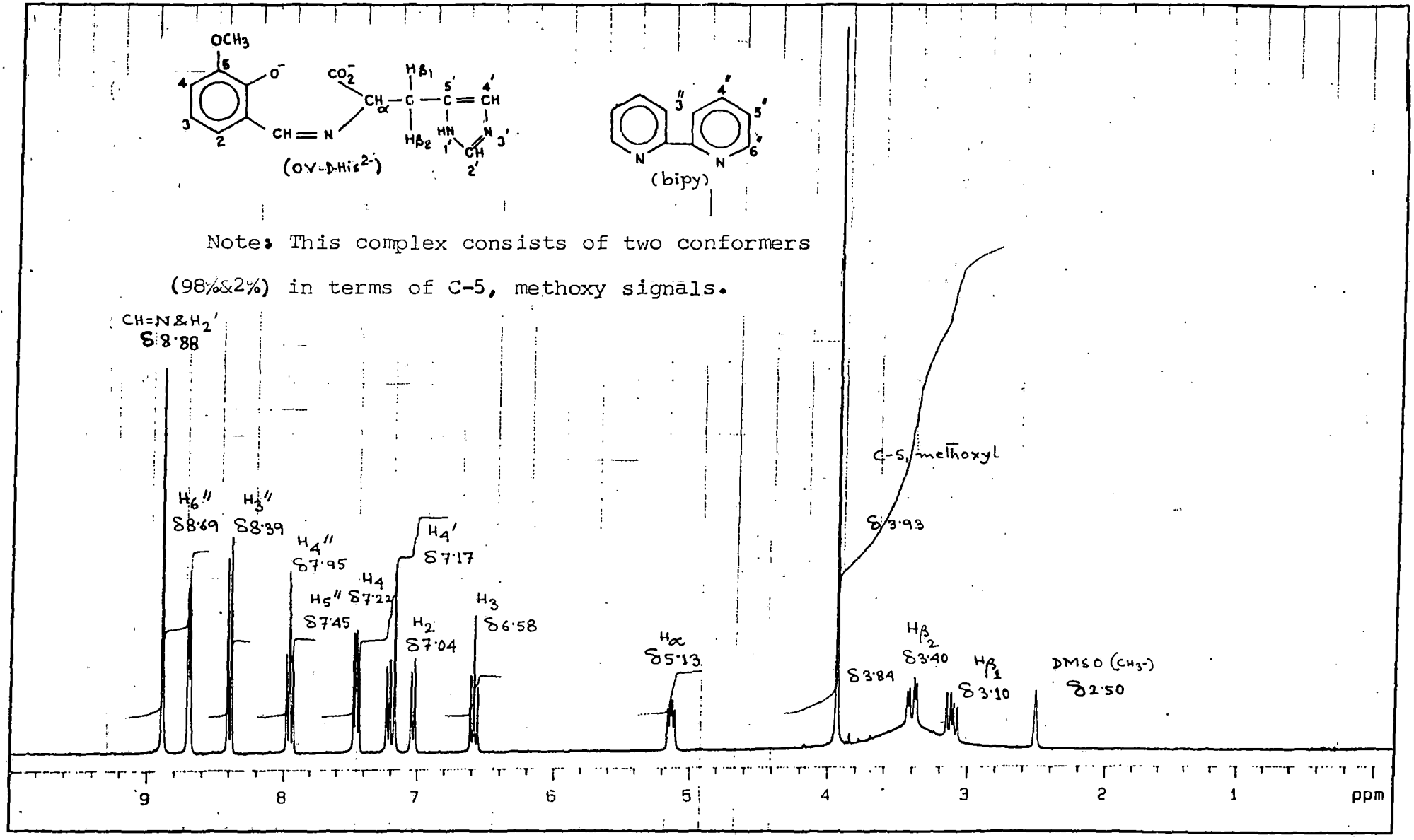

Figure II-9(a): 300 MHz ^{1}H NMR spectrum of $[UO_2(OV\text{-}D\text{-}His)(bipy)].3H_2O$ in DMSO.

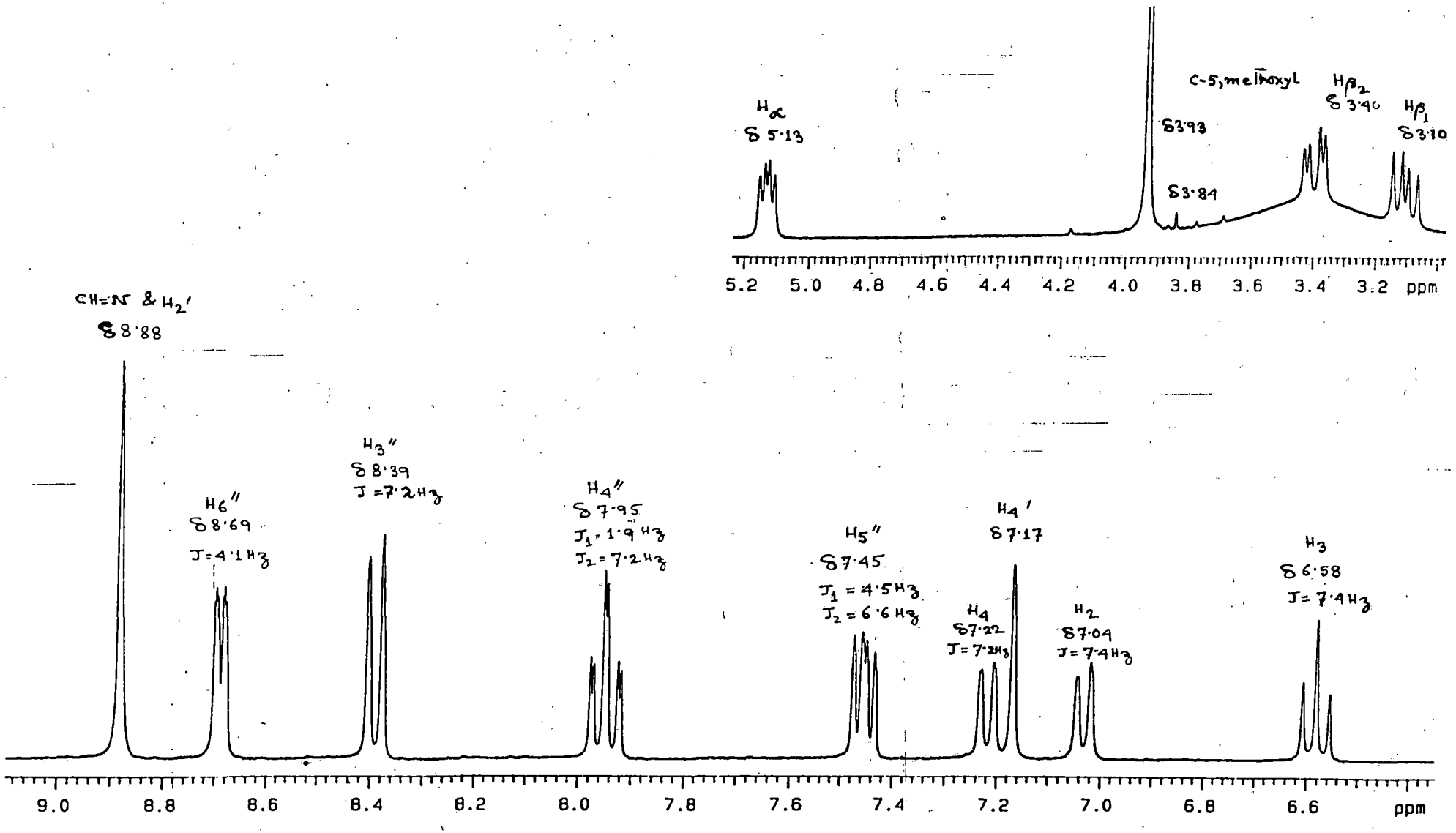

FigureII-9(b): 300 MHz ^{1}H NMR spectrum of $[UO_2(OV\text{-}D\text{-}His)(bipy)].3H_2O$ in DMSO showing the expansion of δ 9.0-6.4 ppm and δ 5.2-3.0 ppm region .

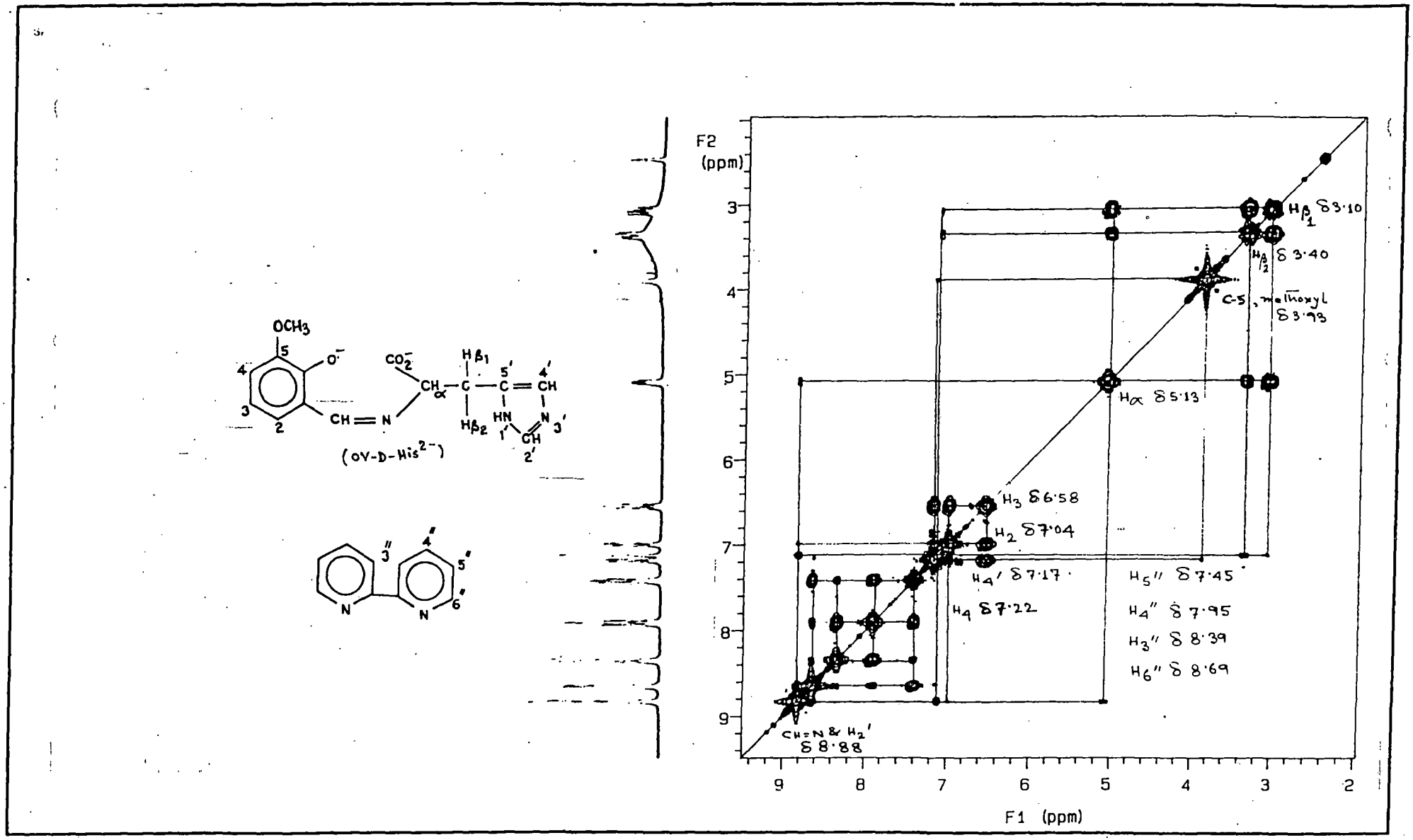

Figure II-9(c): 300 MHz H-H COSY spectrum (symmetrized) of $[UO_2(OV\text{-}D\text{-}His)(bipy)]\cdot 3H_2O$.

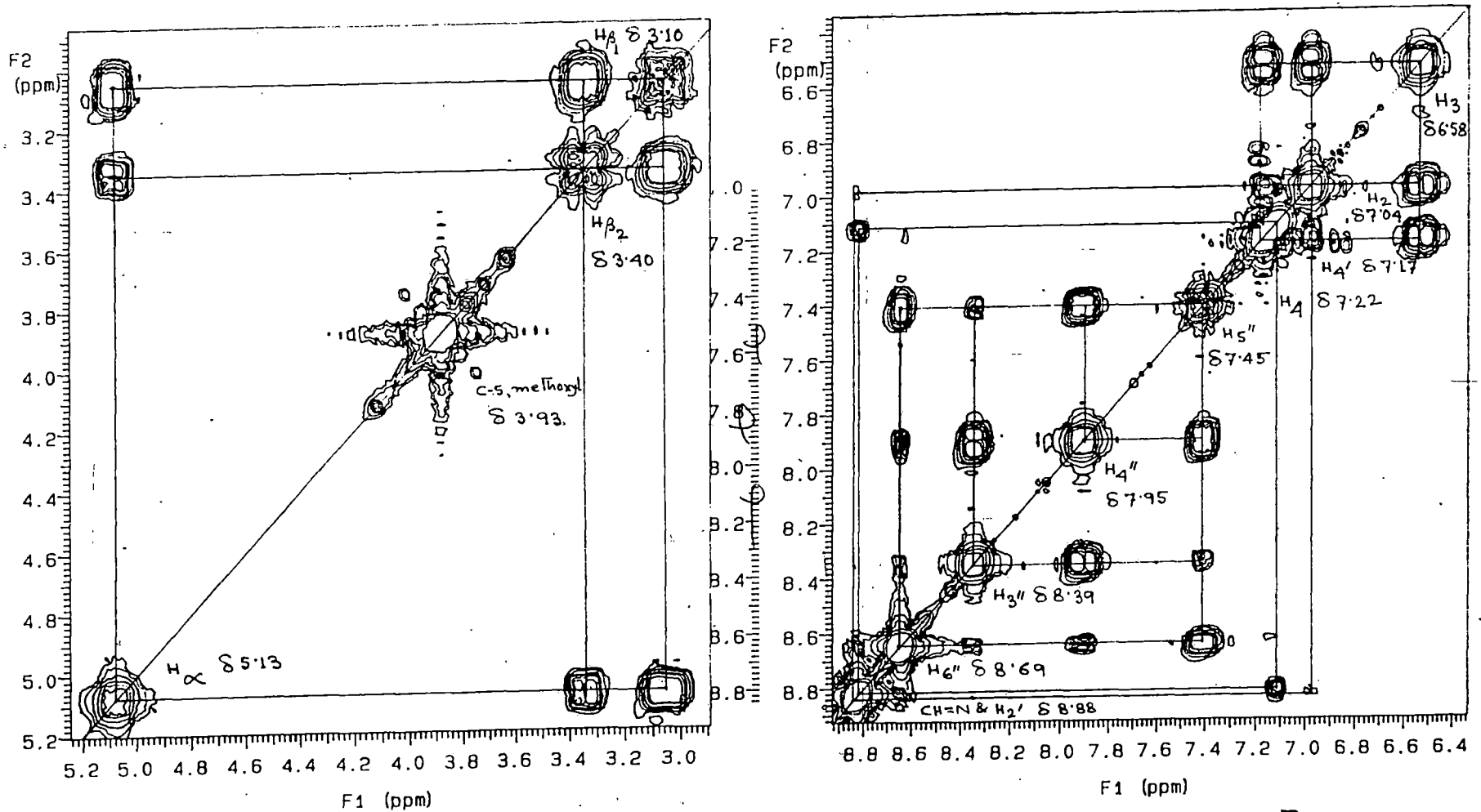

FigureII-9(d): 300 MHz H-H COSY spectrum(symmetrized) of $[UO_2$(OV-D-His)(bipy)$]3H_2O$ showing the expansion of δ 8.8-6.4 ppm and δ 5.2-3.0 ppm region .

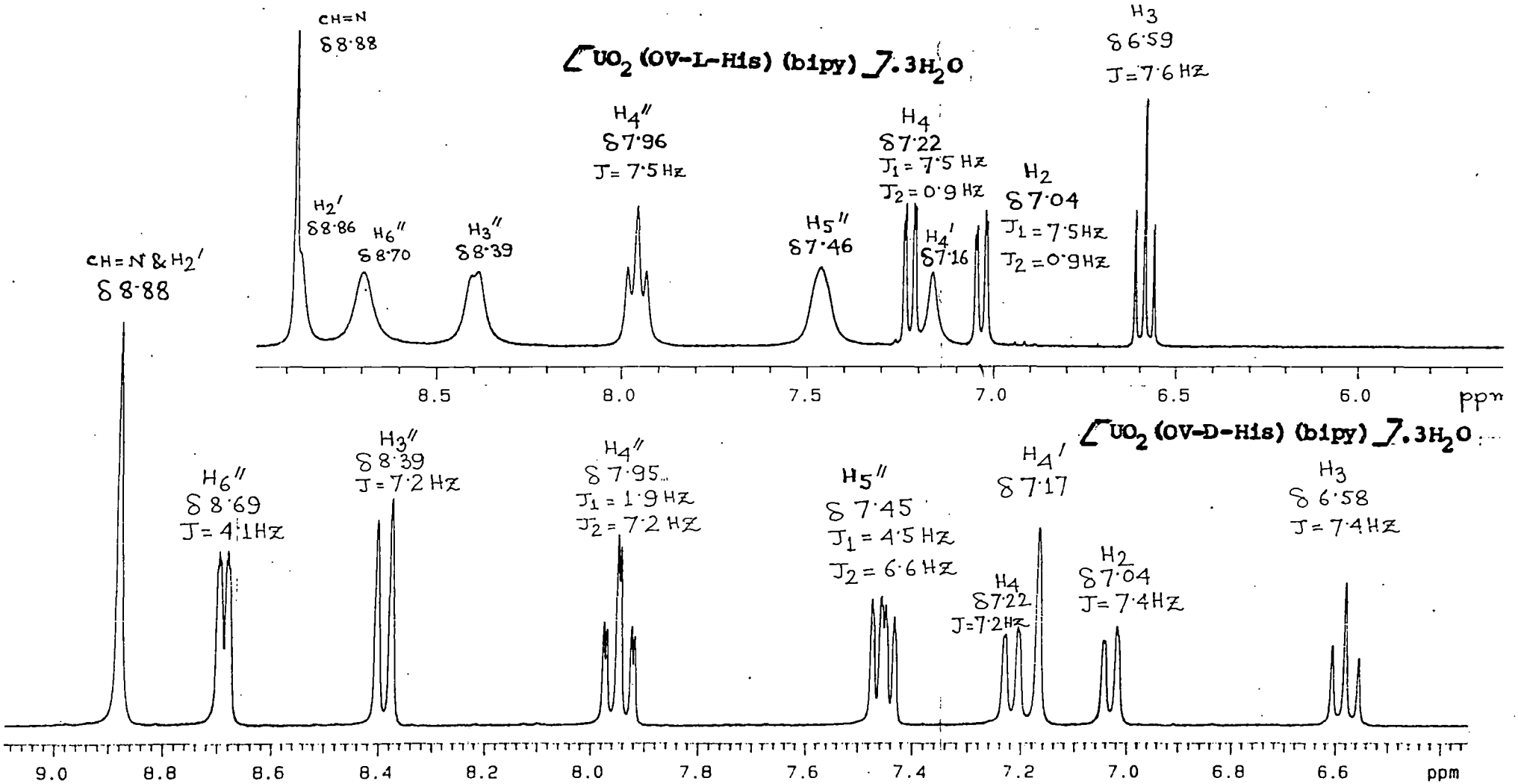

Figure II-10: Comparative ^{1}H NMR spectra of [UO_2 (OV-L-His) (bipy)].$3H_2O$ and [UO_2 (OV-D-His) (bipy)].$3H_2O$ over the region δ 6.50-9.00 ppm.

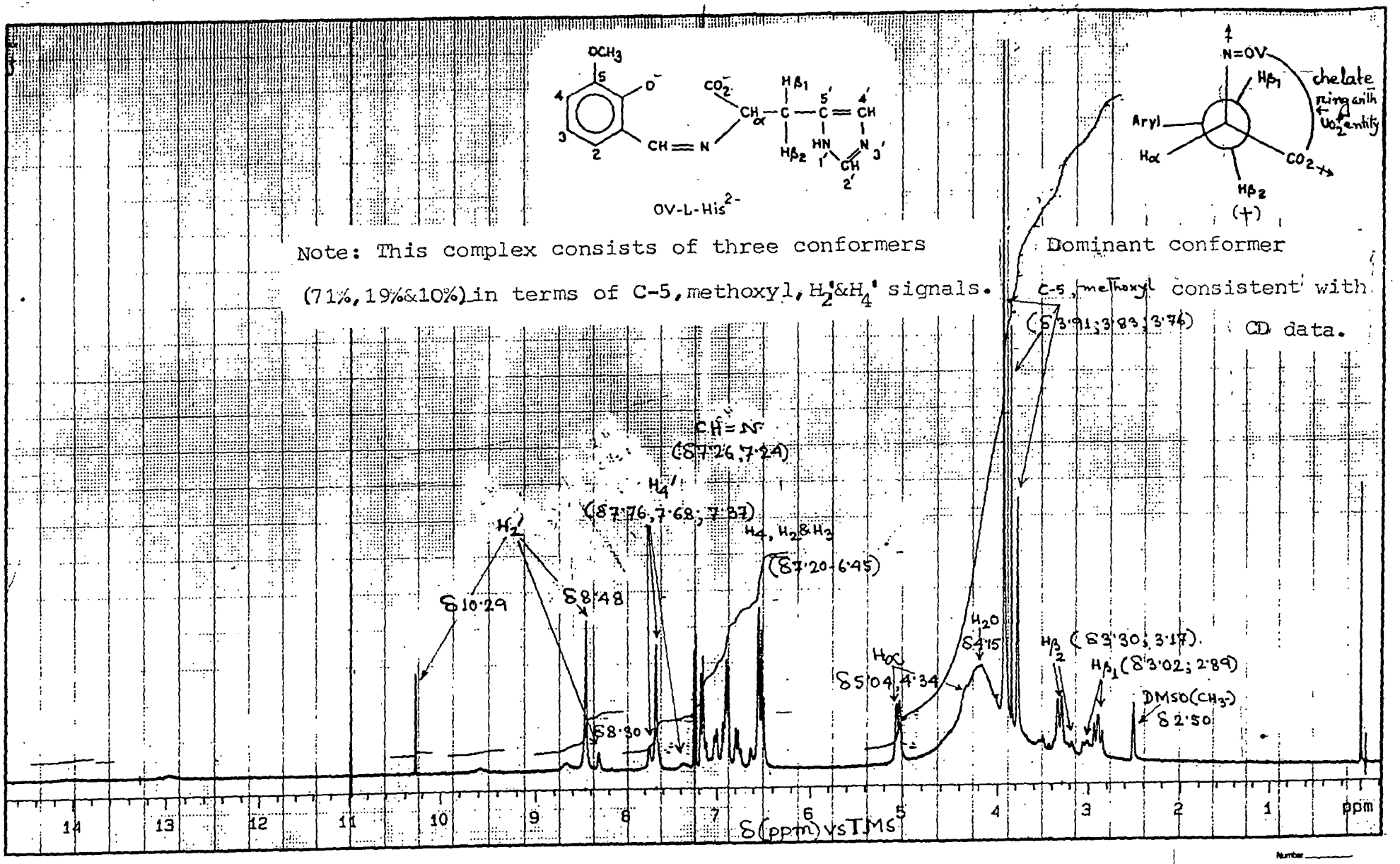

Figure II-11(a): 300 MHz ^1H NMR spectrum of $K_2[UO_2(OV\text{-}L\text{-}His)_2]\cdot 4H_2O$ in DMSO.

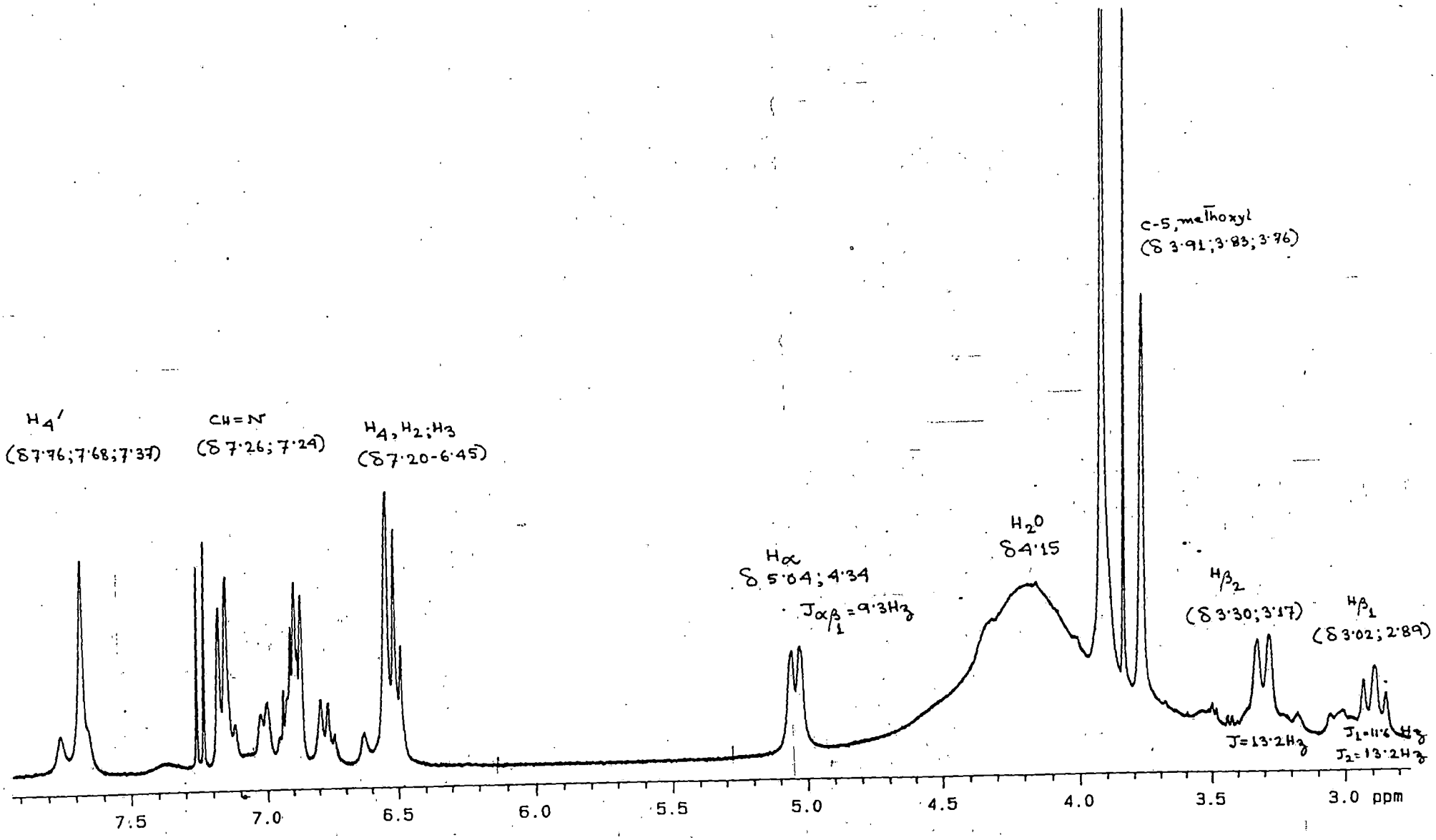

FigureII-11(b): 300 MHz ^1H NMR spectrum of $K_2[UO_2(OV\text{-}L\text{-}His)_2].4H_2O$ in DMSO showing the expansion of δ 7.8-2.8 ppm region.

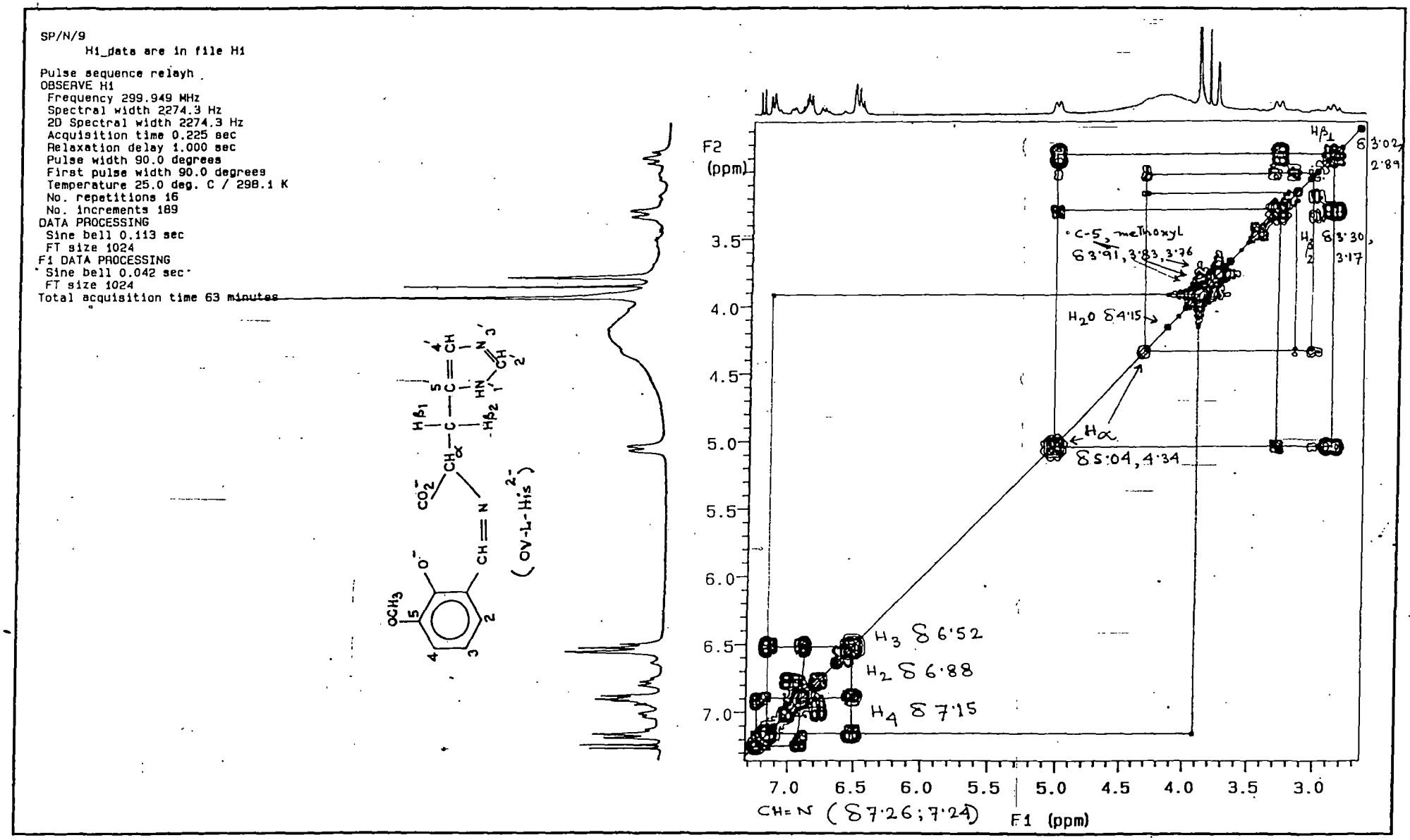

Figure II-11(c): 300 MHz H-H COSY spectrum (symmetrized) of

$K_2[UO_2(OV\text{-}L\text{-}His)_2]\cdot 4H_2O$ in the region δ 2.7-7.3 ppm.

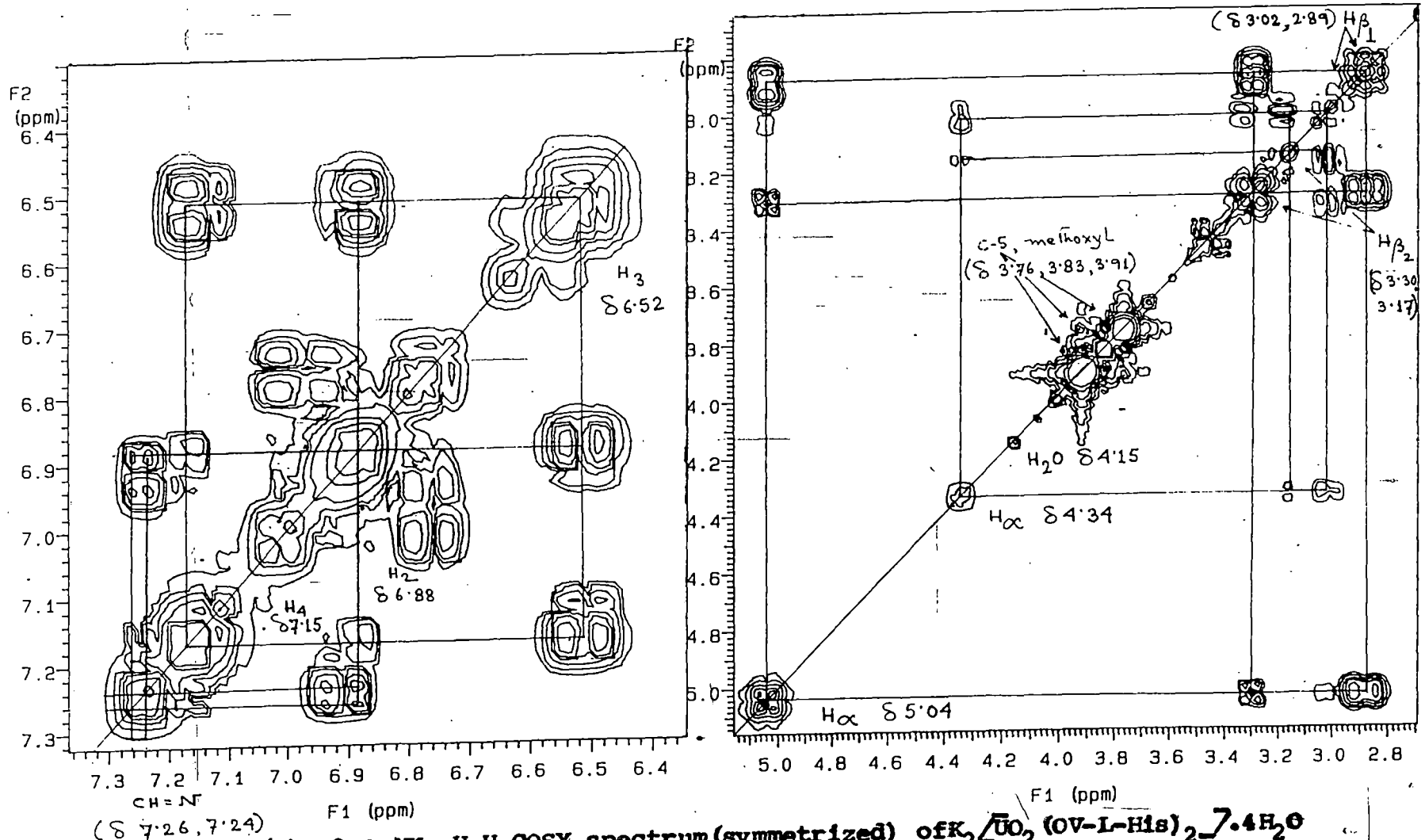

FigureII-11(d): 300 MHz H-H COSY spectrum (symmetrized) of $K_2[UO_2(OV\text{-}L\text{-}His)_2]\cdot 7.4H_2O$ showing the expansion of δ 7.34-6.36 ppm and δ 5.1-2.7 ppm region.

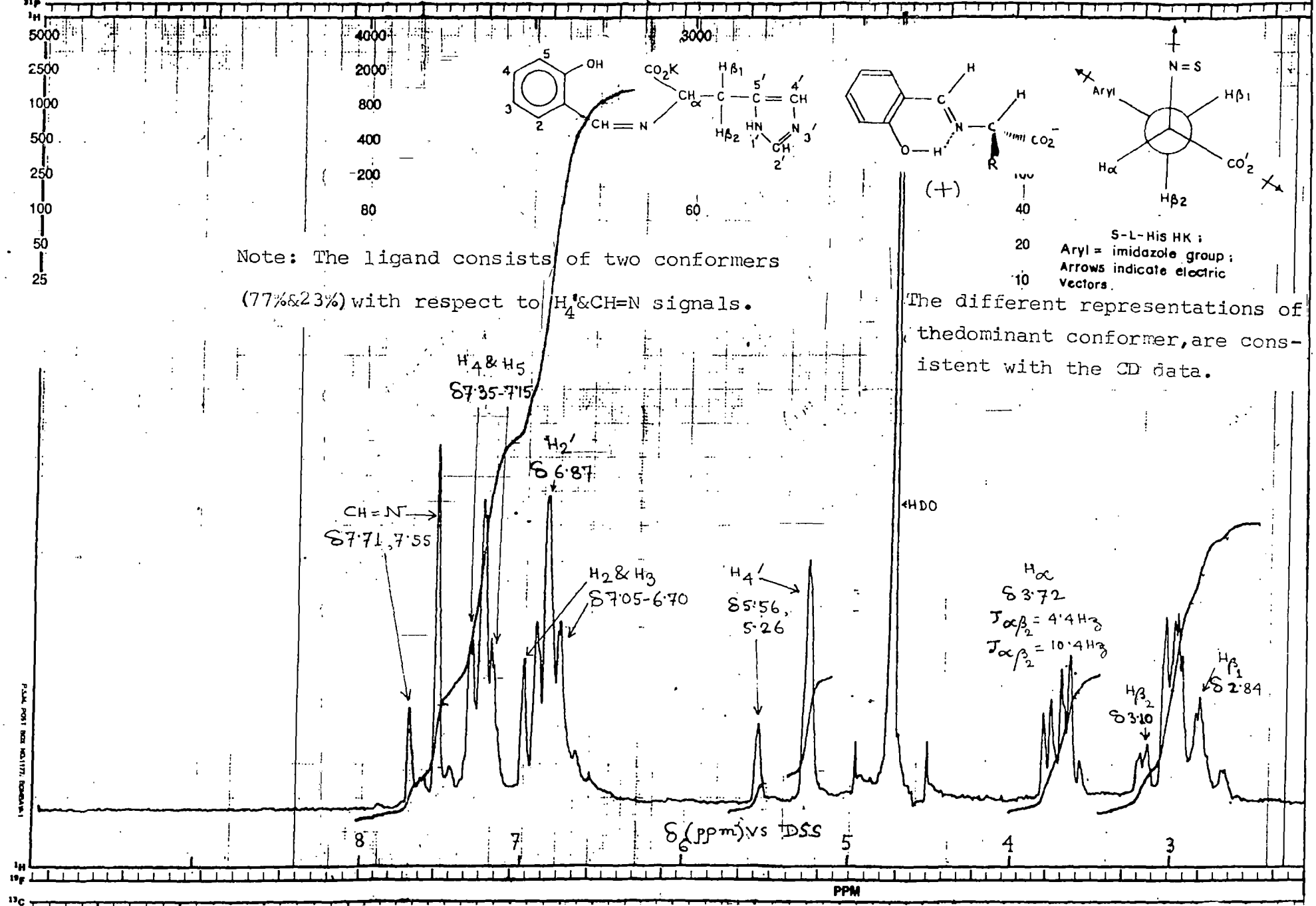

Figure II-12: 100 MHz ^{1}H NMR spectrum of S-L-HisHK in D_2O vs DSS.

$^3J_{\alpha\beta_2}$) using the Pachler method[2]. ^{1}H NMR spectrum of S-L-HisHK (Figure II-12) also indicates the presence of two conformers (77% and 23% respectively) by their two sets of signals for the CH=N (δ 7.55 and 7.71 ppm) and H_4' (δ 5.56 and 5.26 ppm) protons. CD spectral data (a negative Cotton effect at 315 nm) of S-L-HisHK (obtained in situ) is also consistent with the assignment of I (Scheme I) as the major conformer[1]. The 2D H-H correlation spectrum of OV-L-HisHK.$2H_2O$ (Figure II-7) indicates that H_{β_1}, H_{β_2} and H_α protons are mutually connected to each other by cross peaks; both H_{β_1} and H_{β_2} protons are connected by cross peaks to H_4' (δ 5.05 ppm) which in turn is connected by off diagonal peaks to H_2' (δ 6.81 ppm). The C_5-methoxyl (δ 3.68 ppm) group is connected by cross peaks to H_4 (δ 6.83 ppm) which in turn is related by off diagonal peaks to H_3 (δ 6.68 ppm). The upfield shift of H_{β_1} relative to H_{β_2} is probably due to the field shielding effect of the imino and the carbonyl groups[2].

These ligands possess three different spin systems :-

(a) ABX pattern of the H_{β_1}, H_{β_2} and H_α protons;
(b) AA'BB' (S-L-HisHK) or ABC (OV-L-HisHK.$2H_2O$) pattern of the substituted benzene ring of the aldehyde part; (c) the imidazole ring CH protons (H_2' and H_4') are separated by nitrogen atoms with no apparent spin-spin coupling and appear as singlets in most cases.

Further complications to these spectra are added by the presence of more than one conformer; this is true for some of these pertinent complexes as well.

The differences in positions of these spin systems, are enhanced to a considerable extent by complexation, to the UO_2^{2+} entity; this is evident from figures II-7 & II-8, which show that the H_α proton of the free ligand OV-L-HisHK.$2H_2O$ is deshielded by δ 1.96 ppm, crossing over the C_5, methoxyl proton signal; the H_α, H_{β_1}, H_{β_2} proton signals get spread over a larger ppm range (from δ 2.52-3.15 ppm to δ 2.89-5.04 ppm). This makes proton identification easier in spite of the inherent complexity, induced by the presence of the chiral centre[13].

$[UO_2$(OV-L-His)(bipy)$].3H_2O$ consists of two conformers (Scheme I, type II and the other one obtained by rotation about the C_α- C_β bond; 95% and 5% respectively) as indicated by two sets of signals for the C_5, methoxyl, H_α, H_{β_1} and H_{β_2} protons; H_2O proton signal overlaps with that of the H_{β_2} proton of the major conformer. The symmetrized 2D H-H COSY of $[UO_2$(OV-L-His)(bipy)$].3H_2O$ [Figure II-8 (c) &(d)] shows interactions among not only the different types of aromatic protons of the 2,2'-bipyridyl, imidazole, benzene rings but also that between H_2 and -CH=N- protons; the main H-H COSY (δ 2.20 to 9.60 ppm) shows that the -CH=N- proton is connected by cross peaks to the H_α proton as well. On comparing the

positions of the different proton signals of the major conformers in the ligands and the corresponding complexes (Table II-7), some interesting points are observed. Although the protons situated around the immediate coordination zone (e.g., H_α and -CH=N-) are deshielded in most cases by δ 1.20-1.90 ppm, other protons undergo smaller deshielding (up to δ 0.58 ppm for $^{H}\beta_1$, $^{H}\beta_2$ and H_4 protons). Small shielding of the H_3 proton is caused by the delocalisation of part of the electron density into the benzene ring, released as a result of deprotonation of the phenolic -OH group during coordination. The most noteble feature is exhibited by the 2,2'-bipyridyl ring protons which are deshielded by only δ 0.06-0.11 ppm[26,27]. The X-ray crystal structure data of $[UO_2(OV\text{-}L\text{-}His)(bipy)].CH_3OH.H_2O$ indicate that the heterocyclic nitrogen atoms are almost as equally strongly coordinated (σ-bonding) as the azomethine (-CH=N-) nitrogen atom (with $\Delta = \delta$ 1.58 ppm). In the typical dioxouranium(VI) complexes of 8-quinolinol, the H_2 proton undergoes a deshielding of ca. δ 1.40 ppm from the corresponding free ligand value[53]. Evidently electron density has drifted into the 2,2'-bipyridyl ring to cause this upfield shift by ca. δ 1.50 ppm (δ 1.58-0.06/0.11 = δ 1.52/1.47 ppm), of its ring protons.

A logical explanation for this unusual behaviour of the 2,2'-bipyridyl ring protons, is possible involving π -bonding

among the 2,2'-bipyridyl π^* orbitals and the suitable uranium orbitals (e.g., those with their lobes directed in between the Z-axis and the xy plane, assuming the latter as the equatorial one)[9,41,44]; this process leads to extensive occupation of the former type of orbitals (π^*) by the electron density accumulated on the uranium atom through coordination (involving $L \rightarrow M$ σ bonding with the imine acid residue and the 2,2'-bipyridyl moiety). This is a specific instance where a typical hard acid like the UO_2^{2+} entity is transmitting electron density into a π-acid type ligand through $M \rightarrow L$ π bonding[44]. Similar type of shielding is observed for the other 2,2'-bipyridyl and 1,10-phenanthroline complexes of this series (Table II-7).

The one dimentional ^1H NMR spectrum and the corresponding 2D H-H COSY together with the associated expanded spectra of $[UO_2(OV\text{-}D\text{-}His)(bipy)].3H_2O$ (Figure II-9) indicate the presence of two conformers (98% and 2% respectively, by the appearance of two C_5, methoxyl signals). Most of the proton signals exhibit much well-resolved splittings, along with the -CH=N- and H_2' signals overlapping together of the three contributing factors (configurational/conformational/vicinal) to the observed optical activity of these systems, the effect of conformation is evident from the comparative ^1H NMR spectra (Figure II-10) of the two quasi-enantiomorphous complexes (serial no.2, Table II-5 and the corresponding D-histidine

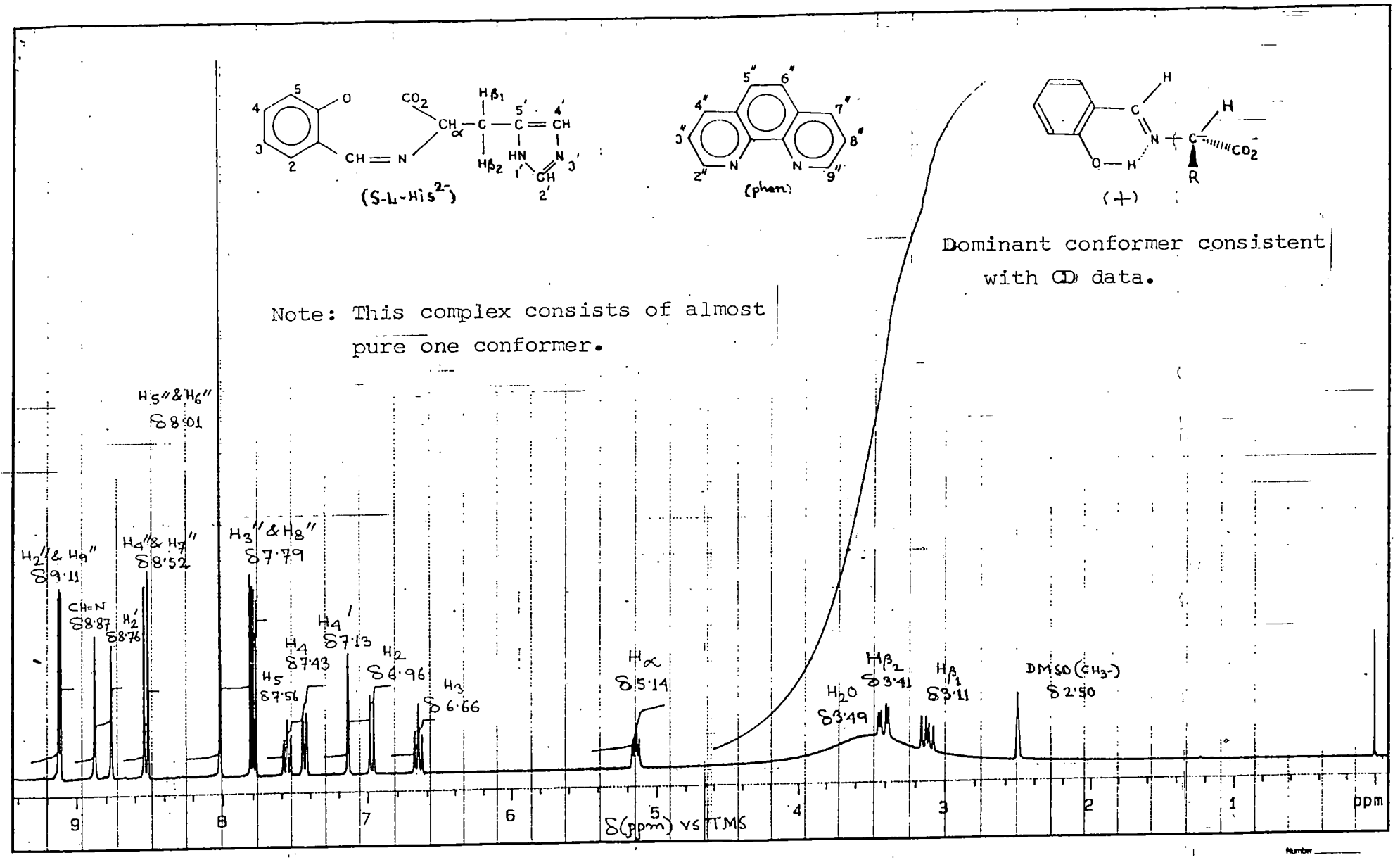

Figure II-13(a): 300 MHz ^{1}H NMR spectrum of $[UO_2(S\text{-}L\text{-}His)(phen)]\cdot 4H_2O$ in DMSO.

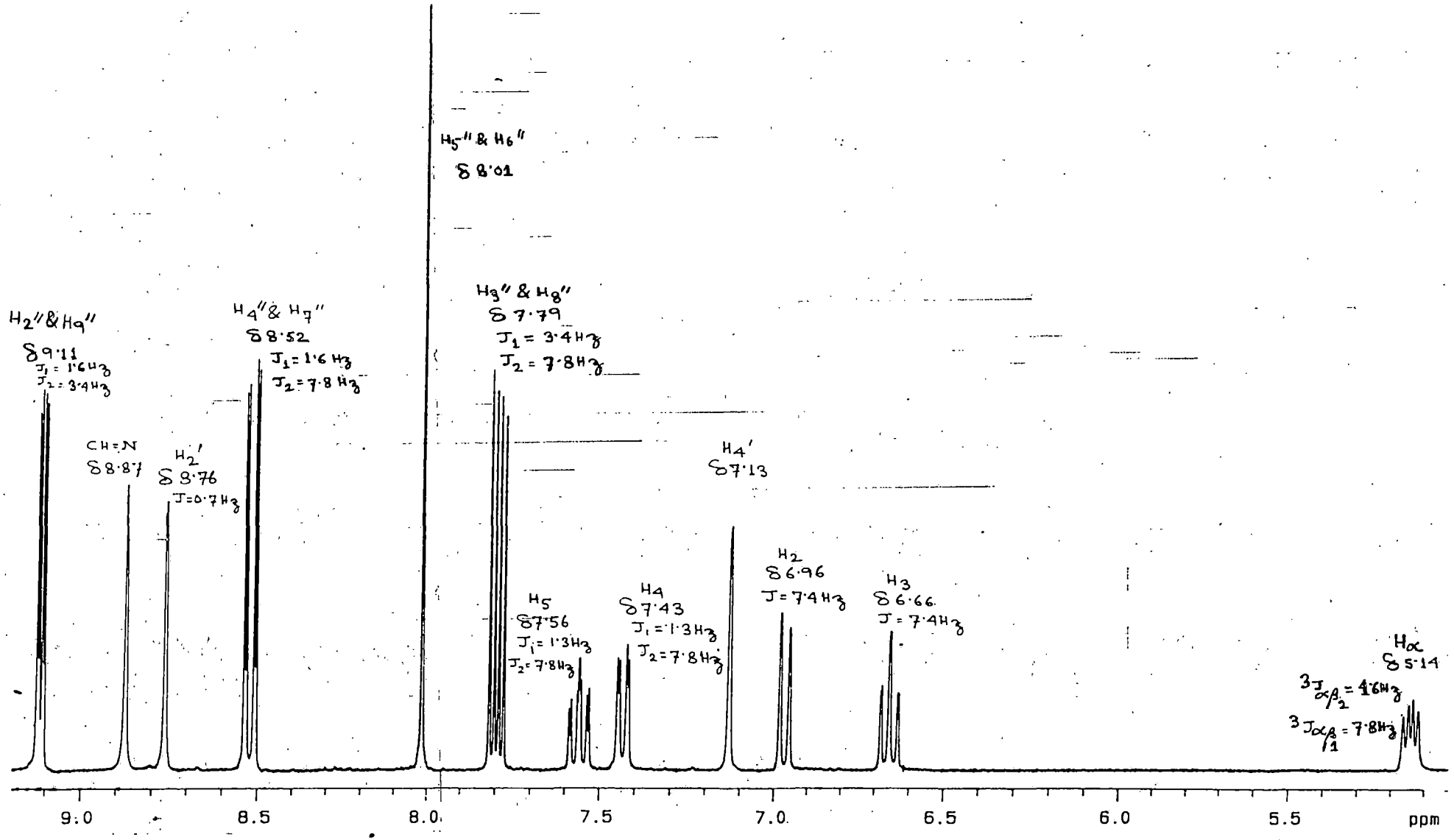

FigureII-13(b): 300 MHz ^{1}H NMR spectrum of $[UO_2(S\text{-}L\text{-}His)(phen)]\cdot 4H_2O$ in DMSO showing the expansion of δ 9.2-5.1 ppm .

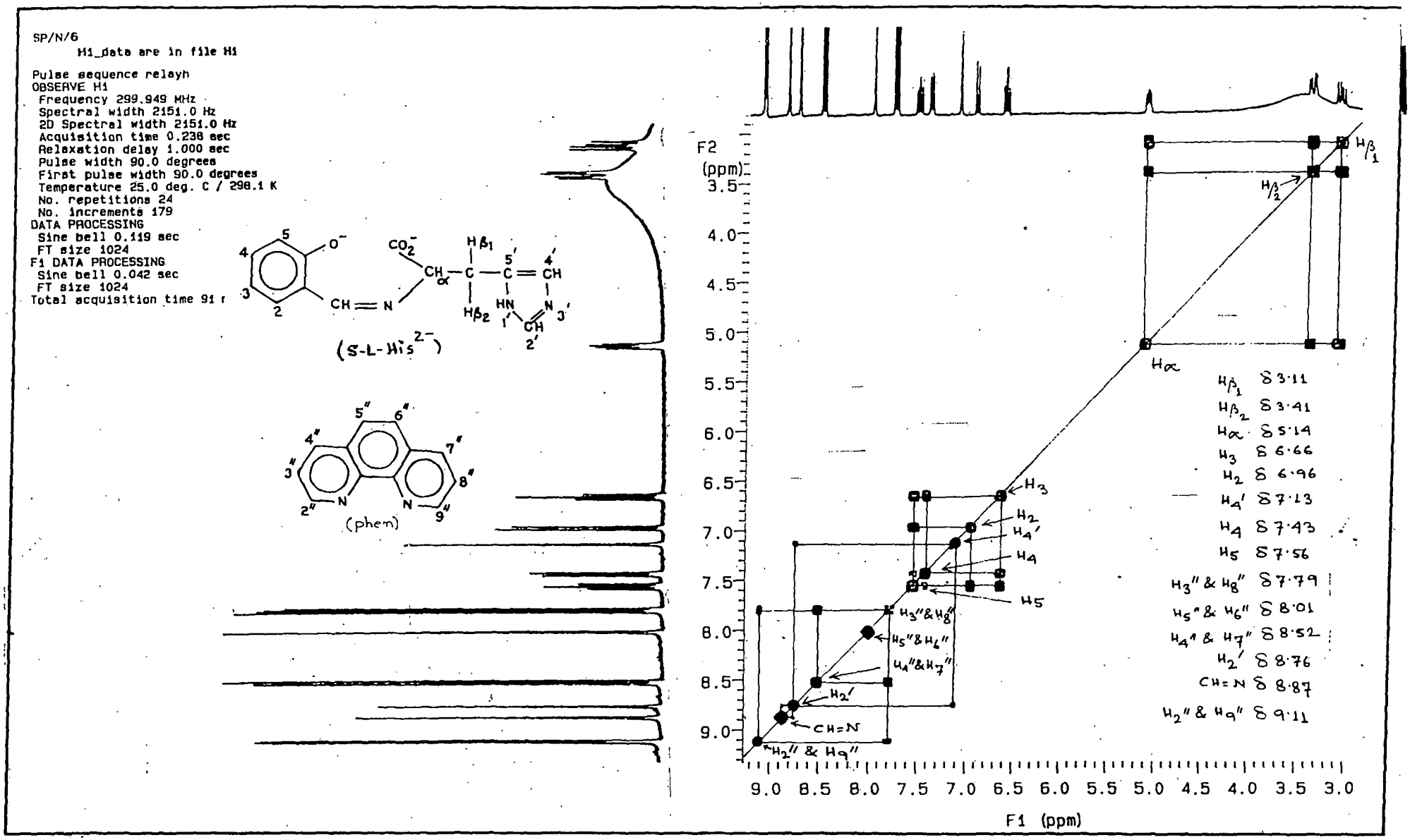

Figure II-13(c): 300 MHz H-H COSY spectrum of $[UO_2(S\text{-}L\text{-}His)(phen)].4H_2O$ in DMSO (symmtrized).

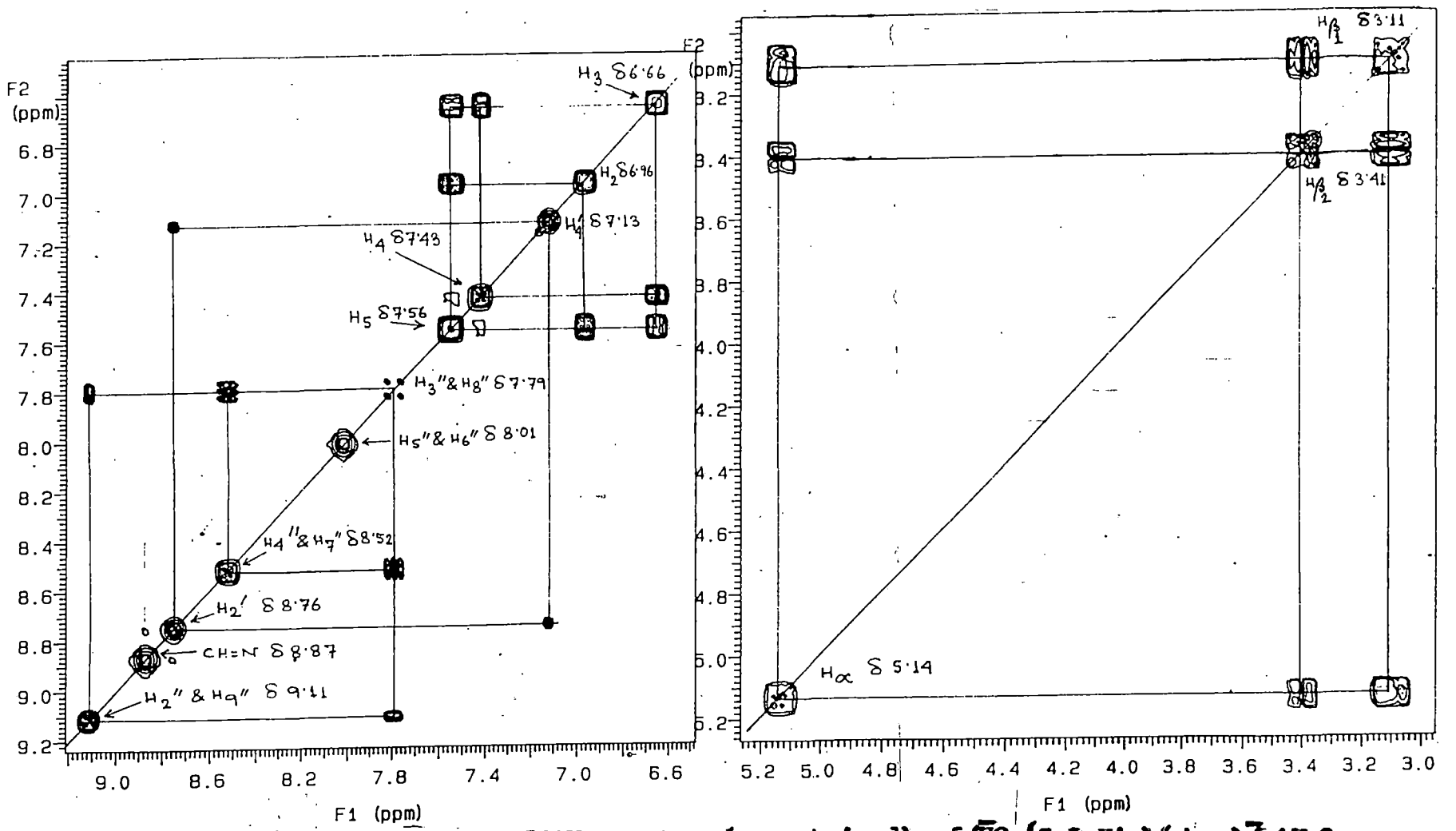

Figure II-13 (d): 300 MHz H-H COSY spectrum (symmetrized) of $[UO_2$ (S-L-His) (phen)$]_2 \cdot 4H_2O$ showing the expansion of δ 9.2-6.5 ppm and δ 5.2-3.0 ppm region.

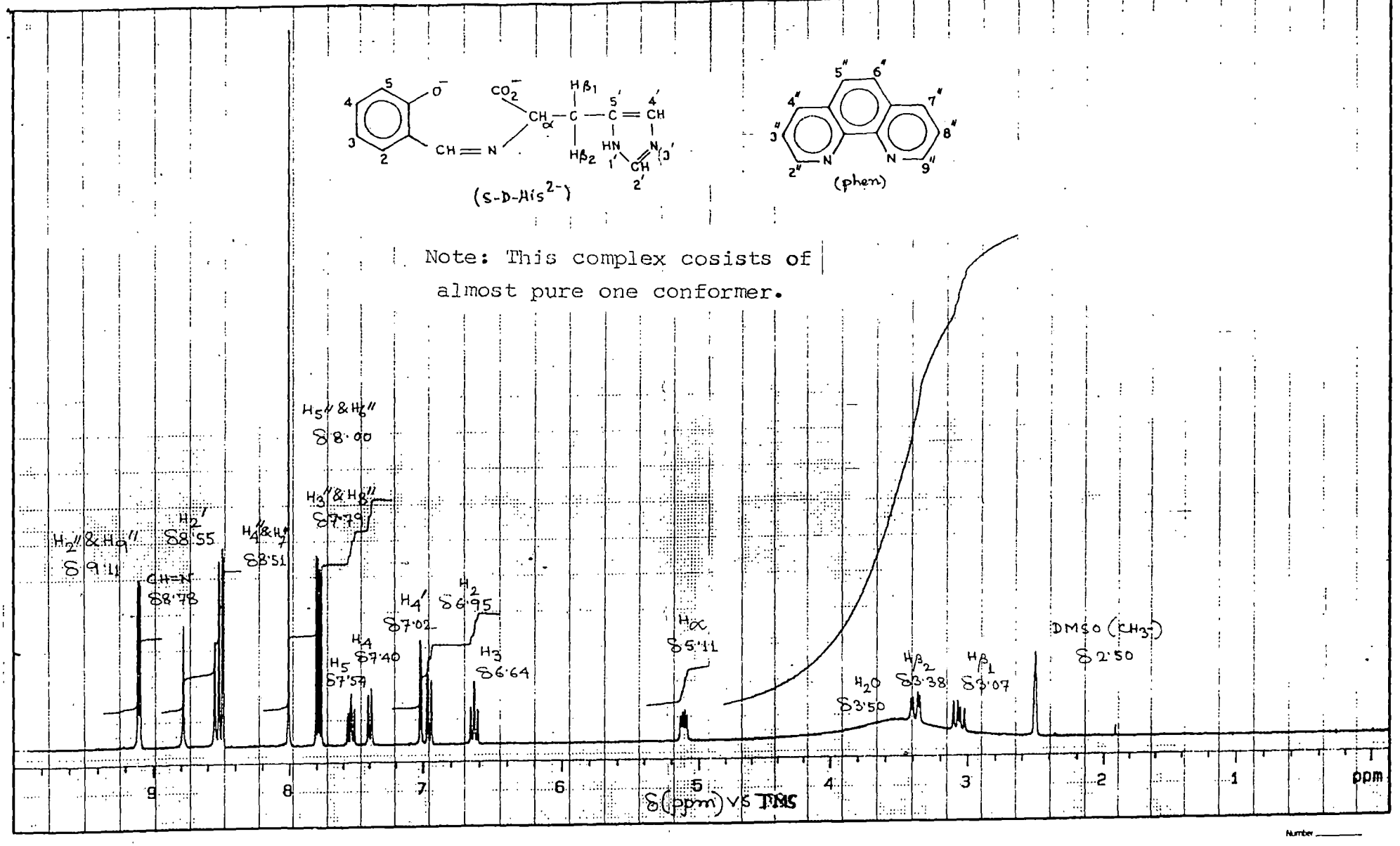

Figure II-14 (a): 300 MHz ^{1}H NMR spectrum of $[UO_2(S\text{-}D\text{-}His)(phen)]\cdot 2H_2O$ in DMSO.

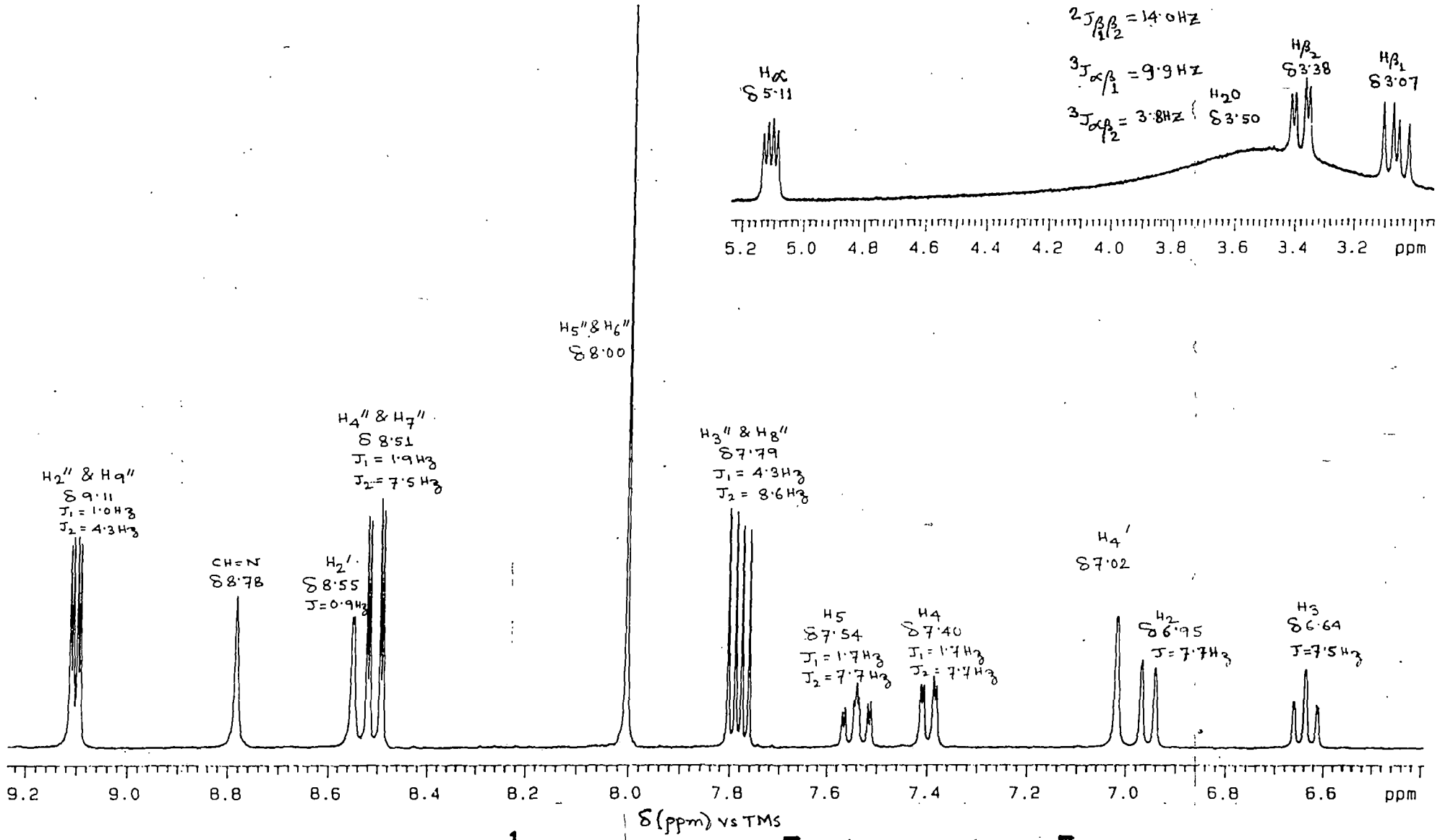

FigureII-14 (b): 300 MHz ^{1}H NMR spectrum of $[UO_2(S\text{-}D\text{-}His)(phen)].2H_2O$ in DMSO showing the expansion of δ 9.2-6.4 ppm and δ 5.2-3.0 ppm region .

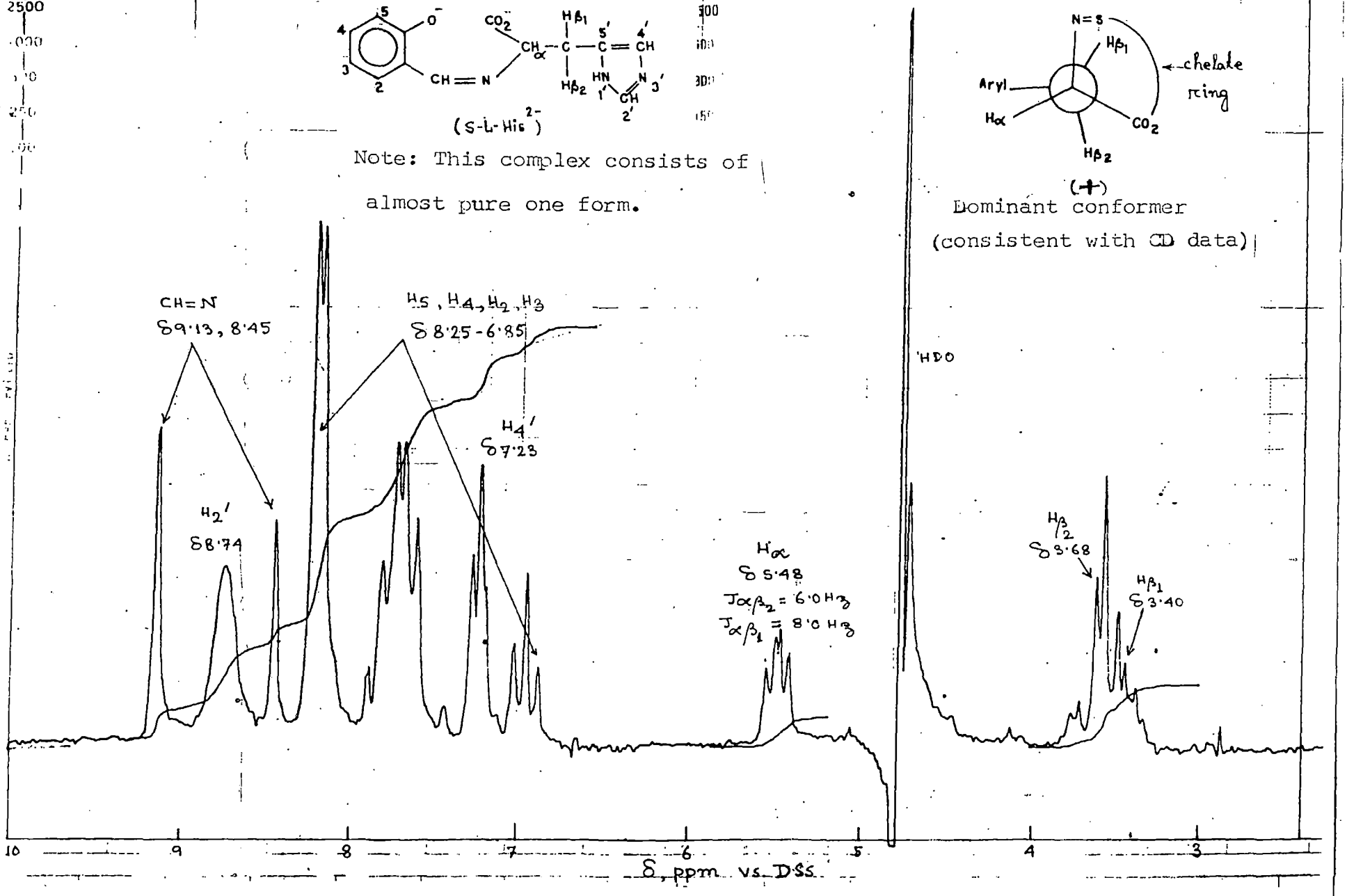

Figure II-15: 100 MHz ^{1}H NMR spectrum of $[(UO_2)_2(S\text{-}L\text{-}His)(S\text{-}L\text{-}HisH)_2(H_2O)_2].4H_2O$ in D_2O vs DSS.

derived complex); the differences in splitting patterns of the proton signals as well as small changes in chemical shift values result from conformational differences (about the N-C_α and C_α-C_β bonds), leading to the different $[\theta]$ values in their CD curves (Figure II-17), whereas the positive and negative signs of these CD curves are determined by configurational factors (discussed later).

Differences in the ^{1}H NMR and CD spectra (Figure II-19) are also observed for the two quasi-enantiomorphous complexes of the N-(salicylidene) series (serial number 7 and its quasi-enantiomer, Table II-5; Figures II-13 and II-14).

For $[(UO_2)_2(S\text{-}L\text{-}His)(S\text{-}L\text{-}HisH)_2(H_2O)_2]\cdot 4H_2O$ (Figure II-15) two signals (2:1 intensity ratio) appear at δ 9.13 ppm (2H, singlet) and δ 8.45 ppm (1H, singlet) due to the presence of coordinated and uncoordinated azomethine groups respectively (Table II-7); most likely two of the ligand residues are acting as tridentate ones as in case of $[UO_2(OV\text{-}L\text{-}His)(bipy)]\cdot CH_3OH\cdot H_2O$, along with the third one using its phenoxide and $-CO_2^-$ groups for bridging purpose, leaving the -CH=N- group free (vide the IR spectral data in Table II-6 and Figure II-12).

For $K_2[UO_2(OV\text{-}L\text{-}His)_2]\cdot 4H_2O$ (Figure II-11) the two ligand residues consist of all the three classical staggered rotamers (obtained by rotation about the C_α-C_β bond) as

indicated by three different signals for each of the H_2', H_4' and C_5- methoxyl protons (71%, 19% and 10% respectively). The two CH=N proton signals differ slightly in chemical shift values. The identifications of different proton signals (Table II-7) are based on the usual molecular connectivity relations, as revealed by the 2D H-H COSY data. This is the only case where the -CH=N- proton signal is shielded from its free ligand position on coordination, although its IR spectral data [of ν (CH=N) mode, Table II-6] is consistent with the presence of coordinated azomethine group; the H_α proton is strongly deshielded ($\Delta = \delta 1.86$ ppm) as usual.

The observed changes in chemical shift values of ligand protons upon chelation depend on several factors, mainly on the nature of the metal-ligand bonds (σ and π types as mentioned earlier), magnetic anisotropy of the UO_2^{2+} entity and intramolecular ring current effects determined by the geometry of the chelate in question[13,26,27,41,53-56].

The changes in chemical shift values ($\Delta\sigma_m$, ppm) for protons in the neighbourhood of the anisotropic field of the UO_2^{2+} entity, is given by $\Delta\sigma_m = \Delta\chi$ atomic $(1-3\cos^2\gamma/3R^3)$, where $\Delta\chi = -2.74 \times 10^{-29}$, R is the distance (cm) of the proton from the anisotropic group and γ is the angle between a line joining the proton to the centre of the anisotropic group and the axis of symmetry of the latter[54-56].

From the Darling model of the complex 3 (Table II-5), R values for H_α and H_{β_1}/H_{β_2} protons are taken as 4.7Å and 6.5Å, along with γ values of 80° and 70°, respectively; $\Delta\sigma_m$ values are calculated to be δ 0.80 ppm and δ 0.21 ppm, respectively. So other factors, especially the deshielding due to the drainage of electron density from the ligand to the metal, make definite contributions to the observed Δ values (e.g., of CH=N and H_α protons) in Table II-7.

For $[(UO_2)_2(S\text{-}L\text{-}His)(S\text{-}L\text{-}HisH)_2(H_2O)_2]\cdot 4H_2O$ the deshielding (Δ = 0.90 ppm) of the -CH=N- proton of the third ligand molecule, may be regarded as due mainly to the $\Delta\sigma_m$ factor, which gives a contribution of δ 0.45 ppm per UO_2^{2+} entity. This data indicate that the bridging unit (or at least its ONO donor part) resides at an angle of 16° from the equatorial plane (R and γ values are being taken from the Darling model to be 5.4Å and 74° respectively)[157-159,162].

The most important factor influencing the vicinal HH couplings ($^3J_{\alpha\beta_1}$, $^3J_{\alpha\beta_2}$) is the dihedral angle between the C-H bonds (e.g., $J = 4.2 - 0.5 \cos\phi + 4.5 \cos 2\phi$ when ϕ is a dihedral angle)[13,15,30,35]. In terms of this equation the dihedral angles (ϕ) $H_\alpha C_\alpha C_\beta H_{\beta_1}$ and $H_\alpha C_\alpha C_\beta H_{\beta_2}$ are taken to be 180° and 60°, respectively, for the free ligands; for the pertinent complexes the corresponding average ϕ values are taken to be 170° and 70°, respectively (i.e., a maximum deviation of 10° is assumed, as evident from Darling model

studies in the light of X-ray and CD data, Scheme I). J_{av} is the average of $^3J_{\alpha\beta_1}$ and $^3J_{\alpha\beta_2}$ values and is helpful for comparison with the theoretical J_{av} value calculated using the equation.

$J_{av} = 17.97-0.8 \sum_{1}^{6} E$, where $\sum_{1}^{6} E$ is the sum of electronegativities (Pauling) of the six groups attached to the $C_\alpha-C_\beta$ bond. Observed data show that most of the complexes have J_{av} values in the range ca.6.1 Hz, although calculated J_{av} values on related ligand systems, show a variation around 7.0 Hz[2]. This lowering of J_{av} values on complexation can be attributed to the increase in electronegativities of some of the relevent atoms in the chelated ligands as a result of $L \rightarrow M$ σ bonding as well as restriction to rotation in these complexes.

Electronic and CD spectra : Figures II-16 to II-19 show some of the representative electronic absorption (EA) and circular dichroism (CD) spectra of the pertinent complexes; quasi-enantiomorphous CD curves have been obtained (Figure II-17 and II-19) using L- and D- histidine derived ligands, stressing the importance of absolute configuration of the amino acid in determining the overall chirality of these complexes.

The characteristic EA bands around 330 nm, 265 nm and 230 nm are assigned to $\pi \rightarrow \pi^*$ transitions of the intramolecularly hydrogen-bonded N-orthovanillidenamino (OVA) chromophore

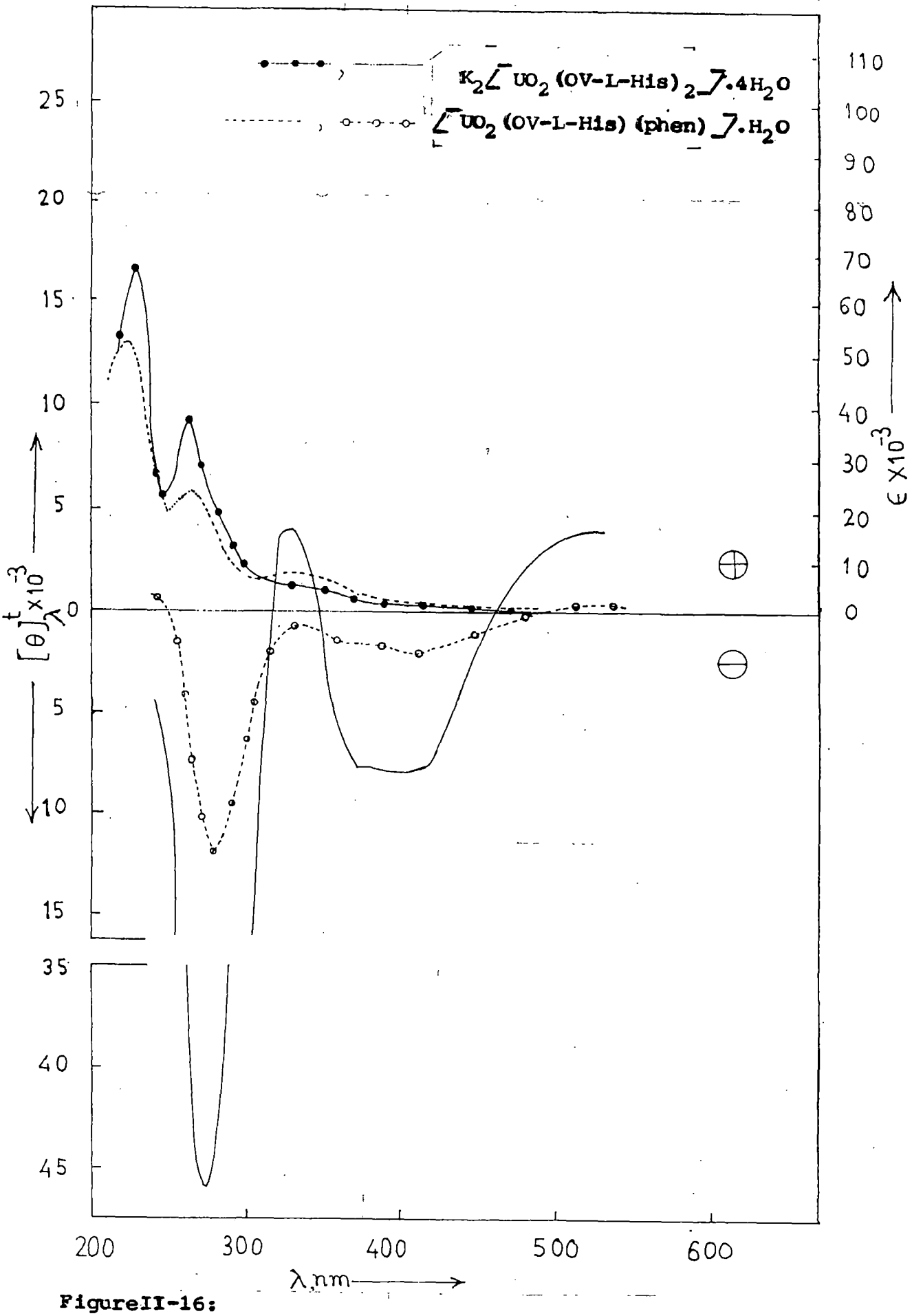

FigureII-16:

Uv-visible and CD spectra of $K_2[UO_2(OV\text{-}L\text{-}His)_2].4H_2O$ and $[UO_2(OV\text{-}L\text{-}His)(phen)].H_2O$ in methanol.

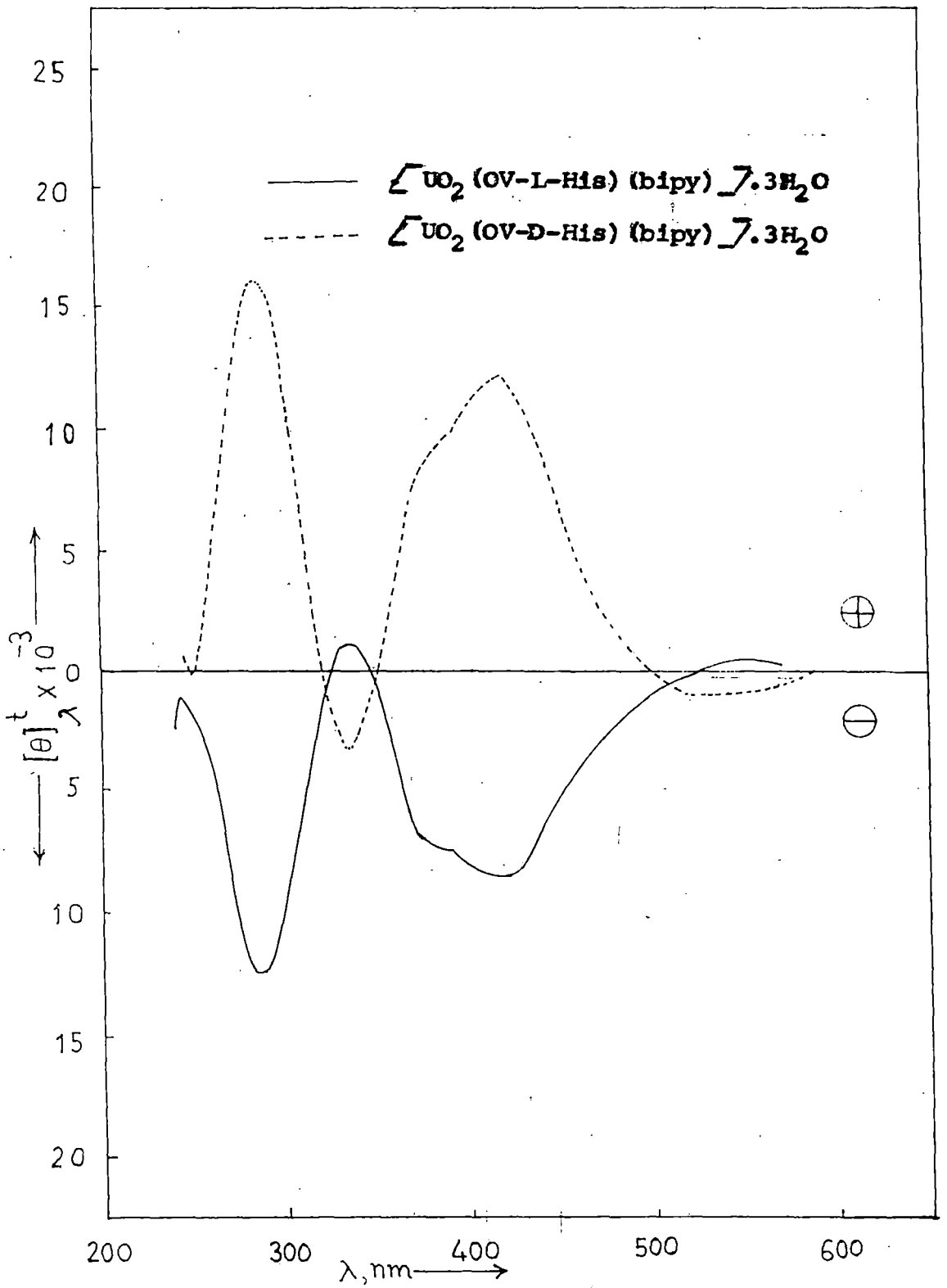

FigureII-17:

CD spectra of $[UO_2(OV\text{-}L\text{-}His)(bipy)].3H_2O$ & $[UO_2 OV\text{-}D\text{-}His)(bipy)].3H_2O$ in methanol .

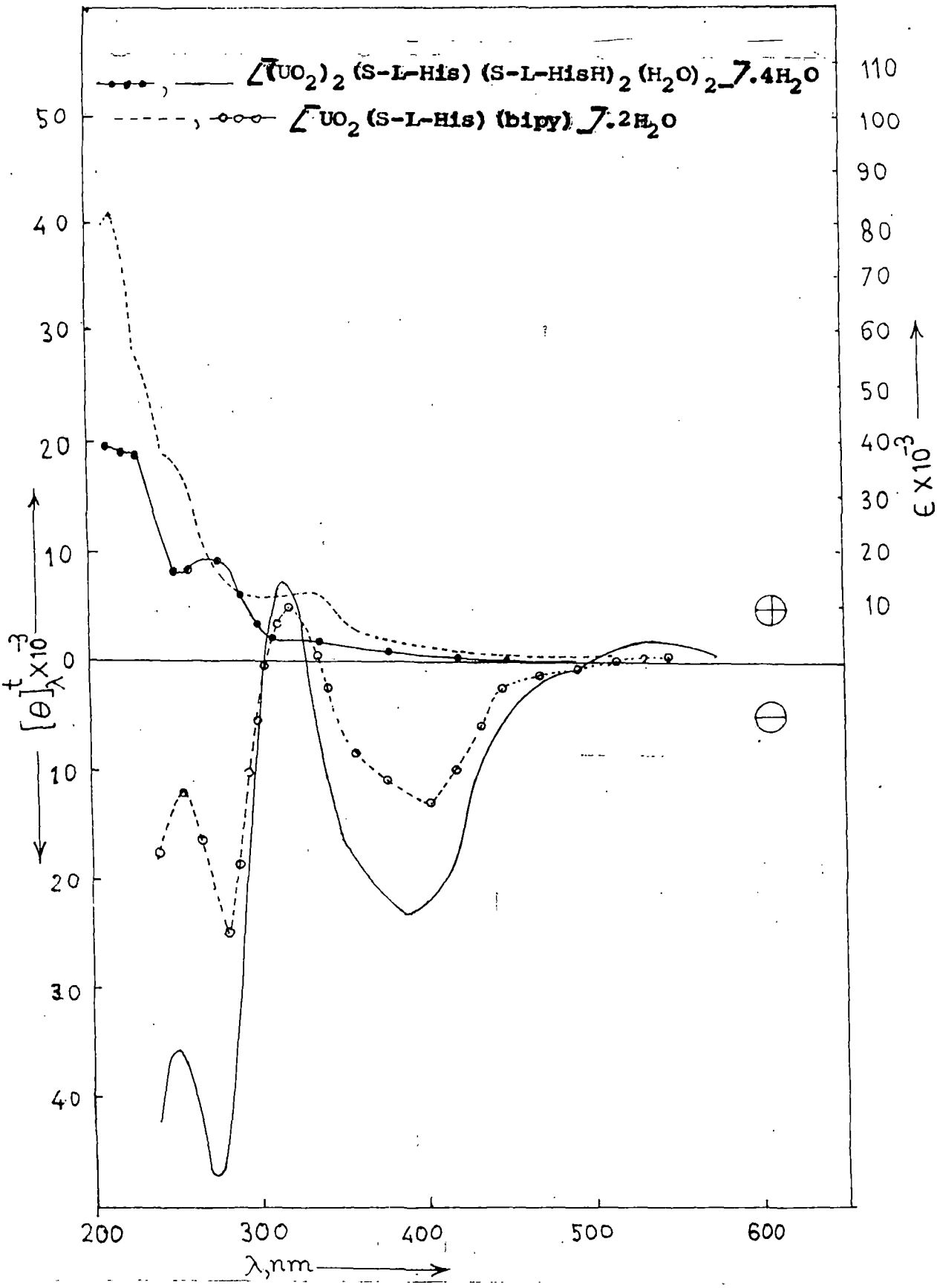

FigureII-18:

UV-visible and CD spectra of $[(UO_2)_2(S\text{-}L\text{-}His)(S\text{-}L\text{-}HisH)_2(H_2O)_2].4H_2O$ and $[UO_2(S\text{-}L\text{-}His)(bipy)].2H_2O$ in methanol .

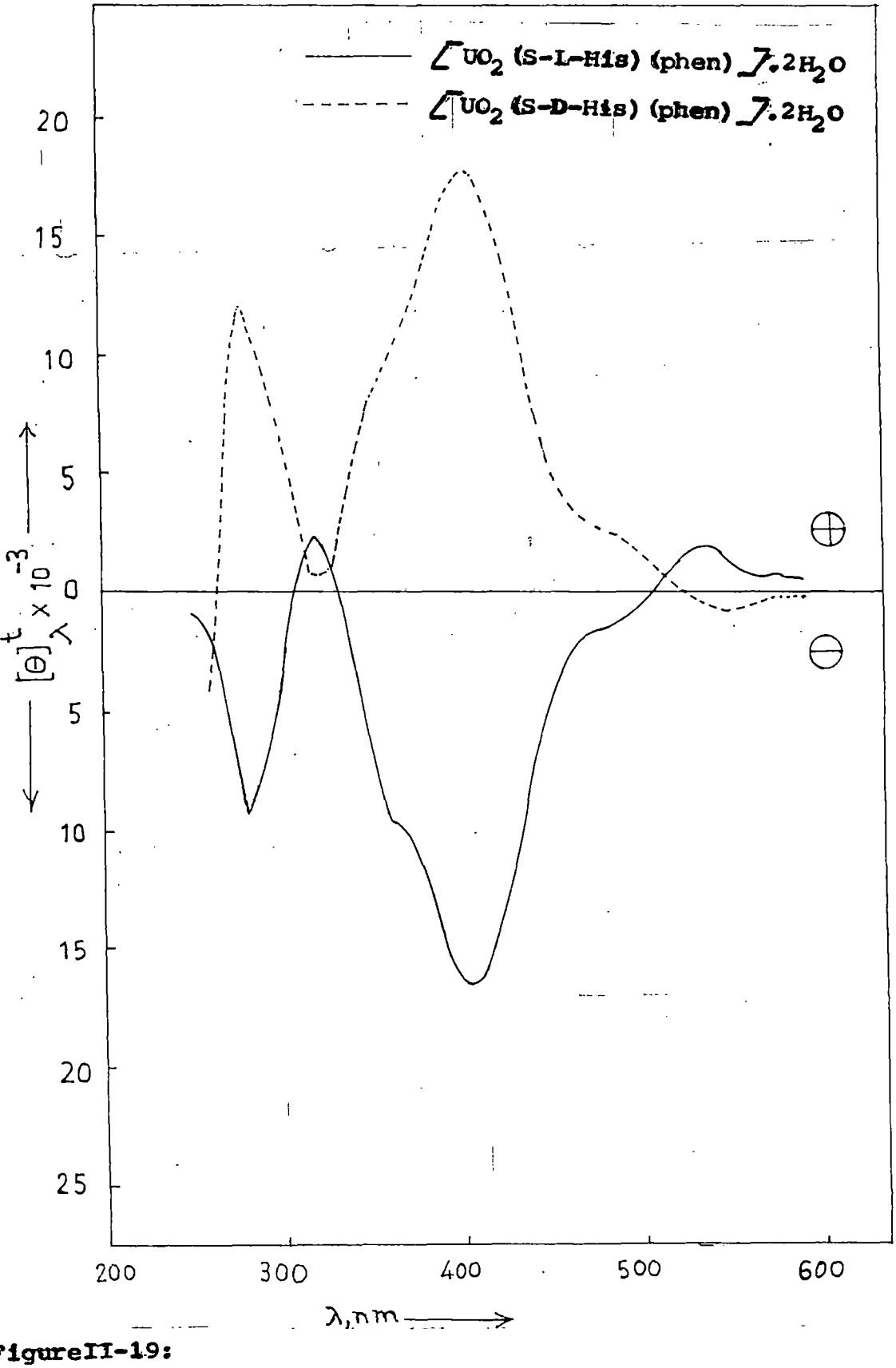

FigureII-19:

CDspectra of $\lceil UO_2$ (S-L-His) (phen) $\rfloor .4H_2O$ & $\lceil UO_2$ (S-D-His) (phen) $\rfloor .2H_2O$ in methanol.

(Scheme II, Figures II-16 and II-18). For the corresponding

Scheme II

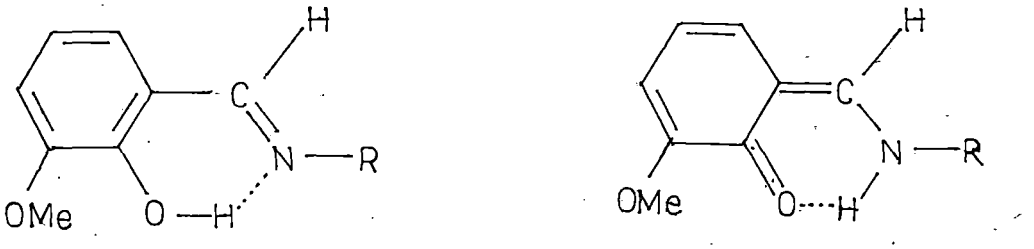

N-salicylidenamino (SA) chromophore, an additional shoulder appears around 240-247 nm; in some of the base adducts new bands appear around 260 nm and 280 nm due to $\pi \longrightarrow \pi^*$ transitions of the 1,10-phenanthroline and 2,2'-bipyridyl moieties respectively[163]. Although the free ligand EA band at 400 nm is assigned to a quinoid form (Scheme II), stabilized in polar solvents[1], for the corresponding dioxouranium(VI) complexes a charge transfer transition of comparable intensity, of the type from the equatorial ligand $p\pi$ orbital to the 5f and/or 6d orbital of the uranium atom, is observed in this region; the apical oxygen $\longrightarrow$ f transition within the UO_2^{2+} entity, centred at about 390-450 nm, has been covered by the aforesaid strong absorption occuring in the range 350-550 nm[55,57,59].

These CD spectra (Figures II-16 to II-19) can be divided into three distinct regions :-

(i) the 240-340 nm region, where an exciton type band is observed with a negative CD maximum around 275 nm and a positive one around 330 nm; the latter band is of much reduced intensity and in some of the 1,10-phenanthroline derivatives, it is totally absent;

(ii) the 340-460 nm region, which exhibits a broad negative CD band around 400 nm with a shoulder at 365 nm; and

(iii) the 460-550 nm region, possessing a weak broad CD maximum around 520-530 nm.

The negative cotton effect around 275 nm is assigned to a $n \rightarrow \pi^*$ transition of the azomethine group strongly coupled to the electronically allowed $\pi \rightarrow \pi^*$ transition below 210 nm of the $-CO_2^-$ group[1].

In terms of the SA chirality rule the decisive CD maximum around 330 nm is generated by the coupled oscillator mechanism[1,64,66] and two major situations may arise :
(A) aliphatic α-amino acid derivatives where the sign of this band in the CD spectrum can be predicted from the preferred chirality that the attachment bond of the $-CO_2^-$ group has with

the phenyl group methine carbon in the OVA/SA chromophore; (B) α and β aryl α-amino acid derivatives where the sign of this CD maximum is determined by the chirality of interaction of the OVA/SA chromophore with the aryl group which overshadows that with the carboxylate group[1]. The molecular structure of $[UO_2(OV\text{-}L\text{-}His)(bipy)].CH_3OH.H_2O$ can be represented in different ways with the help of a Darling model[159] as shown in either Scheme-I or Scheme III (the 2,2'-bipyridyl moiety is omitted) in either case there are opposing contributions

Scheme III

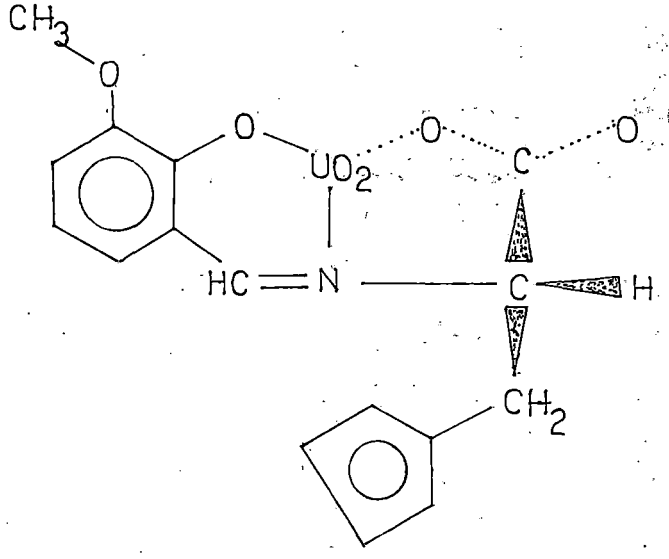

from the aryl group (left handed, negative) and the carboxylate group (right handed, positive) respectively. The negative CD maximum at 315 nm for the free ligand S-L-HisHK (in situ)[1], indicates the dominant conformer I

(Scheme I) to possess left handed chirality (left handed screw), with the contribution from the carboxylate group being overshadowed by that from the aryl group (situation B). On complexation to the UO_2^{2+} entity, a positive CD maximum appears at ca.330 nm (Figures II-16 & II-18) indicating a greater contribution from the carboxylate group in the resulting complexes. This change of sign of the diagnostic CD band, may be ascribed to steric factors existing in the complex molecule II (or V) (Schemes I & III), forcing the electric vector of the aryl group away (Figure II-1), so as to make its coupling with that of the SA chromophore less significant and essentially situation A prevails (leading to right handed chirality in II, Scheme-I). Nevertheless, the weak nature of the positive CD band around 330 nm reflects a residual negative contribution from the imidazole group. The complete absence of this band in some of the 1,10-phenanthroline adducts (Figures II-16 to II-19), is ascribed to the opposing contribution from the electric vector of the $\pi \rightarrow \pi^*$ transition of this neutral donor ligand, which may act in a direction either parallel (short/y axis) or perpendicular (long/x axis) to its C_2 axis; in this region the latter one makes the stronger contribution[63,64,66]. The two rings of the 2,2'-bipyridyl moiety are slightly bent away from the molecular plane (Figure II-3), thereby upsetting the above mentioned contribution from the long/x axis are polarized transition (Figures II-17 & II-18).

The strong broad negative CD band (Figure II-17) around 400 nm of $[UO_2(OV\text{-}L\text{-}His)(bipy)]\cdot 3H_2O$, where ligand-to-metal charge transfer occurs, may be related to the λ-puckering of the six membered chelate ring; a positive CD maximum around 400 nm observed for the corresponding D-histidine derived system (Figures II-17 & II-19)[9].

Essentially the pertinent dioxouranium(VI) complexes have CD spectral characteristics which are quite similar (except the reduced intensity of the CD band around 330 nm) to those of the dioxouranium(VI) complexes of aldimine derivatives of L-alanine and L-valine, possessing alkyl R groups[12,38].

The relatively weak broad CD band around 500-550 nm, is associated with a magnetically allowed uranyl charge transfer transition from a π-oxygen orbital to a f orbital of the uranium atom; the corresponding EA band is scarcely detectable[57]. This transition couples with some uranyl vibration frequency and the vibronic bands generally appear as shoulders at a distance of ca.700-850 cm^{-1} from the main peak[59]. In quasi-enantiomorphous CD curves (Figures II-17 & II-19), the corresponding CD maxima related to this $\pi \longrightarrow f$ transition, differ in position by about 20 nm for the two complexes, whereas for the other peaks, this difference in position usually does not exceed 5 nm.

Cyclic voltammetric studies and conformational effects

The electrochemical data are summarized in Table II-9 & II-10; Figures II-20 to II-22 show some of the representative cyclic voltammograms. For each system an extended cyclic voltammogram was run initially at slow scan (0.01-2.00 V) to establish the limits imposed by the potential at which the ligand begins to reduce (E_{pc} = -1.63V at 50 mvs^{-1}, an irreversible process) and in subsequent cyclic voltammetric measurements, the potential range was limited (-0.80 to -1.20V) to include only that interval in which the complex itself was being reduced and oxidised. The cathoanodic peak system is due to the uncomplicated one-electron charge transfer UO_2^{2+}/UO_2^{+} for the mononuclear complexes[46]. This assignment has been checked through controlled-potential coulometric reductions; for example, controlled-potential coulometry of $[UO_2(OV\text{-}L\text{-}His)(bipy)].CH_3OH.H_2O$ at -1.10 V vs SCE showed a consumption of 1.06 electron/molecule of complex, verifying the one-electron nature of the reduction wave. For the binuclear complex $[(UO_2)_2(S\text{-}L\text{-}His)(S\text{-}L\text{-}HisH)_2(H_2O)_2].4H_2O$ a two-electron transfer due to $2U(VI) \underset{-2e}{\overset{2e}{\rightleftharpoons}} 2U(V)$ occurs[48]. Most of the systems studied tended to show an increase in the cathodic and anodic peak separation as a function of scan rate corresponding to quasi-reversible behaviour.

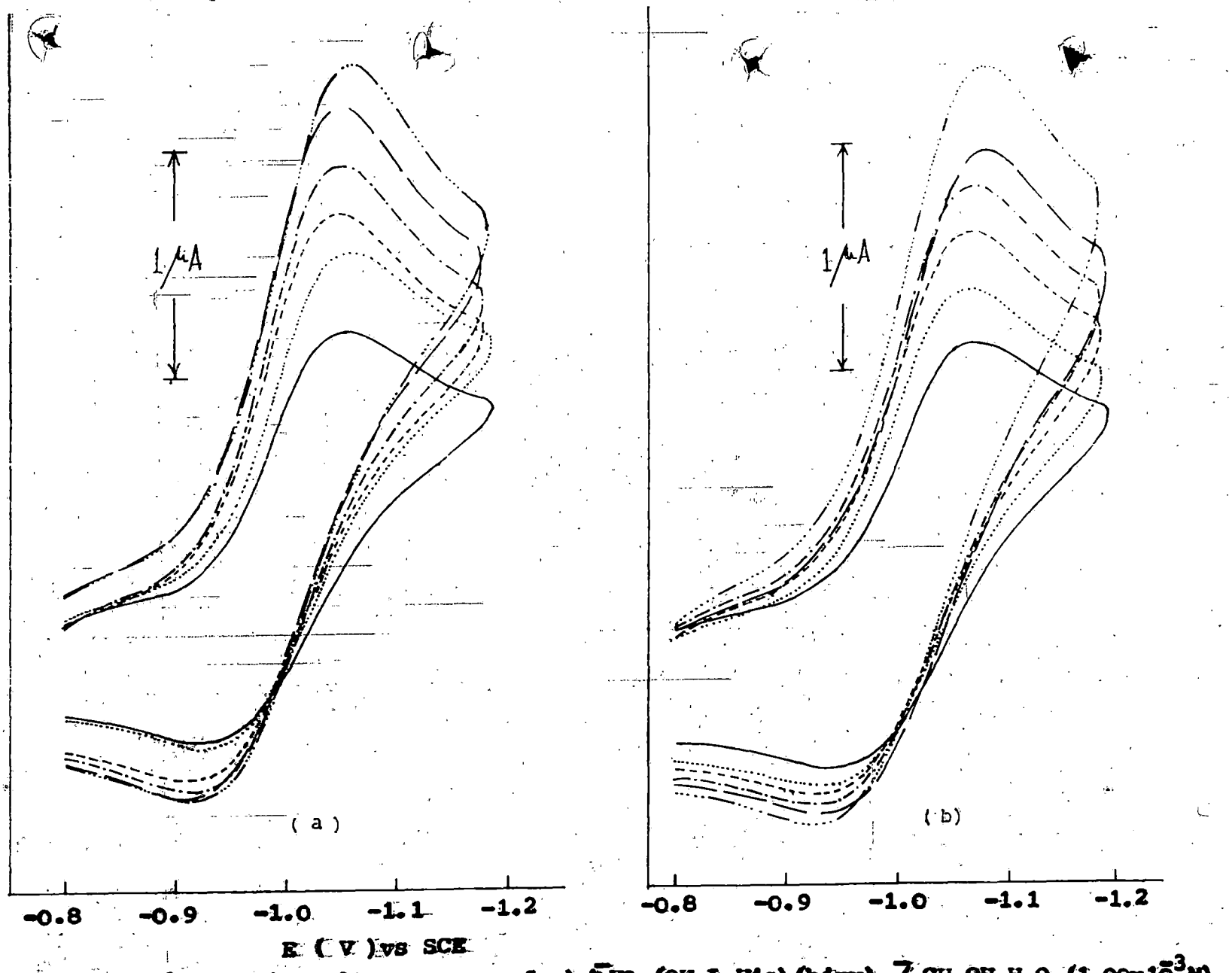

FigureII-20:Cyclic voltammograms of a) $[UO_2(OV\text{-}L\text{-}His)(bipy)].CH_3OH.H_2O$ (1.00×10^{-3} M) and b) $[UO_2(OV\text{-}D\text{-}His)(bipy)].3H_2O$ (0.97×10^{-3} M) in DMSO with 0.1 M $[NBu_4]ClO_4$; scan rates i) 50 (——), ii) 75 (·····), iii) 100 (- - - -), iv) 125 (—·—·—), v) 150 (— —), vi) 175 (—·····—) and vii) 200 (·····) mVS^{-1}. Platinum working electrode .

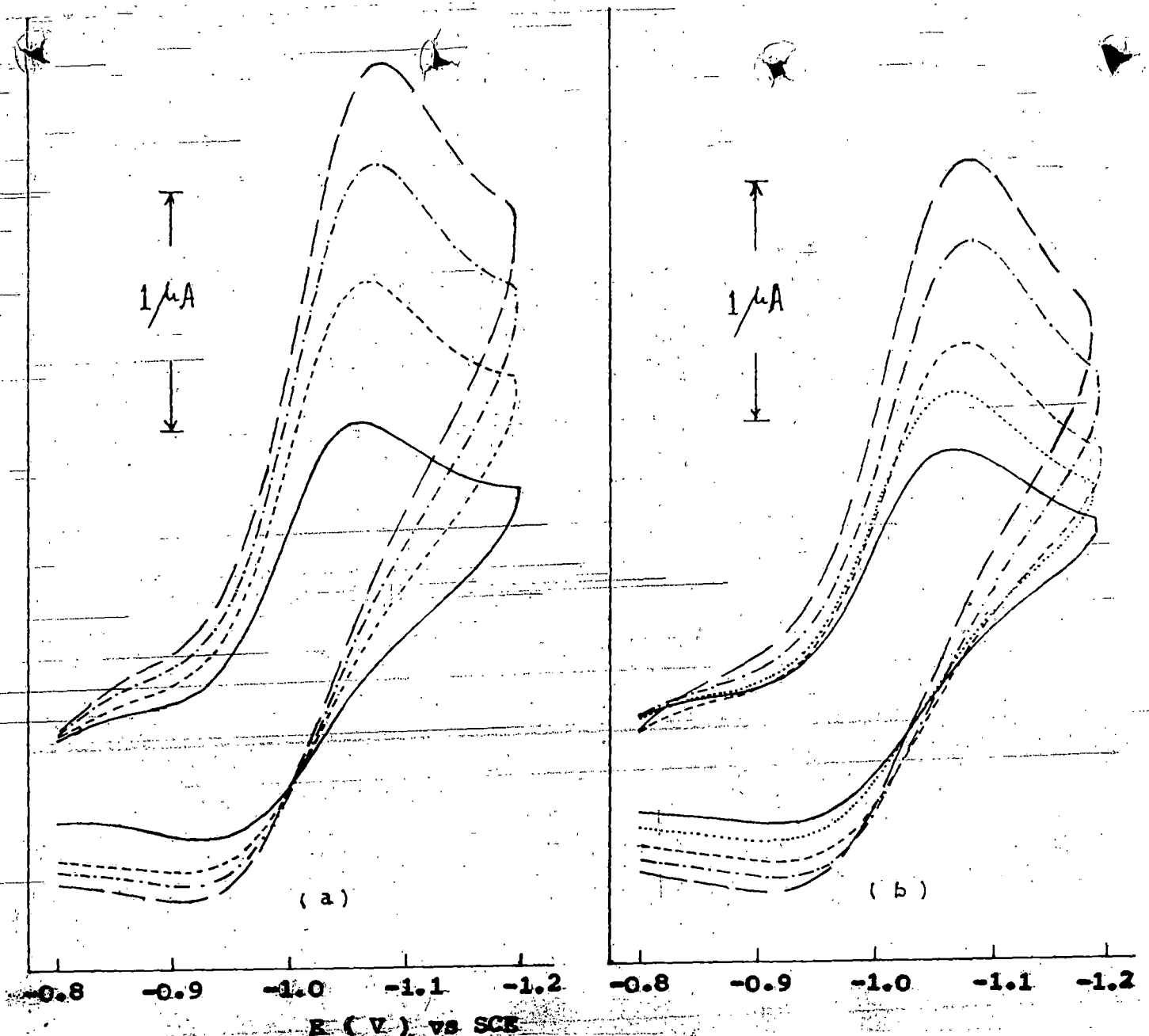

Figure II-21: Cyclic voltammograms of a) $[(UO_2)_2(S\text{-}L\text{-}His)(S\text{-}L\text{-}HisH)_2(H_2O)_2].4H_2O$ (0.61×10^{-3} M) and b) $[UO_2(S\text{-}L\text{-}His)(phen)].4H_2O$ (0.92×10^{-3} M) in DMSO with 0.1 M $[NBu_4]ClO_4$; scan rates i) 50 (——), ii) 75 (·····), iii) 100 (- - - -), iv) 150 (—·—) and v) 200 (— — —) mVS^{-1}. Platinum working electrode.

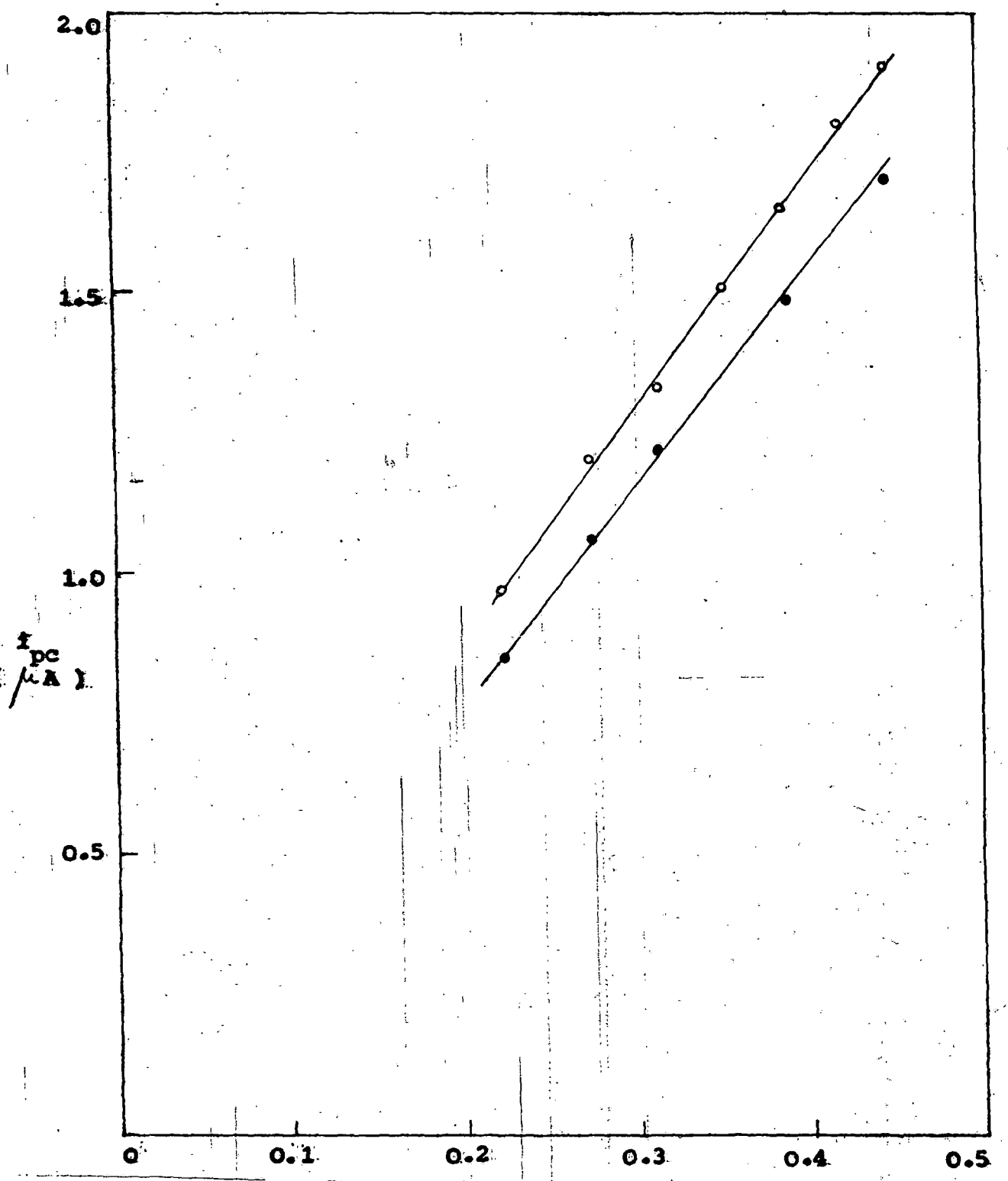

Figure II-22:

Linear dependency of peak current on square root of scan rate for the reduction of i) $[UO_2(OV\text{-}L\text{-}His)(bipy)].CH_3OH.H_2O$ (1.00×10^{-3} M ○) and $[UO_2(S\text{-}L\text{-}His)(phen)].4H_2O$ (0.92×10^{-3} M ●) on a platinum working electrode ; scan rate range : 50-200 mVS^{-1} .

The cyclic voltammogram [Figure II-20 (a)] of [UO_2(OV-L-His)(bipy)].$CH_3OH.H_2O$ in the scan rate range 50-175 mVS^{-1} reveals the following electrochemical parameters :

$E_{\frac{1}{2}}$ = -0.98V, ΔE_p = 145 (± 15) mV and i_{pc}/i_{pa} = 1.78 (± 0.07) and a linear dependency i_{pc} vs $v^{\frac{1}{2}}$ (Figure II-22). The characteristics of the cyclic voltammetric wave [Figure II-20 (b)] at comparable scan rates for [UO_2(OV-D-His)(bipy)].$3H_2O$ are $E_{\frac{1}{2}}$ = -1.00V, ΔE_p = 145 (± 15) mV, i_{pc}/i_{pa} = 1.77 (± 0.17). These two complexes display quasi-enantiomeric CD curves over the entire range from 250-570 nm, except for the difference in [θ] values of the Cotton effects. They also possess noticeable differences in their ^1H NMR spectra [e.g δ (ppm) values as well as splitting patterns of comparable proton signals]. These differences in chiroptical properties resulting from conformational differences, account for the differences in their thermodynamic and kinetic parameters of electrochemical behaviour (Table II-9)[75,76,138,203].

The cyclic voltammograms of the two complexes of S-L-$HisH_2$ series also exhibit quasi-reversible waves in the scan rate range 50 to 200 mVS^{-1}. The characteristics of the cyclic voltammetric wave [Figure II-21 (a)] for [$(UO_2)_2$(S-L-His)(S-L-HisH)$_2$(H_2O)$_2$].$4H_2O$ are $E_{\frac{1}{2}}$ = -0.99V, ΔE_p = 155 (± 15) mV and i_{pc}/i_{pa} = 2.47 (± 0.17); the corresponding values [Figure II-21 (b)] of these parameters for

$[UO_2(S\text{-}L\text{-}His)(phen)].4H_2O$ are -0.99 V, 155 (± 15) mV and 2.27(± 0.15); a linear dependency of i_{pc} vs $v^{\frac{1}{2}}$ is also observed (Figure II-22). The i_{pc}/i_{pa} values indicate lesser susceptibility of the latter complex towards post-chemical reactions. Besides this, the much lower i_{pc}/i_{pa} values (Table II-9) for complexes of the orthovanillidene series, also points towards their greater stability as far as post-chemical reactions are concerned. Both the U(VI) atoms of $[(UO_2)_2(S\text{-}L\text{-}His)(S\text{-}L\text{-}HisH)_2(H_2O)_2].4H_2O$ undergo reduction at the same cathodic peak potential (E_{pc}), i.e., this complex possesses a symmetrically bridged structure (on cyclic voltammetric time scale), with both the metal centres possessing similar coordination environment.

The anodic peak of $K_2[UO_2(OV\text{-}L\text{-}His)_2].4H_2O$ is poorly defined and the relevant cyclic voltammetric response is essentially an irreversible reduction process $[U(VI) \xrightarrow{e^-} U(V)]$, involving extensive post-chemical reactions, before start of the anodic scan (Table II-9).

In terms of HOMO-LUMO approach, during electrochemical reductions the relevant half-filled/vacant MOs accept electrons and the conformational factors have a direct bearing on their energy[75-77]. The stronger the interaction between the $p\pi$ orbitals of the donor atoms and the 5f/6d orbitals of the uranium atom, the more the energy of the HOMO will be raised, making the complex more difficult to reduce[77].

The MO picture reveals that the twelve electrons of the UO_2^{2+} entity fill up the available bonding orbitals $[(1\sigma_g)^2(1\sigma_u)^2(\pi_u)^4(\pi_g)^4]$. Leaving the δ_u, ϕ_u and δ_g orbitals empty; the first two orbitals are of the f-type and the latter one consists of d-orbitals[23,44,58,59]. The electrons donated by the equatorial ligands almost fill up the f-type orbitals of lower energy (these orbitals undergo a degree of modification through metal-ligand mixing), thereby leaving the ϕ_u orbital partly filled and the δ_g orbital empty; they are responsible for the observed electrochemical behaviour. Consequently, the chelation process makes the UO_2^{2+} entity less susceptible to reduction as compared to that in the free state and a reduction to the UO_2^{+} state is accompanied by an increase in size[46]. The ligand should be sufficiently flexible/sterically demanding to bear with the electro-induced stereochemical rearrangement. Otherwise, the relevent cyclic voltammetric wave should be irreversible due to destruction of the cathodic reduction product through a subsequent chemical reaction before start of the anodic scan. Accordingly, the cyclic voltammogram of $UO_2(NO_3)_2 \cdot 6H_2O$ in DMSO (vide chapter III, Figure III-18, Inset) is characterized by a single irreversible reduction peak (E_{pc} = -0.52 V at 50 mVs^{-1}, scan range 0.00 to -1.10 V) corresponding to the U(VI) $\longrightarrow$ U(V) reduction and the latter is rendered irreversible by hydrolysis/solvolysis. The net effect of coordination with these aldimine ligands, is to shift the

cathodic peak potential (ΔE_{pc}) to a more negative value and to impart a quasi-reversible nature to it. Presence of a large R group makes such ligands quite sterically demanding and in conjugation with the neutral bidentate donors (2,2'-bipyridyl/1,10-phenanthroline), they form a relatively compact equatorial donor set around the UO_2^{2+} entity. The i_{pc}/i_{pa} values (at 50 mVS^{-1}, Table II-9) indicate that $[UO_2(OV\text{-}D\text{-}His)(bipy)].3H_2O$ possesses the most compact aldimine chelate ring of this series of complexes.

Imposition of a coordination number of six, coupled with the resulting bi-negative charge on the anionic complex $K_2[UO_2(OV\text{-}L\text{-}His)_2].4H_2O$, makes the relevant metal centred electron transfer process essentially irreversible (Table II-9). Presence of additional electrons in the ϕ_u and δ_g orbitals as well as steric crowding may be regarded as pertinent reasons for this type of electrochemical response. There is hardly any scope of the metal atom for shedding the accumulated electron density on it through π-bonding ($M \longrightarrow L$ type), as in case of the mononuclear complexes containing 2,2'-bipyridyl/1,10-phenanthroline.

Conclusion

The pentagonal planar coordination geometry of the diamagnetic UO_2^{2+} entity, which it achieves here along with a

neutral bidentate donor (e.g. 2,2'-bipyridyl), coupled with its high atomic weight, allows strong ligand coordination; usually the proton signals of the chelated ligand, get well separated in position, thereby assisting their identification. The ligand chiral centre remains unaffected and the extent of different conformer formation as a result of rotation around the $C_\alpha - C_\beta$ bond, is usually not large. Configurational/conformational arguments based on CD and ^1H NMR data for such a mononuclear system, can be correlated in a straight forward manner[28]. Of the three distinct portions in the CD spectra, the region below 350 nm is valuable in determining the conformation about the $N-C_\alpha$ bond as well as the contributions to the diagnostic CD band around 330 nm from the adjacent chromophores, whereas the middle region (350-500 nm) is dependent on the puckering (λ-/δ-) of the chelate rings; the third portion above 500 nm reflects the fact that absolute configuration (L-/D-) of the amino acid residue decides the chirality of the $\pi \longrightarrow f$ charge transfer transition within the UO_2^{2+} entity (vicinal effect).

Both the thermodynamic ($E_{\frac{1}{2}}$) and kinetic (i_{pc}/i_{pa}) parameters of the cyclic voltammetric waves of these complexes throw light on the major factors influencing their electrochemical behaviour, e.g., conformation (their compactness, extent of puckering/twisting) of the chelate rings as well as the accumulated charge on their metal atom through complex

formation. In cases where there is scope for M $\longrightarrow$ L type π -bonding, the chelate rings are usually capable of adjusting (tuning) with the size increase accompanying cathodic reduction (to the UO_2^+ state) and essentially quasi-reversible type of electrochemical behaviour is observed. The irreversible electron transfer process for the anionic complex $K_2[UO_2(OV\text{-}L\text{-}His)_2].4H_2O$, amply demonstrates the inability of the particular chelate rings to cope with the electroinduced size increase of the metal atom as well as the dependence of this process on the electron density on the latter.

Table II-1

Data for X-ray diffraction study of

$[UO_2(OV\text{-}L\text{-}His)(bipy)]\cdot CH_3OH\cdot H_2O$.

formula	$C_{25}H_{27}N_5O_8U$
diffractometer	Nicolet P3
monochromator	graphite
radiation (MoKα)	0.71069
orientation reflections	15
2θ range	9.0 - 20.4
temperature (°C)	20
scan method	ω-scan
scan speed (°/min)	2 - 25
range in h,k,l	min 0,-11,-13
	max 9,10,13
meas. range	$3.0 < 2\theta < 53.0$
check reflections	2
observed refl. [$F_o > 5\sigma(F_o)$]	2818
no of variables	349
R	0.041
Rw [$w = 1/\sigma^2(F_o)$]	0.037
max (Δ/ρ)	0.94
ρ in ΔF map ($e\text{Å}^{-3}$)	min -1.70
	max 2.94

Table II-2

Atomic coordinates ($x10^4$) and equivalent isotropic thermal parameters ($x10^2$) for $[UO_2(OV\text{-}L\text{-}His)(bipy)].CH_3OH.H_2O$.

	x	y	z	U_{eq}
U	0	0	0	2.8
O(1)	1322(43)	981(33)	-1102(26)	5.4
O(2)	-1156(31)	-909(27)	1151(23)	3.9
O(3)	-2427(17)	-2104(13)	-1572(12)	5.1
O(4)	-5294(15)	-3436(11)	-2975(10)	4.0
O(5)	393(17)	2374(13)	861(11)	4.8
O(6)	2296(18)	4806(14)	2739(11)	5.1
O(7)	7802(24)	-3945(15)	5441(22)	8.7
O(8)	476(19)	-5478(16)	-3998(14)	5.8
N(1)	-2995(16)	465(13)	-1042(11)	3.0
N(2)	-7028(24)	2439(19)	-3770(22)	6.7
N(3)	-3865(21)	3015(16)	-3284(13)	4.6
N(4)	3204(17)	687(15)	1701(11)	3.7
N(5)	1542(18)	-2023(15)	-6(11)	3.7
C(1)	-4005(31)	-2217(21)	-2274(19)	2.6
C(2)	-4424(17)	-699(16)	-2171(13)	2.8
C(3)	-4227(20)	66(15)	-3419(12)	3.6
C(4)	-4898(18)	1380(14)	-3490(11)	3.1
C(5)	-6839(18)	1054(13)	-3784(15)	3.9
C(6)	-5230(19)	3660(14)	-3421(13)	3.5
C(7)	-3334(41)	1651(39)	-737(34)	5.5
C(8)	-2434(20)	2830(15)	410(12)	3.3
C(9)	-3300(33)	3848(24)	655(22)	5.0
C(10)	-2297(30)	5175(20)	1622(18)	5.4
C(11)	-426(27)	5526(17)	2333(15)	4.8
C(12)	501(23)	4584(15)	2100(13)	4.0
C(13)	-663(46)	3167(29)	1015(27)	3.1
C(14)	4050(57)	1988(37)	2589(27)	5.3
C(15)	5735(26)	2524(22)	3487(16)	5.4
C(16)	6781(23)	1631(24)	3523(16)	5.3
C(17)	6017(21)	225(21)	2646(16)	4.6
C(18)	4202(20)	-218(20)	1729(15)	3.4
C(19)	3523(48)	-1557(31)	656(30)	4.5
C(20)	4196(22)	-2736(19)	721(18)	4.6
C(21)	3209(30)	-4132(25)	-136(25)	5.0
C(22)	1376(28)	-4485(20)	-931(16)	4.9
C(23)	393(58)	-3406(40)	-954(44)	5.4
C(24)	3317(27)	6134(21)	3773(15)	5.6
C(25)	9064(24)	-2296(15)	5437(22)	4.9

Table II-3

Interatomic distances (Å) and angles (°)
of $[UO_2(OV\text{-}L\text{-}His)(bipy)]\cdot CH_3OH\cdot H_2O$

U - O(1)	1.784(26)	N(5)-C(19)	1.418(35)
U - O(2)	1.743(20)	N(5)-C(23)	1.419(37)
U - O(3)	2.340(11)	C(1) -C(2)	1.563(22)
U - O(5)	2.211(11)	C(2) -C(3)	1.552(16)
U - N(1)	2.559(12)	C(3) -C(4)	1.498(17)
U - N(4)	2.554(11)	C(4) -C(5)	1.374(18)
U - N(5)	2.596(12)	C(7) -C(8)	1.441(34)
O(3)-C(1)	1.249(24)	C(8) -C(9)	1.409(25)
O(4)-C(1)	1.225(23)	C(9) -C(10)	1.391(26)
O(5)-C(13)	1.336(34)	C(10)-C(11)	1.380(28)
O(6)-C(12)	1.338(20)	C(11)-C(12)	1.386(23)
O(6)-C(24)	1.436(19)	C(12)-C(13)	1.523(28)
O(7)-C(25)	1.430(00)	C(14)-C(15)	1.325(40)
N(1)-C(2)	1.474(16)	C(15)-C(16)	1.371(29)
N(1)-C(7)	1.271(37)	C(16)-C(17)	1.392(26)
N(2)-C(5)	1.339(20)	C(17)-C(18)	1.414(19)
N(2)-C(6)	1.344(20)	C(18)-C(19)	1.488(36)
N(3)-C(4)	1.361(17)	C(19)-C(20)	1.381(24)
N(3)-C(6)	1.401(18)	C(20)-C(21)	1.367(28)
N(4)-C(14)	1.327(34)	C(21)-C(22)	1.385(27)
N(4)-C(18)	1.350(19)	C(22)-C(23)	1.479(50)

O(1) -U -O(2)	176.4(17)	N(1) -C(2) -C(1)	109.4(12)
O(1) -U -O(3)	94.2(10)	N(1) -C(2) -C(3)	110.0(10)
O(2) -U -O(3)	88.9(8)	N(1) -C(7) -C(8)	129.5(23)
O(1) -U -O(5)	89.1(10)	N(2) -C(5) -C(4)	109.6(11)
O(1) -U -N(1)	94.3(9)	N(3) -C(4) -C(5)	107.3(11)
O(1) -U -N(4)	90.0(9)	N(3) -C(6) -N(2)	108.7(12)
O(1) -U -N(5)	87.8(9)	N(3) -C(4) -C(3)	130.7(12)
O(2) -U -O(5)	89.8(9)	N(4) -C(14)-C(15)	129.1(32)
O(2) -U -N(1)	88.6(8)	N(4) -C(18)-C(17)	121.2(16)
O(2) -U -N(4)	86.5(8)	N(4) -C(18)-C(19)	118.8(15)
O(2) -U -N(5)	91.2(9)	N(5) -C(19)-C(18)	110.8(20)
O(3) -U -O(5)	135.8(4)	N(5) -C(19)-C(20)	117.6(21)
O(3) -U -N(1)	65.0(4)	N(5) -C(23)-C(22)	110.4(31)
O(3) -U -N(4)	141.0(4)	O(6) -C(12)-C(11)	126.1(13)
O(3) -U -N(5)	78.7(4)	O(6) -C(12)-C(13)	118.0(17)
O(5) -U -N(1)	70.8(4)	C(1) -C(2) -C(3)	107.8(12)
O(5) -U -N(4)	82.9(4)	C(2) -C(3) -C(4)	111.3(10)
O(5) -U -N(5)	145.5(4)	C(3) -C(4) -C(5)	122.0(11)
N(1) -U -N(4)	153.2(4)	C(7) -C(8) -C(9)	119.4(19)
N(1) -U -N(5)	143.8(4)	C(7) -C(8) -C(13)	118.0(20)
N(4) -U -N(5)	62.7(4)	C(8) -C(9) -C(10)	120.4(19)

Table II-3
(continued)

U -O(3)-C(1)	130.2(11)	C(8) -C(13)-C(12)	121.2(23)
U -O(5)-C(13)	140.0(13)	C(9) -C(8) -C(13)	120.8(17)
U -N(1)-C(2)	117.1(8)	C(9) -C(10)-C(11)	120.2(16)
U -N(1)-C(7)	126.9(13)	C(10)-C(11)-C(12)	121.3(13)
U -N(4)-C(14)	122.7(18)	C(11)-C(12)-C(13)	115.9(18)
U -N(4)-C(18)	122.2(10)	C(14)-C(15)-C(16)	116.8(21)
U -N(5)-C(19)	120.7(11)	C(15)-C(16)-C(17)	119.0(14)
U -N(5)-C(23)	113.1(21)	C(16)-C(17)-C(18)	118.9(16)
O(3)-C(1)-O(4)	125.8(17)	C(17)-C(18)-C(19)	119.4(17)
O(3)-C(1)-C(2)	116.7(15)	C(18)-C(19)-C(20)	122.6(22)
O(4)-C(1)-C(2)	117.3(17)	C(19)-C(20)-C(21)	120.0(19)
O(5)-C(13)-C(8)	128.3(21)	C(20)-C(21)-C(22)	120.0(15)
O(5)-C(13)-C(12)	110.5(22)	C(21)-C(22)-C(23)	124.1(20)

Table II-4

Anisotropic temperature factors ($\times 10^2$) for $[UO_2(OV\text{-}L\text{-}His)(bipy)] \cdot CH_3OH \cdot H_2O$.

	U_{11}	U_{22}	U_{33}	U_{23}	U_{13}	U_{12}
U	2.3(0)	2.7(1)	3.2(1)	0.1(1)	0.1(1)	1.3(1)
O(1)	4.5(15)	4.7(12)	6.6(11)	0.9(9)	-0.4(11)	2.7(12)
O(2)	3.8(10)	5.0(9)	2.8(9)	0.9(7)	1.3(8)	1.5(8)
O(3)	4.3(6)	3.7(5)	6.4(7)	-1.1(5)	-1.9(5)	2.7(5)
O(4)	4.0(5)	2.7(4)	4.4(5)	-0.5(4)	-0.4(4)	1.5(4)
O(5)	4.0(5)	3.9(5)	5.2(6)	-1.5(4)	-1.0(4)	2.0(4)
O(6)	4.5(6)	4.1(5)	4.9(6)	-0.4(4)	-0.8(5)	1.4(5)
O(7)	5.1(8)	6.2(9)	12.0(15)	-2.0(9)	1.3(9)	0.5(7)
O(8)	4.8(6)	4.8(6)	6.8(8)	0.6(5)	1.0(6)	1.4(5)
N(1)	2.4(5)	2.9(5)	3.1(5)	-0.3(4)	-0.1(4)	1.0(4)
N(2)	4.3(8)	3.8(7)	11.1(14)	0.6(8)	0.9(8)	1.6(6)
N(3)	4.7(7)	3.8(6)	4.6(6)	0.1(5)	0.3(5)	1.9(6)
N(4)	3.3(6)	4.3(6)	3.3(5)	0.2(4)	-0.2(4)	2.1(5)
N(5)	3.6(6)	4.0(6)	3.7(5)	-0.1(4)	0.1(5)	2.4(5)
C(1)	2.8(7)	2.1(6)	3.1(8)	0.7(5)	-0.6(6)	1.9(5)
C(2)	2.4(6)	1.8(6)	3.6(6)	0.4(5)	-0.1(5)	0.8(4)
C(3)	4.3(7)	3.0(5)	3.8(6)	0.4(4)	0.8(5)	2.0(5)
C(4)	3.1(6)	2.8(5)	3.0(5)	0.6(4)	0.3(4)	1.1(4)
C(5)	2.5(5)	1.6(5)	6.4(8)	0.3(5)	-0.1(5)	0.5(4)
C(6)	3.4(6)	2.0(5)	5.0(7)	0.2(4)	0.3(5)	1.5(5)
C(7)	2.9(11)	7.3(17)	4.7(15)	-0.6(11)	-1.3(10)	2.0(10)
C(8)	4.1(7)	2.6(5)	3.2(5)	0.6(4)	0.6(5)	1.6(5)
C(9)	5.5(11)	4.4(9)	5.7(10)	0.7(8)	1.5(9)	2.8(8)
C(10)	6.7(10)	4.3(8)	6.4(9)	-0.2(7)	1.5(8)	3.6(8)
C(11)	6.4(9)	3.1(6)	4.2(7)	-0.4(5)	1.4(6)	1.6(6)
C(12)	5.1(8)	2.6(5)	3.3(6)	0.1(4)	0.2(5)	1.2(5)
C(13)	1.8(11)	2.4(8)	4.4(8)	-0.6(7)	0.3(8)	0.5(8)
C(14)	5.8(13)	5.1(13)	4.1(12)	0.2(9)	-0.7(10)	2.6(11)
C(15)	4.7(8)	5.3(9)	4.3(7)	-0.6(7)	-0.2(6)	1.3(7)
C(16)	3.1(7)	6.9(10)	4.3(7)	0.4(7)	-0.8(6)	1.5(7)
C(17)	2.7(6)	5.3(8)	4.9(7)	0.5(6)	-0.5(6)	1.7(6)
C(18)	2.6(6)	3.3(8)	3.9(7)	0.7(6)	0.6(6)	1.1(5)
C(19)	7.1(20)	3.0(9)	4.7(13)	-0.1(8)	-0.9(12)	4.9(12)
C(20)	3.8(7)	4.0(7)	7.1(9)	1.3(6)	1.1(7)	2.9(6)
C(21)	4.5(9)	5.2(9)	7.1(13)	1.2(9)	1.7(9)	3.8(8)
C(22)	6.2(10)	4.4(8)	4.7(7)	-0.3(6)	0.4(7)	3.5(8)
C(23)	3.1(15)	3.7(12)	7.1(16)	-1.6(10)	0.7(11)	-0.3(9)
C(24)	5.3(9)	4.7(8)	3.9(7)	0.1(6)	0.2(6)	0.1(7)
C(25)	2.6(6)	3.3(7)	7.7(10)	-0.7(6)	0.6(6)	0.7(5)

N.B. The listing of observed and calculated structure factors (12 pages) is available with the author.

Table II.5. Characterization data for the dioxouranium(VI) complexes of N-(orthovanillidene)-L-histidine ($OV\text{-}L\text{-}HisH_2$) and N-(salicylidene)-L-histidine ($S\text{-}L\text{-}HisH_2$).

Sl. No.	Complex	Color	Analysis, % found (calc.) U	C	H	N	TGA, total mass loss (%) found (calc.)	λ_{max}^{nm} ($\log\epsilon$) in methanol+
1.	$K_2[UO_2(OV\text{-}L\text{-}His)_2].4H_2O$	Dark red	25.3 (23.9)	33.8 (33.8)	3.5 (3.8)	7.3 (8.4)	63.5 (64.9)	224br (4.72), 265br (4.37), 340sh (3.86), 404sh (3.36), 497sh (2.81).
2.	$[UO_2(OV\text{-}L\text{-}His)(bipy)].3H_2O$*	Deep brown	29.7 (31.0)	36.7 (37.6)	3.3 (3.8)	10.1 (9.1)	65.7 (64.8)	231 (4.59), 277br (4.36), 325sh (3.61), 400sh (3.17), 485sh (2.71).
3.	$[UO_2(OV\text{-}L\text{-}His)(bipy)]$ $.CH_3OH.H_2O$	Deep brown	30.1 (31.2)	38.4 (39.3)	3.2 (3.5)	8.2 (9.2)	65.1 (65.4)	231 (4.51), 277br (4.36), 325sh (3.62), 400sh (3.19), 485sh (2.74).
4.	$[UO_2(OV\text{-}L\text{-}His)(phen)].H_2O$	Deep brick red	32.2 (31.5)	41.5 (41.3)	3.2 (3.3)	8.9 (9.3)	62.5 (64.2)	224sh (4.8), 229 (4.82), 263 (4.57), 330sh (3.67), 400 (3.1), 495 (2.65).
5.	$[(UO_2)_2(S\text{-}L\text{-}His)(S\text{-}L\text{-}HisH)_2$ $(H_2O)_2].4H_2O$	Yellowish red	32.5 (33.5)	33.3 (32.9)	3.2 (3.3)	7.9 (8.8)	62.4 (62.0)	212(4.92), 233sh (4.73), 255sh (4.56), 330br (4.12), 389sh (3.5), 470sh (2.95).
6.	$[UO_2(S\text{-}L\text{-}His)(bipy)].2H_2O$	Brick red	32.6 (33.1)	37.4 (38.4)	3.0 (3.2)	8.9 (9.7)	62.4 (62.5)	214sh (4.6), 229sh (4.57), 275br (4.28), 340sh (3.56), 390sh (3.11), 475sh (2.56).

contd ...

Table II-5 contd ...

7. [UO_2(S-L-His)(phen)].$4H_2O$*	Reddish orange	30.8 (30.6)	38.8 (38.5)	2.9 (3.4)	10.1 (9.0)	65.5 (65.34)	225sh(3.86), 229(3.86), 262(3.59), 330sh(2.78), 385sh(3.16), 475sh(2.61).

OV-L-HisH$_2$: $C_{14}H_{15}N_3O_4$; S-L-HisH$_2$: $C_{13}H_{13}N_3O_3$. *The corresponding complexes containing the D-histidine derivatives have been synthesized and characterized through elemental analysis and other physico-chemical data. †Electronic spectral data in methanol : i) OV-L-HisHK.$2H_2O$: 225sh(4.17), 254br(3.57), 279br(3.78), 415(3.02) and ii) S-L-HisHK : 215sh(4.19), 255br(3.57), 275br(3.51), 320sh(3.02), 382(2.76).

Table II-6. Characteristic IR spectral data (cm^{-1}) of the ligands and the corresponding dioxouranium(VI) complexes.

Sl.no.*	ν (CH=N)	ν_{as}, ν_s, Δ value of $-CO_2^-$ group	ν (C-O) + δ (OH) or ν (C-O) of phenolic -OH or phenoxide group	ν_3, F_{UO} (mdynes/A) & R_{UO} (Å) of UO_2^{2+} entity
OV-L-HisHK $\cdot 2H_2O$	1635	1615,1413, 202	1245 (sh) 1231 (br)	-
S-L-HisHK	1635	1575,1415, 160	1240 (br)	-
1	1610	1575,1410, 165	1220 (sh), 1208	895 (br); 6.66; 1.74
2	1615	1602,1410, 192	1222	919,908 (sh); 6.94; 1.74
3	1611	1592,1402, 190	1220	910,897 (sh); 6.79; 1.74;
4	1613	1580,1413, 167	1223	913; 6.93; 1.74
5	1630 (sh) 1619 (br)	1600,1585, 1408,1398, 192,187	1210 (br) 1190 (sh)	908 (br); 6.85; 1.74
6	1630 (sh) 1615	1599,1412, 187	1212	914,898 (sh); 6.82; 1.74
7	1650 (sh) 1620	1600,1415, 185	1210	905,913 (sh); 6.87; 1.74

*These serial numbers refer to those in Table II-5.

Table II-7. Chemical shift (δ, ppm) values of protons of major conformers of the ligands and those of the corresponding dioxouranium(VI) complexes along with the Δ (= δcomplex - δ ligand) ppm values for the latter.

		Amino acid residue			Aldehyde Residue					Imidazole residue		bipy, phen parts[d]			
		$H\beta_1$	$H\beta_2$	H_α	CH=N	C_5, OCH_3	H_2	H_3	H_4	H_2'	H_4'	H_6''	H_5''	H_4''	H_3''
												$H_{2\&9}''$	$H_{3\&8}''$	$H_{4\&7}''$	$H_{5\&6}''$
OV-L-His HK.$2H_2O$[a]		2.52	2.84	3.18	7.29	3.68	6.77	6.68	6.83	6.81	5.05	-	-	-	-
300 MHz															
$K_2[UO_2(OV\text{-}L\text{-}His)_2].4H_2O$[a]		2.89	3.30	5.04	7.26	3.91	6.88	6.52	7.15	8.45	7.58	-	-	-	-
300 MHz	Δ =	0.37	0.46	1.86	-0.03	0.23	0.11	-0.16	0.32	1.64	2.53				
$[UO_2(OV\text{-}L\text{-}His)(bipy)].$		3.10	3.39	5.14	8.87	3.93	7.02	6.60	7.20	8.86	7.16	8.69	7.46	7.96	8.38
$3H_2O$[a]	Δ =	0.58	0.55	1.96	1.58	0.25	0.25	-0.08	0.37	2.05	2.11	0.06	0.11	0.11	0.07
300 MHz															
$[UO_2(OV\text{-}D\text{-}His)(bipy)].$		3.06	3.33	5.08	8.84	3.87	7.01	6.53	7.16	8.84	7.10	8.66	7.41	7.9	8.35
$3H_2O$[a]	Δ =	0.54	0.49	1.90	1.55	0.19	0.24	-0.15	0.33	2.03	2.05	0.03	0.06	0.05	0.04
300 MHz															
S-L-His HK[b]		2.84	3.10	3.72	7.55	-	c	c	c	6.87	5.26	-	-	-	-
100 MHz															

contd ...

Table II-7 contd...

$[(UO_2)_2(S\text{-}L\text{-}His)(S\text{-}L\text{-}HisH)_2(H_2O)_2]\cdot 4H_2O$ [b] 100 MHz	3.40	3.68	5.48	9.13 [e] 8.45 [e]	-	c	c	c	8.74	7.23	-	-	-	-
	0.56	0.58	1.76	1.58					1.87	1.97				
$[UO_2(S\text{-}L\text{-}His)(phen)]\cdot 4H_2O$ [a] 300 MHz	3.11	3.40	5.15	8.87	-	6.96	6.65	7.43	8.76	7.13	9.10	7.79	8.52	8.02
	0.27	0.30	1.43	1.32	-	-	-	-	1.89	1.87	0.0	0.08	0.06	0.05
$[UO_2(S\text{-}D\text{-}His)(phen)]\cdot 2H_2O$ [a] 300 MHz	3.07	3.39	5.11	8.78	-	6.95	6.64	7.40	8.55	7.02	9.11	7.79	8.51	8.01
	0.23	0.29	1.39	1.23	-	-	-	-	1.68	1.76	0.01	0.08	0.05	0.04

[a] In DMSO ; [b] In D_2O; [c] H_2, H_3, H_4, H_5 protons could not be resolved at 100 MHz; [d] δ, ppm values for free bipy & phen protons have been obtained from references 26 & 27; [e] Two singals (1:2 ratio).

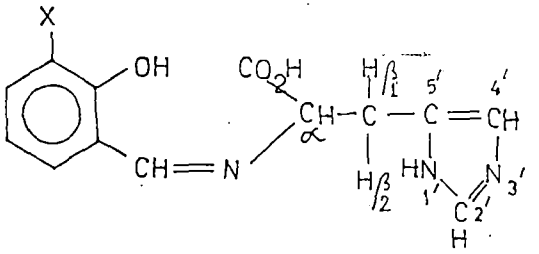

X = H; S-L/D-$HisH_2$;
X = OCH_3; OV-L/D-$HisH_2$.

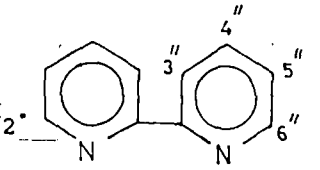

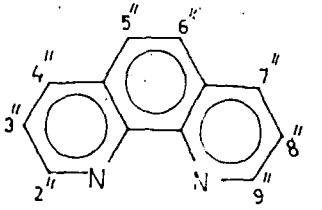

Table II-8. Vicinal coupling constants, average coupling constants and populations of conformers.

	$^3J_{\alpha\beta_1}$ (Hz)	$^3J_{\alpha\beta_2}$ (Hz)	J_{av} (Hz)	$^3J_{\alpha\beta_1} \sim {}^3J_{\alpha\beta_2}$	Population of conformers (%)
OV-L-HisHK.$2H_2O$	12.3	3.7	8.0	3.3	89 & 11
S-L-HisHK	10.4	4.4	7.4	2.4	77 & 23
$[UO_2$(OV-L-His)(bipy)$]$.$3H_2O$	10.0	2.2	6.1	4.4	95 & 5
$[UO_2$(OV-D-His)(bipy)$]$.$3H_2O$	8.5	4.8	6.6	1.8	98 & 2
$K_2[UO_2(OV\text{-}L\text{-}His)_2]$.$4H_2O$	9.3	Overlapping signals	-	-	71,19 & 10
$[UO_2$(S-L-His)(phen)$]$.$4H_2O$	7.7	4.6	6.1	1.7	almost pure one form
$[UO_2$(S-D-His)(phen)$]$.$2H_2O$	8.6	3.8	6.2	2.3	* *
$[(UO_2)_2$(S-L-His)$_2$(S-L-HisH)$_2$(H_2O)$_2$$]$.$4H_2O$	8.0	6.0	7.0	1.3	*

*Presence of two types of ligand residues makes identification of conformers difficult.

Table II-9. Summary of electrochemical data of the dioxouranium complexes.[a,b]

Compound	$UO_2^{2+} + e \rightleftharpoons UO_2^{+}$				
	E_{pc} (V)	E_{pa} (V)	ΔE_p (mV)[c]	$E_{1/2}$ (V)[d]	i_{pc}/i_{pa}
$[UO_2(OV\text{-}L\text{-}His)(bipy)].CH_3OH.H_2O$[e]	-1.05	-0.92[h]	130[c]	-0.98	1.76
$[UO_2(OV\text{-}D\text{-}His)(bipy)].3H_2O$[e]	-1.07	-0.94[h]	130	-1.00	1.60
$K_2[UO_2(OV\text{-}L\text{-}His)_2].4H_2O$[e]	-1.08	-[g]	-	-	-
$[(UO_2)_2(S\text{-}L\text{-}His)(S\text{-}L\text{-}HisH)_2(H_2O)_2].4H_2O$[e]	-1.06	-0.92[h]	140	-0.99	2.64
$[UO_2(S\text{-}L\text{-}His)(phen)].4H_2O$[e]	-1.06	-0.92[h]	140	-0.99	2.43

[a]Conditions : Cyclic voltammetry, platinum working electrode, 0.61-2.06 mM in DMSO, 0.1M $[NBu_4]ClO_4$ as supporting electrolyte. [b]Potentials reported vs SCE, 25°C.
[c]$\Delta E_p = E_{pc} - E_{pa}$. E_{pc} and E_{pa} are cathodic and anodic peak potentials respectively; i_{pc} and i_{pa} are the corresponding peak currents (μA). [d]$E_{1/2} = 0.5(E_{pc} + E_{pa})$. [e]At 50 mVs^{-1}.
[f]vide reference 46 & 48 regarding one-electron nature of this redox process. [g]The anodic peak is poorly defined and the cyclic voltammetric process is essentially irreversible.
[h]The broad anodic response becomes more well-defined at faster scan rates.

Table II-10. Detailed electrochemical characterization of (A) $[UO_2(OV\text{-}L\text{-}His)(bipy)]\cdot CH_3OH\cdot H_2O$ and (B) $[UO_2(S\text{-}L\text{-}His)(phen)]\cdot 4H_2O$[a,b].

(A)

Scan rate v (mVs^{-1})	$v^{1/2}$ $(V/S)^{1/2}$	E_{pc} (V)	E_{pa} (V)	ΔE_p (mV)	$E_{1/2}$ (V)	i_{pc} (μA)	i_{pa} (μA)	i_{pc}/i_{pa}
50	0.224	-1.05	-0.92	130	-0.98	0.97	0.55	1.76
75	0.274	-1.05	-0.92	130	-0.98	1.20	0.65	1.85
100	0.316	-1.05	-0.91	140	-0.98	1.33	0.75	1.77
125	0.353	-1.05	-0.91	140	-0.98	1.50	0.86	1.74
150	0.387	-1.05	-0.91	140	-0.98	1.65	0.96	1.71
175	0.418	-1.06	-0.91	150	-0.98	1.80	1.02	1.76
200	0.447	-1.07	-0.91	160	-0.99	1.90	1.09	1.75

(B)

50	0.224	-1.06	-0.92	140	-0.99	0.85	0.35	2.43
75	0.274	-1.07	-0.91	160	-0.99	1.06	0.45	2.35
100	0.316	-1.07	-0.91	160	-0.99	1.22	0.57	2.12
150	0.387	-1.08	-0.91	170	-0.99	1.49	0.67	2.22
200	0.447	-1.08	-0.91	170	-0.99	1.70	0.71	2.39

[a]Conditions : Vide the foot-note of Table II-9 regarding the details.

[b]Concentration : 0.92-1.00 mM.